ABSTRACTS BOOK

ELyT workshop 2022

International Research Network
IRN CNRS "ELyT Global"

Engineering and science Lyon Tohoku

November 16th – 18th, 2022 - Lyon, France

ELyT workshop 2022

November 16th - 18th, 2022 - Lyon, France

Program

Wednesday, November 16th
INSA - Rotonde / Agora

8:30	9:00	Welcome coffee
9:00	11:10	Doctor Honoris Causa ceremony for Professor Toshiyuki Takagi Round table Picture
11:10	11:30	Opening of the workshop

11:30	13:30	Cocktail

13:30	14:10	Invited talk by Valéry Botton (INSA Lyon)
14:10	15:50	Session 1 (chairs: T. Uchimoto & G. Sébald)
15:50	16:10	Coffee break
16:10	18:30	Session 2 (chairs: M. Ohta & J.-Y. Cavaillé)

Thursday, November 17th
Ecole Centrale de Lyon - Building W1 / Amphi 3

7:40		Bus departure from INSA to ECL
9:00	9:40	Invited talk by Anne-Lise Cristol & Yannick Desplanques (Centrale Lille)
9:40	10:20	Session 3 (chairs: K. Funamoto & M. Lallart)
10:20	10:40	Coffee break
10:40	12:00	Session 4 (chairs: K. Funamoto & M. Lallart)

12:00	14:00	Lunch and poster session

14:00	14:40	Invited talk by Ausrine Bartasyte (Université de Franche-Comté)
14:40	16:00	Session 5 (chairs: H. Abe & N. Mary)
16:00	17:00	Coffee break and poster session
17:00	18:00	Session 6 (chairs: H. Abe & N. Mary)

20:00	23:00	Banquet

Friday, November 18th
INSA - Building H. Lamarr / Amphi Chappe

9:00	11:00	JSPS Core-to-Core symposium
11:00	12:00	Double-degree PhD Round table
12:00	13:30	Lunch
13:30	14:10	Invited talk by Kostas Danas (Ecole Polytechnique)
14:10	15:30	Session 7 (chairs: A. Komiya & F. Gillot)
15:30	15:50	Coffee break
15:50	18:10	Session 8 (chairs: H. Kurita & V. Fridrici)
18:10	18:30	Closing session

Wednesday, November 16th

INSA - Rotonde / Agora

8:30	9:00	Welcome coffee
9:00	11:10	Doctor Honoris Causa ceremony for **Professor Toshiyuki Takagi** Round table Picture
11:10	11:30	Opening of the workshop
11:30	13:30	Cocktail
13:30	14:10	Flows driven by ultrasounds in liquids in a wall mass transfer enhancement perspective **Valéry Botton** *et al.* (INSA Lyon)
14:10	14:30	Kinetics of Polyurethane Bending over Long Times under Electric Field (TEmPuRA) **Gildas Coativy** *et al.* (INSA Lyon)
14:30	14:50	Thermodynamic modelling of liquid metal dealloying **Pierre-Antoine Geslin** *et al.* (INSA Lyon)
14:50	15:10	Fracture behavior of Al-Fe welds **Kiyoaki Suzuki and Sylvain Dancette** (TU and INSA Lyon)
15:10	15:30	Tensile properties of silk fibers obtained from silkworms fed cellulose nanofibers **Hiroki Kurita** *et al.* (TU)
15:30	15:50	NDT based on the magnetization mechanisms: last progress in the frame of BENTO **Benjamin Ducharne** *et al.* (INSA Lyon)
15:50	16:10	Coffee break
16:10	16:30	Making cool with elastocaloric polymers: progress of the ELyT Global REFRESH project **Gaël Sebald** *et al.* (TU)
16:30	16:50	Modelling of elastocaloric polymers-based heat pump: heat transfer analysis & improved design **Giulia Lombardi** *et al.* (TU)
16:50	17:10	Analysis of energy conversion potentials of Metglas 2605SA1 for energy harvesting applications by measuring Ericsson cycle **Yuanyuan Liu** *et al.* (INSA Lyon)
17:10	17:30	Calibration of an in vivo biomechanical characterisation device for unruptured cerebral aneurysms: first results on polymeric phantom arteries **Guillaume Plet** *et al.* (ECL)
17:30	17:50	Design of a polymeric cerebral aneurysm based on numerical modelling for the development of an aneurysm mechanical characterisation device **Jolan Raviol** *et al.* (ECL)
17:50	18:10	Observation of endothelial cell response to various stenting deployment in an *in vitro* flow system **Hanif Saifurrahman** *et al.* (TU)
18:10	18:30	Nd^{3+}-doped $20Al(PO_3)_3$-80LiF glass : a promising VUV scintillator material for high-counting-rate fast neutron detection **Georges Boulon** *et al.* (Univ. Lyon 1 UCBL)

Thursday, November 17th

Ecole Centrale de Lyon - Building W1 / Amphi 3

7:40		Bus departure from INSA to ECL (in front of La Rotonde)
9:00	9:40	Wear and emissions of highly dissipative rubbing systems: how to learn from experiment? **Anne-Lise Cristol, Yannick Desplanques** *et al.* (Centrale Lille)
9:40	10:00	Atomic structure of bulk metallic glasses investigated by transmission electron microscopy, synchrotron-radiation X-ray diffraction, scanning tunneling microscopy and ab-initio molecular dynamics simulation **Dimitri Louzguine** (TU)
10:00	10:20	Skyrmion stabilization by geometric confinement and uniaxial strain **Hiroshi Koibuchi** (National Institute of Technology (KOSEN), Ibaraki College)
10:20	10:40	Coffee break
10:40	11:00	Evaluation of the thermal gradient of in-flight polymer particles during cold spray process **Chrystelle Bernard** *et al.* (TU)
11:00	11:20	EDOT polymerization in an emulsion by plasma enveloped bubble **Kazuhiko Otake** *et al.* (TU)
11:20	11:40	Electrochemical- and gaseous hydrogen monitoring system for thermodynamic equilibrium state using hydrogen-permeable Pd tubes **Helmut Takahiro Uchida** *et al.* (Tokai University)
11:40	12:00	Diffusion of water in epoxy ionic liquid composite polymer cured and its effect on dielectric and mechanical properties **Lucas Ollivier-Lamarque** *et al.* (TU)

12:00	14:00	Lunch and poster session

14:00	14:40	LiNbO$_3$ films for acoustic filters and vibrational energy harvesting **Ausrine Bartasyte** (Université de Franche-Comté)
14:40	15:00	Flow structure extraction related to the noise generation in a subsonic free jet by using mode decomposition methods **Shota Morita** *et al.* (TU)
15:00	15:20	Sensitivity analysis to investigate the secondary structure from atmospheric shear flow **Ryoichi Yoshimura** *et al.* (TU)
15:20	15:40	Superlubricity of a-C/Si$_3$N4 contact in presence of castor oil **Maria-Isabel de Barros Bouchet** *et al.* (ECL)
15:40	16:00	Multi-scale elucidation of friction mechanisms in ice-rubber interfaces **Anderson Dalavale Kaiser Pinto** *et al.* (ECL)
16:00	17:00	Coffee break and poster session
17:00	17:20	Introduction of synthetic artery data **Kazuyoshi Jin** *et al.* (TU)
17:20	17:40	Blood flow simulations in cerebrovascular models from BraVa database **Yutaro Kohata** *et al.* (TU)
17:40	18:00	Robust shape optimization of a disc-brake system under dynamical criterion **Frédéric Gillot, Achille Jacquemond** *et al.* (ECL)

20:00	23:00	**Banquet** On board Hermès II (13 bis quai Rambaud - 69002 Lyon)

Friday, November 18th

INSA - Building H. Lamarr / Amphi Chappe

9:00	11:00	JSPS Core-to-Core symposium 1. Introduction of core to core by Pr. Takashi Tokumasu (online) 2. Introductions of ammonia utilization and combustion by Pr. Akihiko Hayakawa 3. Ammonia : possible free-carbon fuel for energy and transport applications, Invited talk by Pr. Christine Mounaïm-Rousselle
11:00	12:00	Double-degree PhD Round table

12:00	13:30	Lunch

13:30	14:10	Recent advances in the study of magnetorheological elastomers (MREs) **Kostas Danas** *et al.* (Ecole Polytechnique)
14:10	14:30	Material design for corrosion and stress corrosion cracking management in nuclear applications **Hiroshi Abe** (TU) and **Benoît Ter-Ovanessian** (INSA Lyon)
14:30	14:50	Hypoxia triggers collective aerotactic spreading of eukaryotic cells **Nasser Ghazi** *et al.* (Univ. Lyon 1 UCBL)
14:50	15:10	Cancer cell migration under oxygen concentration gradients **Kenichi Funamoto** *et al.* (TU)
15:10	15:30	Effect of wall elasticity on flow instability and wall shear stress of a full-scale, patient-specific phantom in middle cerebral artery **Ryuhei Yamaguchi** *et al.* (TU)
15:30	15:50	Coffee break
15:50	16:10	Effect of difference wall stiffness between single-segment models and two-segments models on velocity map **Daibo Kotaro** *et al.* (TU)
16:10	16:30	Modeling of Olsen cycle for pyroelectric energy harvesting and assessment of abnormal electrocaloric effect in ferroelectric single crystals **Gaspard Taxil** *et al.* (INSA Lyon)
16:30	16:50	Thermal processes in thermomagnetic energy generators **Joel Joseph** *et al.* (Karlsruhe Institute of Technology)
16:50	17:10	Radiative cooling of solar cells: detailed optoelectro-thermal modeling and influence of surface structuring **Mohamed Amara** *et al.* (INSA Lyon)
17:10	17:30	Ferromagnetic alloys for integrated electrical protection circuits **Mickaël Lallart** *et al.* (INSA Lyon)
17:30	17:50	Thermodynamic Analysis of a New Electric Environmental Control System **Takahiro Adachi** (Akita University)
17:50	18:10	CarboEDiffSim :Molecular Theory Analysis of Carbon Diffusion in Iron which is Happened Phase Transformation under Electric Field **Patrice Chantrenne** *et al.* (INSA Lyon)
18:10	18:30	Closing session **Toshiyuki Takagi** (TU)

Wednesday, November 16th

Afternoon

Flows driven by ultrasounds in liquids in a wall mass transfer enhancement perspective.

ELyT Global
Theme: Energy
Scientific topic: Materials & Structure design

Pr. Valéry BOTTON	**Dr. Sophie MIRALLES**	**Dr. Daniel HENRY**

Abstract

"Not only can a jet generate sound but also sound can generate a jet!" [1]. This sentence by Sir J. Lighthill explains in a few words what acoustic streaming is: the possibility of driving stationary and quasi-stationary flows using acoustic waves (see also our video [2]). This phenomenon can be present in many applications ranging from biomedical applications (low intensity ultrasounds-based diagnostics or high intensity ultrasounds-based treatment) to engineering applications (sono-chemistry, velocimetry, and potentially crystal growth). It can be undesired, such as in the case of prenatal echography, or valuable as a stirring solution in applications sensitive to heat and mass transfers. It is this last possibility that we consider. Our team has indeed been working in the field of semiconductors and metallic alloys elaboration from a melt for many years, with a fluid dynamics standpoint. In such processes, the solidification rejects impurity/dopant into the liquid phase in the vicinity of the solidification front. Controlling liquid convection in the melt is then of primary importance in order to control the eventual composition of the elaborated solid ingot, its micro, meso and macro segregations. Electromagnetic fields are a well-known, well-established solution to act on convection, but implementing electromagnets within a furnace can sometimes be considered as too intrusive and detrimental to the thermal uniformity of the furnace. In the framework of photovoltaic silicon growth within directional solidification furnaces, our team has also collaborated on the modelling of a mechanical stirring featuring a rotating propeller, which is still a very intrusive approach [3].

On another hand, the ability of acoustic streaming to induce mixing in a contactless way in a decimetric cavity has poorly been investigated yet. This could be of interest in applications like

crystal growth from a melt, in which relatively slow flows are expected to have dramatic effect on heat and mass transfer at the solid-liquid interface. Similarly, a well-designed ultrasonic field may help controlling detrimental natural convection instabilities occurring in such processes.

The use of ultrasonic actuators operated at relatively low frequencies and high powers – typically hundreds of kHz and watts, respectively - is widely investigated for improving metallic blend solidification processes. The approach is then to rely on the creation of a cavitation cloud to locally increase sound attenuation near the tip of the actuator [4], which converts acoustic energy into momentum and produces strong flows similar to free jets. The coherence of the acoustic beam is thus lost at a quite small distance from the actuator. Our team is rather interested in higher frequencies and lower powers, for which Eckart type streaming occurs in a homogeneous liquid without producing cavitation. The ultrasonic beam is then coherent on long distances, which allows forcing flows far from the actuator since typical attenuation lengths of sound in common liquids are typically decimeters long or even meters long, in the MHz range [5]. In cavities with dimensions comparable to the attenuation length, acoustic reflections on the walls containing the liquid can occur, increasing the geometrical complexity in the acoustic field and thus in the forcing [6,7]. We will present the understanding we got of this type of acoustic streaming along a beam, after a few years of experimental and numerical investigations on the subject. We will eventually focus on our recent experimental and numerical work concerning how acoustic streaming enhances mass transfer at a solid-liquid interface [8]. This work relies on an electrochemical technic, implemented in collaboration with the MATEIS laboratory, to measure the wall mass flux at working electrodes in a ferro-/ferri-cyanide electrolytic solution.

An outlook could be future collaborations in the Lyon-Tohoku collaborative framework, possibly in smaller scale mass-transfer experiments.

[1] S.J. Lighthill, Acoustic streaming, J. Sound Vibr. 61 (1978) 391–418.
[2] Transient Eckart acoustic-streaming flow, 2014. https://www.youtube.com/watch?v=ArpclLD4yP8 (accessed September 26, 2022).
[3] M. Chatelain, V. Botton, M. Albaric, D. Pelletier, B. Cariteau, D. Abdo, M. Borrelli, Mechanical stirring influence on solute segregation during plane front directional solidification, International Journal of Thermal Sciences. 126 (2018) 252–262. https://doi.org/10.1016/j.ijthermalsci.2017.12.024.
[4] G.S.B. Lebon, G. Salloum-Abou-Jaoude, D. Eskin, I. Tzanakis, K. Pericleous, P. Jarry, Numerical modelling of acoustic streaming during the ultrasonic melt treatment of direct-chill (DC) casting, Ultrasonics Sonochemistry. 54 (2019) 171–182. https://doi.org/10.1016/j.ultsonch.2019.02.002.
[5] B. Moudjed, V. Botton, D. Henry, H. Ben Hadid, J.-P. Garandet, Scaling and dimensional analysis of acoustic streaming jets, Phys. Fluids. 26 (2014) 093602. https://doi.org/10.1063/1.4895518.
[6] B. Moudjed, V. Botton, D. Henry, S. Millet, H. Ben Hadid, Y-shaped jets driven by an ultrasonic beam reflecting on a wall, Ultrasonics. 68 (2016) 33–42. https://doi.org/10.1016/j.ultras.2016.02.003.
[7] T. Cambonie, B. Moudjed, V. Botton, D. Henry, H. Ben Hadid, From flying wheel to square flow: Dynamics of a flow driven by acoustic forcing, Phys. Rev. Fluids. 2 (2017) 123901. https://doi.org/10.1103/PhysRevFluids.2.123901.
[8] N. El Ghani, S. Miralles, V. Botton, D. Henry, H. Ben Hadid, B. Ter-Ovanessian, S. Marcelin, Acoustic streaming enhanced mass transfer at a wall, International Journal of Heat and Mass Transfer. 172 (2021) 121090. https://doi.org/10.1016/j.ijheatmasstransfer.2021.121090.

Kinetics of Polyurethane Bending over Long Times under Electric Field

ELyT Global

Project: Theory for Electrostriction of PolymeRic Actuator. TEmPuRA

Theme: Materials and structure design

| 1-G. COATIVY | 2-G. DIGUET | 1,3-K. YUSE | 1-L. SEVEYRAT | 1-V. PERRIN | 4- F. DALMAS |

| 5-S. LIVI | 6-H. TAKANA | 4-J. COURBON | 7-C. BERNARD | 3,8-JY CAVAILLE |

1   Univ. Lyon, INSA-LYON, LGEF, EA682, F-69621 Villeurbanne, France
2   Micro System Integration Center, Micro/Nano-Machining Research and Education Center, Tohoku University, Sendai, Japan
3   Lyon Center, IFS -Tohoku U., Université de Lyon, INSAVALOR, Villeurbanne, 69621, France
4   Univ Lyon, INSA Lyon, UCBL, CNRS, MATEIS, UMR5510, Villeurbanne 69621, France
5   Univ Lyon, CNRS, UMR 5223, Ingénierie des Matériaux Polymères, Université Claude Bernard Lyon 1, INSA Lyon, Université Jean Monnet, F-69623 Villeurbanne Cedex, France
6   Tohoku Univ, Inst Fluid Sci, Aoba Ku, 2-1-1 Katahira, Sendai, Miyagi 9808577, Japan
7   Frontier Research Institute for Interdisciplinary Sciences, Tohoku University, Sendai, Japan
8   ELyTMaX IRL3757, CNRS, Univ Lyon, INSA Lyon, Centrale Lyon, Université Claude Bernard Lyon 1, Tohoku University, Sendai, Japan

Abstract

Dielectric elastomers such as polyurethane (PU) can be used to develop electro-actuators. Most of them have the advantage of being easy to process, lightweights and cheap. The electromechanical behavior of dielectric elastomers in compression is generally described as coming from mechano-dielectric effects without charge transport: the mutual attraction of electrodes of opposite signs (Maxwell stress), the orientation of the dipoles present in the material, and in the case of multiphase materials, the attraction of the different phases [1]. These different phenomena seem to explain the reduction in thickness of thin polyurethane films subjected to an electric field. However, they do not explain the slow kinetics of electro-actuation of polyurethane at constant electric field [2] or its bending [3]. Bending tests consist

of suspending a sample, holding a fixed edge, and measuring the displacement of its free end from the vertical (figure 1). The mechanisms of dielectric elastomers recalled above cannot be used to describe the bending of PU since it requires an asymmetric repartition of mechanic stress. It was shown that after few minutes of applying an electric field, the observed bending is originated from an asymmetric space charge distribution inside the material which can be ionic (impurities) or electronic (charge injection) [3,4]. Our experiments performed over 10^5 s (figure 1) show that the displacement reaches a maximum at t≈100 s and finally tends to zero. It suggests that after such a long period of time, the distribution of electric charges is finally symmetric. In order to explain this behavior, a first attempt of simulation was made. It is based on three main concepts: two types of ions with opposite charges are present inside the material, their mobility is different and the local electric field depends of the charge distribution inside the material. By fixing the parameters of the simulation at an electric field of 10 MV/m, it was possible to obtain the same range of order of bending by simulation as the one measured experimentally at different electric fields. However, our simulation did not involve any measured physical parameters and is not able to quantitively describe the electric current measured experimentally. The objective of our ongoing project is therefore to develop model materials with a controlled amount of charge carriers, to determine their physical parameters such as ion mobility and to move towards a more realistic modelling of their behavior.
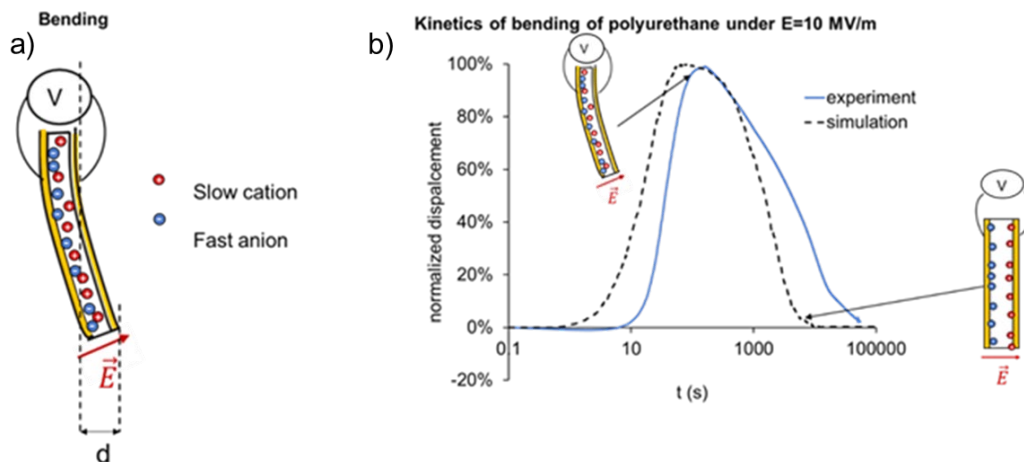
Figure 1 a) Principle of bending test b) normalized displacement measured experimentally and obtained via a simulation involving the presence of two types of ions with opposite charges and having different mobilities

References:

[1]   Jomaa M H, Masenelli-Varlot K, Diguet G, Seveyrat L, Lebrun L, Wongtimnoi K, Vechambre C, Chenal J M and Cavaillé J Y 2015 Modeling of segmented pure polyurethane electrostriction behaviors based on their nanostructural properties *Polymer (Guildf).* **62** 139–47

[2]   Jomaa M H, Seveyrat L, Perrin V, Lebrun L, Masenelli-Varlot K, Diguet G and Cavaille J Y 2017 Difference between electrostriction kinetics, and mechanical response of segmented polyurethane-based EAP *Smart Mater. Struct.* **26** 035049

[3]   Watanabe M, Wakimoto N, Shirai H and Hirai T 2003 Bending electrostriction and space-charge distribution in polyurethane films *J. Appl. Phys.* **94** 2494–7

[4]   Watanabe M, Kato T, Suzuki M, Amaike Y and Hirai T 1999 Bending Electrostriction in Polyurethanes Containing Ions as Contaminants or Additives *Jpn. J. Appl. Phys.* **38** L872–4

Thermodynamic modelling of liquid metal dealloying

ELyT Global
Theme: physical metallurgy
Scientific topic: liquid metal dealloying

	Pierre-Antoine Geslin **MATEIS – INSA Lyon**		**Louis Lesage** **MATEIS – INSA Lyon** **IMR – Tohoku Univ** **ElytMAX – Tohoku Univ / INSA-Lyon / CNRS**
	Nicolas Mary **MATEIS – INSA Lyon**		**Takeshi Wada** **IMR – Tohoku University**
	Hidemi Kato **IMR – Tohoku University**		

Abstract

Liquid metal dealloying has emerged as a promising technique to elaborate finely porous structures of various nature (non-noble metals, refractory metals or semi-conductors) presenting a high surface area, valuable in numerous applications including catalysis, sensors or battery materials [1,2,3]. This process consists of immersing a binary AB precursor alloy in a liquid metal chosen such that only one element (B) of the precursor alloy dissolves selectively into the metallic melt C while the other element (A) reorganizes into a porous structure. Understanding how the resulting microstructure (composition of phases, solid fraction, etc.) depends on the parameters of the process (temperature, compositions of the precursor and the bath) is critical the elaborate microstructures with optimized properties for

functional and mechanical applications.

In particular, experimental evidences point out that tuning the composition of the liquid bath enables to control the residual B content of the resulting solid ligaments. To rationalize these findings, we consider that the composition of the different phases resulting from dealloying process is dictated by a thermodynamic equilibrium. This is justified by the fact the microstructures display large exchange areas between solid ligaments and liquid channels, thereby promoting the convergence to a thermodynamic equilibrium. We show that such equilibrium considerations enables to reproduce experimental results for Fe-Ni precursors immersed into Mg-Ni baths of different compositions.

To go beyond this single equilibrium approach, we also propose a 1D diffusion model to simulate the kinetics of the dealloying process. The dealloying rate and the composition of both solid and liquid phases are again determined from local thermodynamics equilibria while the diffusion equation is integrated in the liquid phase. The model predictions are compared to experimental results for two different systems.

References :

[1] T. Wada, K. Yubuta, A. Inoue and H. Kato, Materials Letters 65, pp. 1076-2078, 2011.

[2] T. Wada, A.D. Setyawan, K. Yubuta, H. Kato, Scripta Materialia 65, pp. 532-535, 2011.

[3] T. Wada, H. Kato, Scripta Materialia 68, pp. 723-726, 2013.

Fracture behavior of Al-Fe welds

ELyT Global
**Theme: Transportation
Scientific topic: Materials & Structure design**

	K. Suzuki [1]		**S. Dancette** [2,3]
	J. Adrien [3]		**Y. Sato** [1]

Affiliation

1: Department of Materials Processing, Graduate School of Engineering, Tohoku University, 6-6-02 Aramaki-aza-Aoba, Aoba-ku, Sendai 980-8579, Japan
2: ELyTMaX IRL3757, CNRS, Univ Lyon, INSA Lyon, Centrale Lyon, Universite Claude Bernard Lyon 1, Tohoku University, Sendai, Japan
3: Univ Lyon, INSA Lyon, CNRS UMR5510, Laboratoire MATEIS, F-69621, Villeurbanne Cedex, France

Abstract

Joining aluminum to steel has been a long-running scientific and technological problem for many applications, starting with those in the transportation industry. It would unlock new designs of optimized vehicle structures combining strength, lightweight and energy absorption ability. Troubles arise from the brittle intermetallic compound layer appearing at the Fe-Al interface during the welding process. Its low fracture toughness causes premature brittle fracture of the weld joint when subjected to load.

In this work, the mechanical behavior of different Al-Fe welds with varying composition of the aluminum alloy is investigated by means of microstructure analysis, *in situ* mechanical tests under X-ray tomography and finite element analysis. Precise control of the alloying elements composition allows to control the nature and thickness of the intermetallic interfacial layer, but also affects the yield strength and deformability of the aluminum alloy.

Different scenarios of weld deformation and crack propagation are analyzed and discussed in

relation with the characteristics of the interfacial layer and the properties of the base metals.
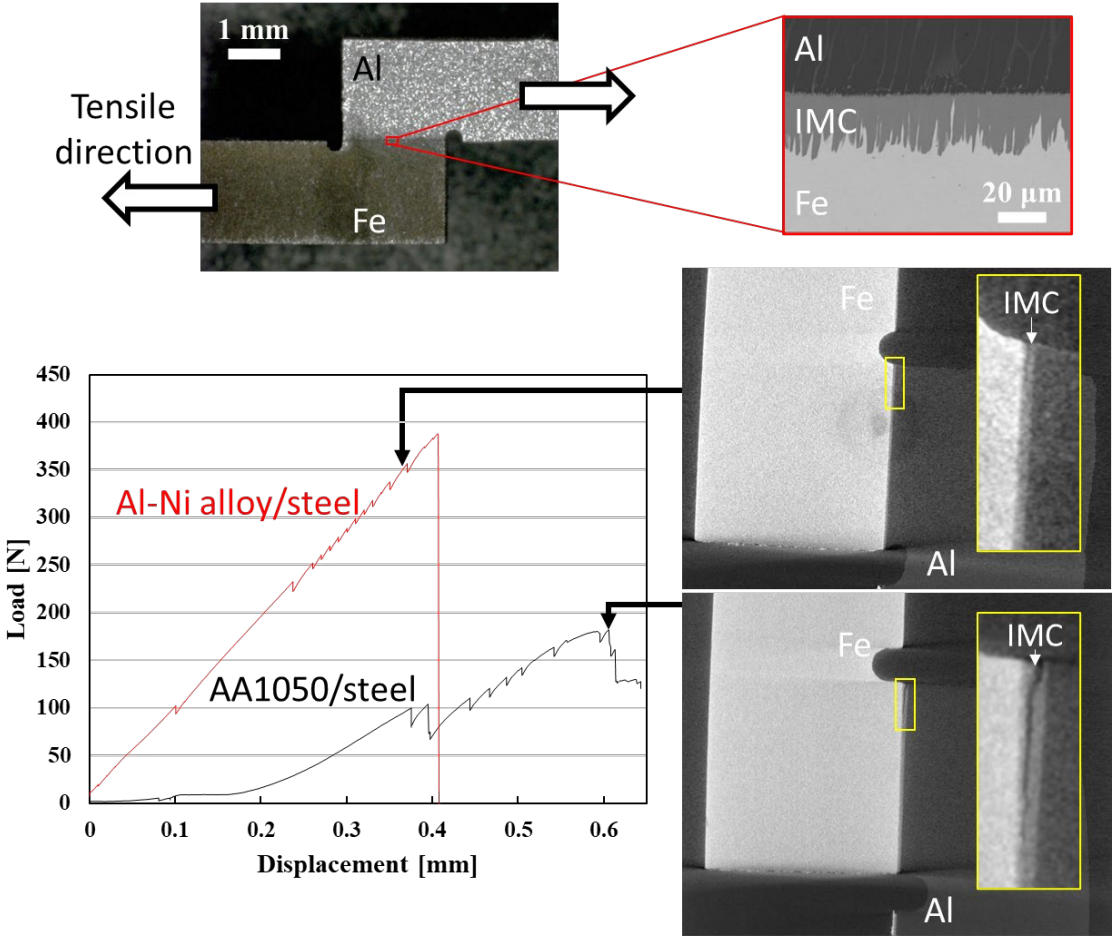
Figure : Lap-shear testing of Al-Fe welds monitored in situ using X-ray tomography.

Tensile Properties of Silk Fibers Obtained from Silkworms Fed Cellulose Nanofibers

ELyT Global
Energy
Materials & Structure design

| | Assist. Prof. Hiroki KURITA | | Teruyoshi KANNO | | Dr. Zhenjin WANG | | Prof. Fumio NARITA |

Abstract

In addition to its traditional applications in the textile industry, Bombyx Mori silk has attracted significant attention in materials science and bioengineering. Recently, the potential for stretching silk fibers with excellent toughness has been particularly investigated. Cellulose nanofibers (CNFs) have been widely studied as reinforcing materials due to their excellent mechanical properties, relatively low density, and promising biocompatibility. We report that silkworm silk fibers with intrinsically dispersed CNFs exhibit superior tensile properties compared to conventional silk fibers. Morphological studies have also revealed that individual fibrils or fibril bundles are aligned and uniformly dispersed in the longitudinal direction of the silk fiber.

Introduction

Silk is the only natural fiber that exists as continuous filaments. This unique advantage contributes to the diversity of potential uses of silk fibers Bombyx Mori (B. Mori) silk is a conventional fiber material produced by the domesticated silkworm. Silk fibers drawn from silkworms have excellent biocompatibility. As a result, they have been widely applied in the medical field due to their low risk of causing inflammatory reactions.

Cellulose nanofibers (CNFs) are promising environmentally friendly next-generation nanomaterials that can be used to synthesize low-cost, lightweight, high-strength, renewable, and sustainable nanocomposites. However, CNF-based composites synthesized in previous studies exhibit moderate mechanical properties, which may be due to poor nanofibril alignment. The flow-focusing method, in which fibrils are dispersed in a liquid and oriented along the flow direction, has effectively improved nanofibril orientation. A similar assembly process is used in the silkworm spinning process, which prompted our research. This example represents a new environmentally friendly method of stretching silk

fibers reinforced with CNF and may provide an alternative to post-functionalization approaches involving harmful organic solvents.

Recently, a novel technique has been reported that can easily and directly obtain silk fibroin solution without using organic solvents using a silk cocoon mill. This study aims to develop a nano-cellulose/silkworm silk composite fiber, focusing on directly feeding nanomaterials to silkworms. To improve the mechanical strength of the silk produced, CNF was added to silkworm feed. Tensile tests were conducted to determine the mechanical properties of the stretched silk fibers. The surface of the silk fibers was also examined to confirm the presence and orientation of nanofibrils.

Results and Discussion

Fig. 1 shows typical stress-strain curves for silk fibers from silkworms fed cellulose nanofibers. The cross-sectional area of silk fibers used for tensile stress measurements was estimated to be 393, 272, and 356 m^2 for the silk fibers obtained from silkworms fed cellulose nanofibers of 0, 5, and 10 wt.% (Pure-F, CNF5-F, CNF10-F specimens), respectively, from SEM images. However, the CNF10-F specimens were not as strong as the Pure-F specimens. However, Young's modulus and fracture strength of CNF10-F specimens were lower than those of Pure-F specimens, despite the higher concentration of CNF (see Fig. 2).
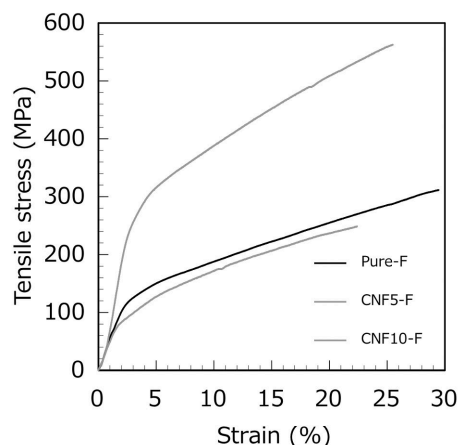
Figure. 1 Typical stress–strain curves of silk fibers obtained from silkworms fed cellulose nanofibers.

Atomic force microscope (AFM) images were obtained to clarify the mechanism of the strengthening effect observed in the CNF5-F specimens. On the other hand, white lines were observed in the two-dimensional AFM surface image of CNF5-F, and these lines appeared as discontinuous fibrous protrusions in the three-dimensional AFM image. Moreover, the height of the protrusions extending outward from the fiber surface is approximately 1 nm. Therefore, these structures were identified as single cellulose fibrils; in CNF5-F and CNF10-F specimens, the nanofibrils were aligned in the axial direction of the silk fiber. AFM images showed that CNF aggregation was more advanced in CNF10-F specimens than in CNF5-F specimens, indicating that the nanofibrils were well dispersed.
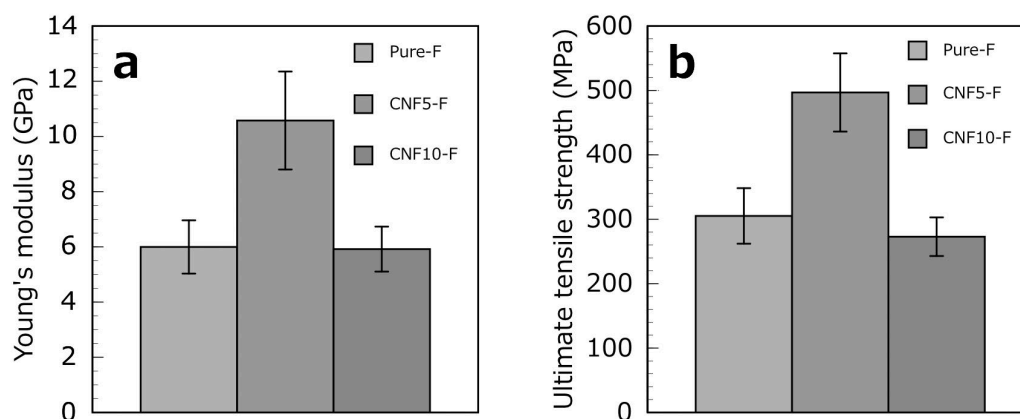
Figure. 2 (a) Young's modulus and (b) ultimate tensile strength of silk fibers obtained from silkworms fed cellulose nanofibers.
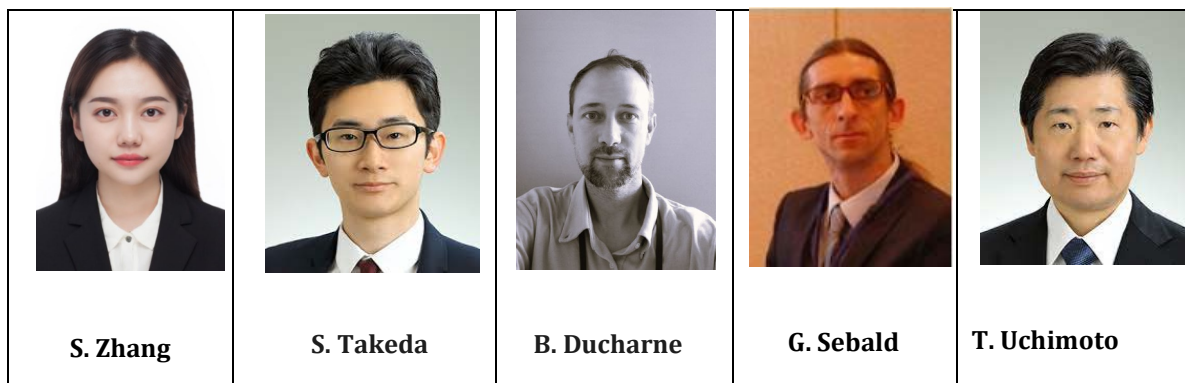
NDT based on the magnetization mechanisms:

last progress in the frame of BENTO.

(Nonlinear and dynamic micromagnetic <u>Be</u>havior modeling and characterization for <u>N</u>on-Destructive <u>T</u>esting techniques <u>o</u>ptimization).

ELyT Global
**Non-destructive testing
Magnetization signatures**

S. Zhang   **S. Takeda**   **B. Ducharne**   **G. Sebald**   **T. Uchimoto**

Abstract

Magnetism entails many facets in contemporary Non-destructive Testing (NDT):
- A way to convey and transmit information like in eddy current testing.
- A source of a mechanical force like in magnetic particle inspection.
- The natural earth field being distorted by defects or properties to be assessed like in metal magnetic memory.
- An induced magnetic field distorted by surface or sub-surface defects like in magnetic flux leakages.

In the frame of BENTO, magnetism is exploited differently, still for an NDT purpose, but the focus is set on the magnetization mechanisms of ferromagnetic components and their capability to indirectly convey information about targeted properties (mechanicals, microstructural, etc.). Steel production is by far more extensive than any other metal production. Steel is used in domains as diverse as transportation (railway tracks, boat tanks, etc.), construction (concrete re-enforcing bars, bridges, etc.), and energy (pipelines, turbines, etc.). In the steel industry, the demand for NDT is immense. Historically, surface defects (porosity, corrosion, cracks, etc.) were first targeted, but internal properties like residual stresses, plastic strains, internal dislocations, and the likelihood of failure due to creep or

fatigue have grown in interest recently. Every NDT method can be applied to steel, but the techniques relying on the magnetization mechanisms are unique to steel. The idea of developing NDT from the magnetization signature is not new, and the first scientific publications on this topic can be found in the sixties. Firstly, developed at the academic level, it soon grew significant interest among steel companies. The first industrial machines dedicated to this topic were commercialized in the eighties and found relative success. Nowadays, devices like the Fraünofer IZFP 3MA or the Stresstech® rollscan are relatively commune. The implementation and configuration of these devices are all based on the same protocols. A large amount of experimental data is collected, then specific indicators evaluated on this data are defined. Eventually, complex mathematical correlations are established with targeted properties predetermined on well-known specimens. This method relies on meticulous experimental campaigns and leads to rejection thresholds setting acceptance limits. This configuration process is tedious and not always reliable, and manufacturers are looking for alternatives. Unfortunately, the configuration issue is not the only one mentioned by the end-users; the signal interpretation, indicators selection, and physical meaning are also recurrently stated as holding back this technological development.

The sensitivity to the targeted properties differs from one magnetization mechanism to the other. Progress in this domain will come from developing experimental situations where those mechanisms happen to be separated. Once the targeted property is well defined, the final step exploits the most sensitive magnetization mechanism.

In the frame of BENTO, progress has been made regarding identifying the targeted property. Progress has been made too concerning the definition and the isolation of the magnetization mechanisms (experimental situations and indicators where these mechanisms can be ideally observed).

Correlations have been established between the targeted properties and the magnetization mechanisms. Together with newly developed simulation tools, they helped understand its physic and converge toward the ideal way to control a targeted property in a real-life situation (industrial context).

Recent papers (less than two years) in the Frame of BENTO collaboration:

[1] S. Zhang, B. Ducharne, G. Sebald, S. Takeda, T. Uchimoto, Magnetic indicators for evaluating plastic strains in electrical steel: toward nondestructive assessment of the magnetic losses. NDT&E Int., under revision, 2022.
[2] B. Ducharne, S. Zhang, G. Sebald, S. Takeda, T. Uchimoto, « Electrical steel dynamic behavior quantitated by inductance spectroscopy: Toward prediction of magnetic losses," J. of Mag and Mag., vol. 560, p.169672, 2022. DOI: 10.1016/j.jmmm.2022.169672
[3] S. Zhang, B. Ducharne, S. Takeda, G. Sebald, T. Uchimoto, "Low-frequency behavior of laminated electric steel sheet: Investigation of ferromagnetic hysteresis loops and incremental permeability," J. of Mag and Mag., Vol. 538, 2021. DOI: 10.1016/j.jmmm.2021.168278
[4] S. Zhang, B. Ducharne, S. Takeda, G. Sebald, T. Uchimoto, "Identification of the ferromagnetic hysteresis simulation parameters using classic non-destructive testing equipment," J. of Mag and Mag. Mat., Vol. 531, 2021. DOI: 10.1016/j.jmmm.2021.167971
[5] B. Gupta, B. Ducharne, T. Uchimoto, G. Sebald, T. Miyazaki, T. Takagi, "Comparison of electromagnetic nondestructive testing of creep-degraded high-chromium ferritic steels," NDT & E Int., vol. 118, 102399, 2021. DOI: 10.1016/j.ndteint.2020.102399
[6] S. Zhang, B. Ducharne, T. Uchimoto, A. Kita, Y.A. Tene Deffo, "Simulation tool for the Eddy Current Magnetic Signature (EC-MS) non-destructive method," J. of Mag. and Mag. Mat., vol. 513, 167221, 2020. DOI: 10.1016/j.jmmm.2020.167221
[7] Z. Xiaodong, T. Uchimoto, B. Wu, T. Toshiyuki, B. Ducharne, L. Xiucheng, H. Cunfu, "Improved dynamic magnetostriction measurement method based on M-EMAT for the characterization of residual strain," Int. J. of App. Electromag. and Mech., vol. 64, n°1-4, pp. 299-306, 2020. DOI: 10.3233/JAE-209334
[8] S. Zhang, B. Ducharne, T. Uchimoto, A. Kita, Y.A. Tene Deffo, "Simulation tool for the Eddy Current Magnetic Signature (EC-MS) non-destructive method," J. of Mag. and Mag. Mat., vol. 513, 167221, 2020. DOI: 10.1016/j.jmmm.2020.167221

Making cool with elastocaloric polymers: progress of the ELyT Global REFRESH project

ELyT Global
Theme: Energy
Scientific topic: Materials and Structures Design

Gaël SEBALD[a]   Atsuki KOMIYA[a,b]   Jacques JAY[c]   Gildas COATIVY[d]

Giulia LOMBARDI[a,b]   Marianne SION[a,b,c]   Xuen Sze WAY[b]   Laurent LEBRUN[d]

[a] *ELyTMaX UMI 3757, CNRS – Université de Lyon – Tohoku University International joint Unit, Tohoku University , 980-8577, Sendai, Japan*
[b] *Institute of Fluid Science, Tohoku University, 980-8577, Sendai, Japan*
[c] *Univ. Lyon, CNRS, INSA-Lyon, CETHIL, UMR5008, F-69621, Villeurbanne, France*
[d] *Univ. Lyon, INSA-Lyon, LGEF, EA682, F-69621, Villeurbanne, France*

Abstract

Refrigeration alternatives are driven by the need of more environmentally friendly solutions while ensuring a high efficiency. In some solid materials – called caloric materials – the entropy may be modified by an external stimuli other than temperature, similarly to a perfect gas or a refrigerant gas under hydrostatic pressure. The temperature variations are usually rather small (i.e. <20K for NiTi elastocaloric alloys, <5K for electrocaloric materials). Nonetheless, several groups attempted to design, fabricate and test lab-scale proofs of concepts, like electrocaloric devices [1] or elastocaloric devices [2]. Such experimental developments are of primary importance for proving the potential of these refrigeration alternatives, but also for material scientists searching for more effective materials [3, 4], in order to determine which properties has to be optimized.

From the state of the art, the development of this refrigeration technology is at its early stage, where both material development and device design require equal attention. Among caloric materials, natural rubber appears to be a promising elastocaloric material offering several advantages [5, 6], although barely investigated in the view of this application. Polymers exhibit low thermal conductivity, thus opening unprecedented questionings on the applicability into a

refrigeration device where a quick heat transfer is needed between the caloric material and its surroundings.

Within ELyT Global REFRESH project, a focus is done on the development of experimental proofs of concept of refrigeration device, assisted by *ad hoc* heat and mass transfer problems models. The material exhibits periodic time variations of temperature when actuated cyclically, and it is required a heat transfer system to induce net heat flux from a cold reservoir to a hot reservoir while controlling thermal losses. One possibility is to move cyclically a fluid in contact with the rubber material while it is stretched and unstretched [2, 7]. Doing so, it is possible, under finely controlled conditions, to induce a net heat flux along one direction, and the fluid can take some heat from the source and to deliver it to the sink. This principle is called regenerative system, since not only the net heat transfer is obtained, but also the heat is stored locally in the solid leading to a temperature gradient along a cooling line if the active material in long enough. In the framework of REFRESH project, it was developed an innovative experimental proof of concept leading to performances as high as other caloric materials.

Alternatively, solid-solid heat transfer might be envisaged, leading to a so-called single stage system. In such a system, the active material is mechanically moved and put into contact with the heat sink (at room temperature) when its temperature increased after the stretching step. After some time, the temperature of the active material stabilizes to that of the heat sink. It is then moved away from the heat sink, un-stretched and put into contact with the heat source (at a temperature lower than room temperature) to absorb heat from it. For an elastocaloric material, the stretching may be combined with the contact with the heat sink using a concave shape. For example Ossmer et al. developed such a system for NiTi elastocaloric alloys [8]. In the frame of REFRESH project, it was started recently the development of two device configurations for transposing this possibility to natural rubber while solving specific issues of this material (cyclic deformations up to 600% and low thermal conductivity).

The potential of natural rubber starts to be confirmed in both material characterization and tentative experimental refrigeration proof of concept. The precise evaluation of the potential of this material as alternative for refrigeration still require extensive work, firstly on the material itself (which is not optimized yet for this application). It is required also further development of the refrigeration proof of concept, where large potential improvement is foreseen.

References
[1] A. Torelló, P. Lheritier, T. Usui, Y. Nouchokgwe, M. Gérard, O. Bouton, S. Hirose, E. Defay, *Science*, 370, (2020), 125–129.
[2] J. Tušek, K. Engelbrecht, D. Eriksen, S. Dall'Olio, J. Tušek, N. Pryds, *Nat. Energy*, 1, (2016), 16134.
[3] P. Lloveras, A. Aznar, M. Barrio, P. Negrier, C. Popescu, A. Planes, L. Mañosa, E. Stern-Taulats, A. Avramenko, N. D. Mathur, X. Moya, J.-L. Tamarit, *Nat. Commun.*, 10, (2019), 1803.
[4] B. Nair, T. Usui, S. Crossley, S. Kurdi, G. G. Guzmán-Verri, X. Moya, S. Hirose, N. D. Mathur, *Nature*, 575, (2019), 468–472.
[5] Z. Xie, G. Sebald, D. Guyomar, *Appl. Phys. Lett.* 108, (2016), 041901.
[6] G. Sebald, Z. Xie, D. Guyomar, *Philos. Trans. R. Soc. A Math. Phys. Eng. Sci.*, 374, (2016), 20150302.
[7] G. Sebald, A. Komiya, J. Jay, G. Coativy, L. Lebrun, *J. Appl. Phys.*, 127, (2020), 094903.
[8] H. Ossmer, F. Wendler, M. Gueltig, F. Lambrecht, S. Miyazaki, M. Kohl, *Smart Mater. Struct.* 25, (2016), 085037.

Modelling of elastocaloric polymers-based heat pump: heat transfer analysis and improved design

ELyT Global
**Theme Energy
Scientific topic Materials and modelling**

| Giulia LOMBARDI[a,b] | Gael SEBALD[a] | Astuki KOMIYA[b] | Sze Xuen WAY[b] | Gildas COATIVY[c] | Jacques JAY[d] |

[a] ELyTMaX IRL3757, CNRS, Univ. Lyon, INSA Lyon, Centrale Lyon, Université Claude Bernard Lyon 1, Tohoku University, 980-8577, Sendai, Japan
[b] Institute of Fluid Science, Tohoku University, 980-8577, Sendai, Japan
[c] Univ. Lyon, INSA Lyon, LGEF EA682, F-69621, Villeurbanne, France
[d] Univ. Lyon, CNRS, INSA-Lyon, CETHIL, UMR5008, F-69621, Villeurbanne, France

Caloric materials have the property to show significant thermal changes when subjected to an external magnetic, electric, or mechanical stimulus, thus classifying these materials into magnetocaloric, electrocaloric and elastocaloric materials, respectively[1]. Among the elastocaloric materials, natural rubber (NR) constitutes a highly-abundant and low-cost alternative, and it does not require high force levels, contrary to SMAs (the most widely used material for elastocaloric systems)[2,3].

The elastocaloric properties of NR tubes were experimentally investigated. They were subjected to different elongations, thus exhibiting different adiabatic temperature variations ΔT_{ad}, as shown in Fig. 1(A). The increase in the recorded temperature is mainly caused by the strain-induced crystallization and the chain orientation toward the strain direction. The NR elastocaloric properties under cyclic elongations were studied by imposing trapezoidal elongations at 0.1 Hz. The temperature reached a stabilization for all the tested elongations after ~20 cycles. Higher applied elongations led to higher values of hysteresis, thus leading to lower values of COP_{mat}. This highlight the interest in employing cycling elongations between $\lambda = 3.5$ and $\lambda = 5.5$ (shown in Fig. 1(B)) representing the appropriate compromise in terms of temperature variations and mechanical losses.
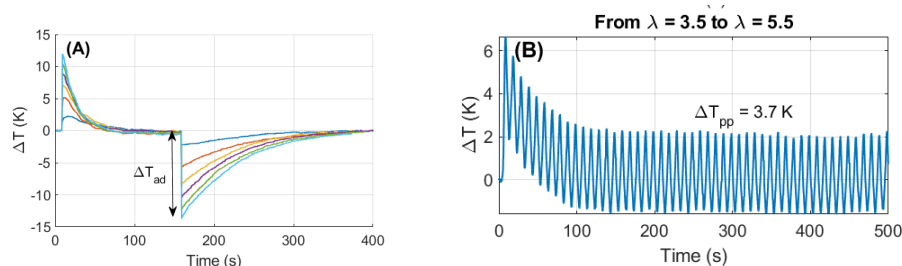
Fig. 1 (A) Adiabatic ΔT as a function of time; (B) ΔT as a function of time for cyclic elongations at 0.1 Hz

The obtained temperature variations need to be converted into a permanent spatial gradient. To do so, a fluid moving cyclically can be used, leading to an active regenerative system[2]. In order to enhance the heat transfer between the NR tubes and the water, a theoretical study is conducted using OpenFOAM. The objective of the simulation, which schematic is given in Fig. 2, is the study of the heat transfer problem between the solid and the fluid region in the transient domain. This is affected by many parameters, for instance: the rubber thickness, the water flow rate, the rubber deformation, the phase difference between the rubber deformation and water flow. Eventually, the final goal would be to evaluate the influence of the listed parameters on the heat transfer process. Fig. 3 represents the temperature profile as a function of time at the water inlet (blue line) and outlet (red line). Although the tendency of the temperature is roughly correct (a temperature span is developed between the tube inlet and outlet), the inlet boundary conditions need to be adjusted.
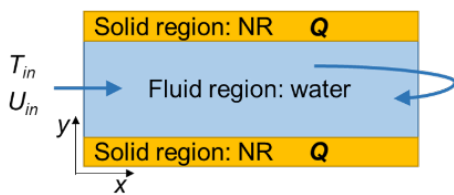
Fig. 2 Schematic diagram of the NR tube and water.
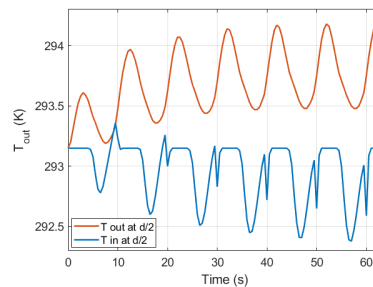
Fig. 3 Outlet temperature profile along the y-axis of the NR tube.

As in the final cooling application several rubber tubes are employed, a global model considering the lumped system parameters has been developed. A schematic of such a model is given in Fig. 4. The model has been used to calculate the influence of the thermal insulation on the final temperature span but it can serve other purposes (for instance, the influence of the void volumes or flow maldistribution). Fig. 5 shows the cooling power as a function of the temperature span: the insulation has a relatively small impact on the final temperature span of the system, giving an increase of the final temperature span of 2 K when considering a 2 cm thick polyurethane foam surrounding the full length of the cooling system.

$$Q_{W} = W_{hyst} V_{tube} f N_{t}$$
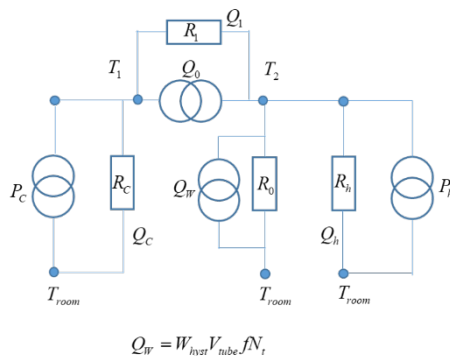
Fig. 4 Schematic of the system model of a cooling device.
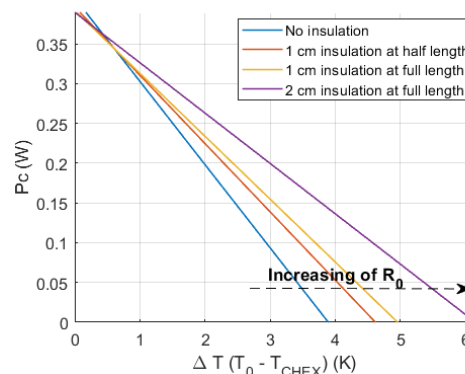
Fig. 5 Variation of the cooling power vs temperature span of a cooling device with 19 NR tubes as a function of the $R_{0.}$

References

[1] I. Takeuchi, T. Yabuki, K. Sandeman, Physics Today, 68, (2015), 12, 48.

[2] A. Torelló, E. Defay, International Journal of Refrigeration 127 (2021), 174-179.

[3] G. Sebald, A. Komiya, J. Jay, G. Coativy, L. Lebrun, Journal of Applied Physics 9 (2020), 094903.

Analysis of energy conversion potentials of Metglas 2605SA1 for energy harvesting applications by measuring Ericsson cycle

ELyT Global
Theme Energy
Scientific topic: - Materials and structure design
- Simulation and modeling

Yuanyuan LIU[1,2,3] **Benjamin DUCHARNE**[3] **Gaël SEBALD**[3] **Kanjuro MAKIHARA**[2] **Mickaël LALLART**[1,*]
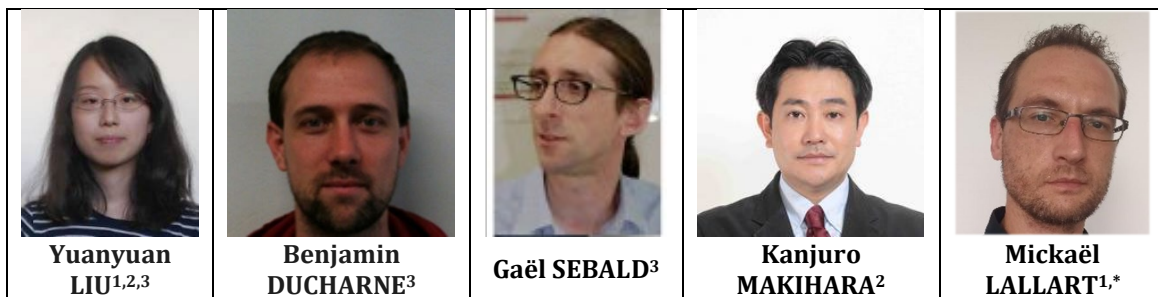
[1]*Univ. Lyon, INSA-Lyon, LGEF EA682, F-69621, France*
[2]*Space Structure Lab, Department of Aerospace Engineering, Tohoku University, Japan*
[3]*ELyTMaX UMI 3757, CNRS, Univ. Lyon, INSA Lyon, Centrale Lyon, Université Claude Bernard Lyon 1, Tohoku University, Sendai, Japan*

mickael.lallart@insa-lyon.fr

Abstract

1. Introduction

With the fast development of the Internet of Things, the number of wireless sensors and sensor networks is increasing. Hence, energy harvesting systems which could convert ambient energy sources, such as vibrations, into electrical energy are a great alternative to batteries and their associated drawbacks such as limited lifespan due to self-discharge. In this framework, magnetostrictive alloys, one of the main categories of energy harvesting materials, have been used for energy conversion by exploiting Villari effect. Compared to conventional materials, namely Galfenol and Terfenol-D, that feature high magnetostrictive effect, amorphous alloys, such as Metglas 2605SA1, show attractive characteristics such as flexibility, low hysteresis, and much lower price. In this study, Metglas 2605SA1 was chosen for its high tensile strength and cost-effectiveness. A specific setup was developed for the measurement of Ericsson cycles, which gives the ultimate amount of converted energy of the materials. The Ericsson cycle measurement for Metglas 2605SA1 ribbon under different tensile stresses in the low frequency range are presented. The converted energy was compared to the harvestable energy of Galfenol and Terfenol-D calculated from the hysteresis curves taken from the literature.

2. Experimental

Two actuators were used for the cyclic application of tensile stress, while the frequency and the amplitude could be controlled precisely. A force sensor was used to monitor the stress. A primary coil of 110 turns was wounded separately and evenly on the two ferrites

as shown in Fig. 1. A 5Ω resistance was connected to the primary coil, allowing to get the excitation field. A sensing coil of 500 turns was wounded on the specimen, allowing the magnetic flux density determination.
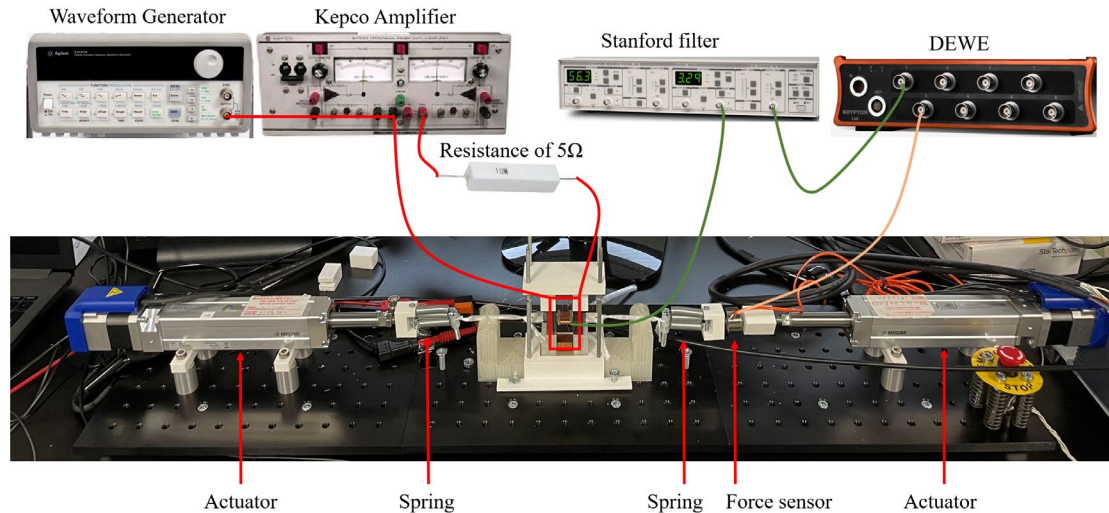
Fig. 1 Set up for the specimen characterization and measurement of Ericsson cycle under different tensile stresses

3. Discussion

The measured Ericsson cycles are presented in Fig.2. From these curves, the maximum harvestable energy in low magnetic field when the tensile stress changes were derived. The total energy available when applying a force of 20N (corresponding to 62MPa) reached 310µJ/cm^3. For Galfenol and Terfenol, the theoretical converted energy under the same conditions were in the range of 100µJ/cm^3.

From a system point of view, for an axial type energy harvester using Terfenol-D presented in [1], the estimated maximum value from the Ericsson cycle is 220 µJ/cycle/cm3, compared to the experimental result of 17µJ/cycle/cm3, with a bias magnetic excitation of 7.2kA/m and a mechanical preload of 6MPa.
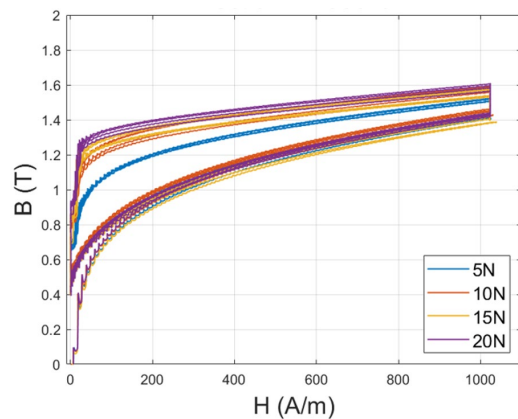
Fig. 2 Ericsson cycles under different tensile stress and magnetic field

These results showed that Metglas 2605SA1 has the potential to harvest more energy than Galfenol and Terfenol-D under low magnetic field conditions, compatible with the use of permanent magnet as magnetic source.

[1]   Zucca, M., Hadadian, A., & Bottauscio, O. (2015). Quantities affecting the behavior of vibrational magnetostrictive transducers. IEEE Transactions on Magnetics, 51(1). https://doi.org/10.1109/TMAG.2014.2359248

CALIBRATION OF AN *IN VIVO* BIOMECHANICAL CHARACTERISATION DEVICE FOR UNRUPTURED CEREBRAL ANEURYSMS: FIRST RESULTS ON POLYMERIC PHANTOM ARTERIES.

ELyT Global
Biomechanics – Cerebral aneurysms

G. Plet [a]	**J. Raviol** [a]	**H. Magoariec** [a]	**C. Pailler-Mattei**[a, b]

Affiliation

[a]*Laboratory of Tribology and Dynamics System, UMR CNRS 5513, Ecole Centrale de Lyon, France*

[b]*University of Lyon, University Claude Bernard Lyon 1, IPSB-Faculty of Pharmacy, France*

Abstract

Introduction

An intracranial aneurysm is an anatomical anomaly resulting from a residual and structural deformation of the wall of a cerebral artery. The estimated prevalence of unruptured intracranial aneurysm is 2-5 % in the world population [1]. Scores exist to assess the risk of rupture [2], but no quantitative information on the biomechanical state of the aneurysm wall is considered, a parameter that is yet predominant in the mechanisms of aneurysm rupture. In this context, we have developed an original device to measure *in vivo* the mechanical behaviour of the aneurysmal wall and predict the risk of rupture. This work deals with the calibration of the device on polymeric phantoms, which is the necessary stage before testing on animal model.

Materials and Methods

Three saccular intracranial aneurysms phantoms representing a bifurcation of the circle of Willis were 3D-printed by stereolitography. For calibration purpose, dimensions of the

phantoms were deliberately not biofidelic: the arteries have a diameter of 8 mm and a thickness of 600 μm, while the aneurysm has a diameter of 16 mm and a thickness of 400 μm. Concerning the mechanical stiffness, Young's modulus of phantoms is 1.57±0.13 MPa. The phantoms were fixed in a tank and a fluid flow of 500 ml/min was controlled using a pump as well as flowmeters at the artery inlet and at both outlets. The device, connected to a syringe pump, was then inserted into the aneurysm in order to stress the wall with physiological fluid at a flow rate between 0 and 150 ml/min. The aneurysmal domes were speckled in order to use a stereo-correlation system allowing the collection of the displacements as well as the strains generated by the experimental probe. Acquisitions of 45 s at 3 Hz (135 images) were recorded with a load of 6 s (18 images) at 150 ml/min in order to observe the maximum strains and displacements generated by the device in the pulsation area.

Results and Discussion

For the three samples, we consider the point of pulse impact on the aneurysm wall, and we compare the repeatability for the strain norms obtained. For the same aneurysm wall thickness and the same Young's modulus, the strains tensor norm are comparable and have been observed in Figure 1.
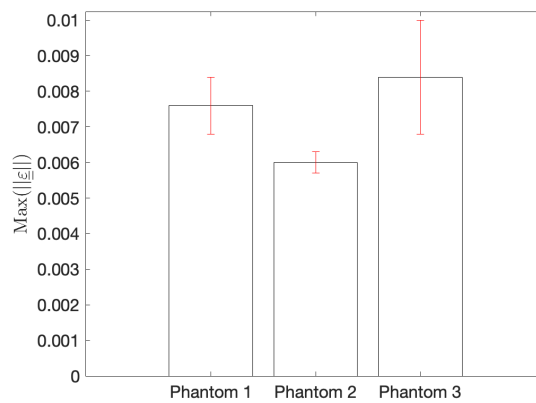
Figure 1: Strains tensor norm at the point of pulse impact on aneurysm wall on three printed polymeric phantoms.

Actually, for the Phantom 1, we obtained for the 6 s of pulsation a mean value of 0.0076±0.0008, for the Phantom 2 a mean value of 0.0060±0.0003 and for the Phantom 3 a mean value of 0.0084±0.0016.

References

1. RinkelGJ,DjibutiM,AlgraA,VanGijnJ.Prevalenceand risk of rupture of intracranial aneurysm: a systematic review. Stroke, 1998; 29:251-6.
2. Greving, J.P., Wermer, M.J.H., Brown, R.D., Morita, A., Juvela, S., Yonekura, M., Ishibashi, T., Torner, J.C., Nakayama, T., Rinkel, G.J.E., Algra, A., 2014. Development of the PHASES score for prediction of risk of rupture of intracranial aneurysms: a pooled analysis of six prospective cohort studies. The Lancet Neurology 13, 59–66.

Acknowledgements

Design of a polymeric cerebral aneurysm based on numerical modelling for the development of an aneurysm mechanical characterisation device

ELyT Global
Biomechanics - Cerebral aneurysms

J. Raviol [a]	**G. Plet** [a]	**H. Magoariec** [a]	**C. Pailler-Mattei**[a, b]

Affiliation

[a]*Laboratory of Tribology and Dynamics System, UMR CNRS 5513, Ecole Centrale de Lyon, France*

[b]*University of Lyon, University Claude Bernard Lyon 1, IPSB-Faculty of Pharmacy, France*

Abstract

Introduction

Intracranial aneurysms (ICA) are a structural and residual deformation of the arterial wall. The estimated prevalence of unruptured ICA is 2-5 % in the world population [1]. ICA rupture leading to subarachnoid haemorrhage has a fatality rate of 30-40 % [2]. None method currently exists to accurately predict the rupture risk. The aim of the MECANEV project is to quantify the in vivo mechanical behavior of unruptured ICA and provide a decision support tool to clinicians. This project encompasses the design of an experimental arterial wall deformation device and of a numerical tool to quantify the wall stress state by inverse analysis.

This device is a guidance flux system that has been calibrated on an experimental bench with a polymeric phantom artery. We present in this study the associated numerical model and its use to estimate the best ratio thickness/stiffness wall linked to the issues of 3D printing or moulding process in designing both thin and soft materials and evaluate the distance device/aneurysm wall effect.

Materials and Methods

The numerical model developed on COMSOL Multiphysics included solid mechanics elements considered as isotropic elastic linear or viscoelastic materials regarding the method considered (SLA 3D printing or injection moulding): the artificial phantom artery (reconstructed 3D geometry) and the deformation device (PTFE). 2 parameters were studied: the thicknesses of the aneurysm

wall and of the artery wall (600,1500 µm for the artery and 400 µm for the aneurysm,) with Young's modulus between 0.2-3 MPa. Several impact locations and several distances of the device to the wall (1-5 mm) were considered.

The model included 2 laminar flows: one for the static artery outer environment, and one for the miscible artery flow and device pulsed flow (water for both flows for calibration purposes). The associated flow rates were 500 mL/min and 150 mL/min respectively. The fluid-structure interaction (FSI) between the aneurysm arterial wall and the artery/device flow was computed using the arbitrary Lagrangian-Eulerian technique (ALE) and considering the loading of the fluid on the surface [3].

Results and discussion

The center of the impact location on the aneurysm wall was considered, the displacement and the strain tensor norms for the couples 600-400, 1500-400 μm were compared for all the Young's modulus between 0.2-3 MPa. For the same aneurysm area wall thickness and a same Young's modulus, the displacement norm was not comparable unlike the strain tensor norms differences which were between 2 % and 3 %. It has been observed for all the Young's modulus (figure 1).
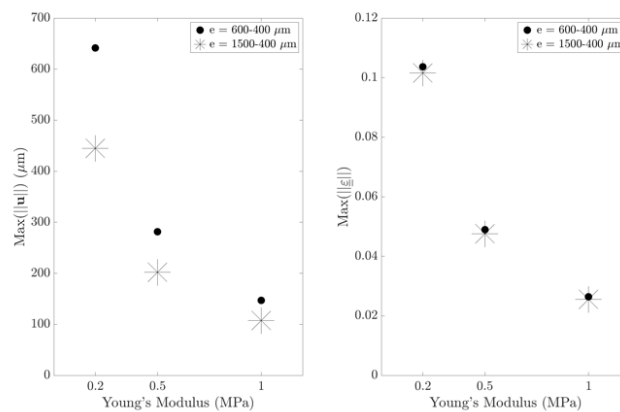
Figure 1 : Strain tensor and displacement norms int the center of the impact location on aneurysm wall for 600-400 μm and E between 0.2 and 1 MPa

It was possible to quantify the device position influence on the displacement and strain norms. As it was difficult to target a specific position in the experimental bench, a range of value regarding the position was valuable.

Conclusion

The developed numerical model was useful for the calibration phase of the device with support in (1) designing the phantom artery: for a strain study, it is important to target the appropriate aneurysm thickness but we have flexibility in other part of the artery and (2) quantifying the uncertainties of the experimental bench to help the further numerical/experimental comparisons.

Acknowledgements

References

1. Rinkel GJ, Djibuti M, Algra A, Van Gijn J. Prevalence and risk of rupture of intracranial aneurysm: a systematic review. Stroke, 1998; 29:251-6.
2. Van Gijn J, Kerr RS, Rinkel GJ. Subarachnoid haemorrhage. Lancet 2007; 369:306-318.
3. COMSOL, Models sme Fluid-structure interaction in a network of blood vessels.

Observation of Endothelial Cell Response to Various Stenting Deployment in an In-Vitro Flow System

ELyT Global
- **Theme: Engineering for Health**

Scientific Topic: Simulation & Modeling

Hanif Saifurrahman Institute of Fluid Science, Tohoku University, Japan Graduate School of Engineering, Tohoku University, Japan	**Zi Wang** Institute of Fluid Science, Tohoku University, Japan Graduate School of Biomedical Engineering, Tohoku University, Japan	**Yukiko Kojima** Institute of Fluid Science, Tohoku University, Japan Graduate School of Engineering, Tohoku University, Japan
Makoto Ohta Institute of Fluid Science, Tohoku University, Japan	**Hitomi Anzai** Institute of Fluid Science, Tohoku University, Japan	

Abstract

1. Introduction

Blood vessel stenosis is a phenomenon where a blood vessel's pathway narrows. The most famous type of stenosis is atherosclerosis, in which blood vessel is blocked by accumulation of fat. Atherosclerosis is also one of the precursors to ischemic heart disease (IHD), which will worsen to heart attack. In Japan themselves, IHD places third in terms of fatality rate compared to other diseases such as cancer[1].

One of the possible devices mainly used to treat such disease are stents[2]. However, in practice stent deployment in blood vessel also leads to a complication termed restenosis. Restenosis is theorized to be a phenomenon where Endothelial Cells (ECs) does not grow fast enough and the cells underneath endothelial cell layer (smooth muscle cell) invade the EC layer, causing the vessel's pathway to be blocked again. It was later discovered that stent deployment resulted in the alteration of flow environment, and the endothelial cells responds sensitively to the wall shear stress generated from the alteration. Thus, it is important to observe how stent designs affect endothelial cells.

There are many investigations revolving around stent development, stent design, and endothelial cell response to such development and design. However, there are little to no published studies which investigate the response of EC in a stent-applied blood vessel via in-vitro means. Hence, the research conducted by Ohta Laboratory intends to tackle this matter by exposing ECs to various stenting conditions in a parallel flow chamber.

2. Method

Firstly, ECs were cultured in a 35-mm petri dish for around six to ten days. Then, ECs were exposed with a laminar flow inside a flow system for 24 hours using an in-vitro system [3]. In this in-vitro system the ECs were exposed to various ranges of flow patterns. At the middle of the flow chamber a bare metal we added Nitinol bare metal stent wire to simulate stented vessels in this flow chamber. Additionally, other experimental setup involving placement of two struts and angled struts were also conducted. These were done to clarify ECs response between two stent gaps and angled struts respectively.

Then, since flow information such as shear stresses cannot be observed directly during in-vitro experiment, CFD was used to analyze the flow pattern and the correlated shear stress. The geometry of the flow area was made to resemble the flow chamber used in the experiment as close as possible, and the boundary condition was set so that the condition emulated was equal to that of the in-vitro flow system.

3. Result and Discussion

From the simulation, it could be seen that the existence of straight stent within the flow chamber causes alteration to the downstream part, creating low WSS-region at the recirculation zone and high-WSS region near the reattachment zone. This similar trend can also be seen when said stent are placed diagonally ($60°$ angular displacement) and when angled stent is deployed. When two stents are deployed instead, the flow between the two stents also shows similar trend where recirculation zone and reattachment zone were seen at the gap.

This flow pattern and the corresponding shear stress distribution turned out to affect the migration of ECs after 24-hours exposure to flow where the ECs seem to migrate to high-WSS region, causing their density distribution to resemble that of the shear stress distribution. Further investigation using the double strut, diagonal strut displacement, and angled strut also shows similar trend.

Thus, since it was already known how ECs respond to installment of stent in a laminar flow environment, in the future it is expected that the response of ECs under pulsatile flow could be investigated in-vitro as well.

4. Conclusion

It could be found based on simulation and in-vitro experiments that stent deployment causes flow property and shear stress distribution to change within a flow area, and that endothelial cells' distribution conforms to such change. Future prospective research includes research to see how endothelial cells response to pulsatile flow.

REFERENCES
[1] Vos, T., Lim, S. S., Abbafati, C., Abbas, K. M., Abbasi, M., Abbasifard, M., Abbasi- Kangevari, M., Abbastabar, H., Abd-Allah, F., Abdelalim, A., Abdollahi, M., Abdollahpour, I., Abolhassani, H., Aboyans, V., Abrams, E. M., Abreu, L. G., Abrigo, M. R., Abu-Raddad, L. J., Abushouk, A. I., … Murray, C. J. (2020). Global burden of 369 diseases and injuries in 204 countries and territories, 1990–2019: A systematic analysis for the global burden of disease study 2019. The Lancet, 396(10258), 1204–1222. https://doi.org/10.1016/s0140-6736(20)30925-9
[2] S. Borhani, S. Hassanajili, S. H. Ahmadi Tafti, and S. Rabbani, "Cardiovascular stents: overview, evolution, and next generation," Prog. Biomater., vol. 7, pp. 175–205, Sep. 2018, doi:10.1007/s40204-018-0097-y.
[3] H. Anzai et al., "Endothelial cell distributions and migration under conditions of flow shear stress around a stent wire," Technol. Health Care Off. J. Eur. Soc. Eng. Med., vol. 28, no. 4, pp. 345–354, 2020, doi: 10.3233/THC-191911.

Nd³⁺-doped 20Al(PO₃)₃-80LiF glass : a promising VUV scintillator material for high-counting-rate fast neutron detection

ELyT Global
Theme : Nano & Micro Scale Materials & Devices (M)
Scientific topic : Materials and structure design

Prof YOSHIKAWA Akira Research Laboratory on Advanced Crystal Engineering, Institute for Materials Research (IMR), Tohoku University, 2-1-1 Katahira, Aoba-ku, Sendai, 980-8577, JAPAN

Akihiro Yamaji

Prof. SARUKURA Nobuhiko Institute of Laser Engineering, (ILE) Osaka University, Yamadaoka 2-6, Suita City, Osaka 565-0871 JAPAN

Melvin Empizo, Yuki Minami, Kohei Yamanoi, Toshihiko Shimizu, Masashi Yoshimura

Prof. BOULON Georges Institut Lumière Matière (ILM) UMR 5306 Université Claude Bernard Lyon 1- CNRS, Campus Lyon Tech-La Doua 69622 Villeurbanne, FRANCE

Yannick Guyot

Faculty of Chemistry, University of Wroclaw, Wroclaw, POLAND
GUZIK Malgorzata

Abstract

Scintillators are luminescent materials that absorb the incident high-energy radiation and convert it into more accessible optical emissions. In particular, scintillators are the core sensing components that drive capabilities and impose limitations on radiation detectors. Research efforts are then geared towards the design and development of potential scintillator materials. For example, bulk single crystals are investigated for their scintillator applications due to their good quantum efficiencies. However, large-area and high-quality crystals that are required for most radiation detection applications are difficult to produce because of the restrictions by their crystal growth technologies including high production costs and slow

growth processes. We have subsequently developed the complex fluorophosphate glass, $20Al(PO_3)_3$-$80LiF$ (APLF) as a host material for rare earth ion-doped neutron scintillators. Similar to other known fluorophosphates, APLF contains aluminum metaphosphate $[Al(PO_3)_3]$ which is more stable to moisture than other metaphosphates. APLF glass also has a lithium (Li) content of 31.6 mmol cm^{-3} which is comparable to that of a commercial cerium-activated Li aluminosilicate glass scintillator, KG2 (36.0 mmol cm^{-3}). This high Li content is essential in enhancing the detector sensitivity to low-energy (270 keV) fast neutrons. We want to take advantage of the rare earth ions' electric-dipole allowed interconfigurational $4f^{n-1}5d \rightarrow 4f^n$ transitions which have fast emission decays from their $4f^{n-1}5d$ excited states. It should be remembered that electric dipole transitions are allowed when the initial and final states have opposite parity just like the case of both $4f^{n-1}5d$ and $4f^n$ configurations.

Among other available rare earth ion dopants, neodymium (Nd^{3+}) is a well-known optical activator of laser crystals for which the Nd^{3+} transitions are largely analyzed in the $4f^3$ configuration, which lies from the UV to the near-infrared (NIR) regions (200 nm to 1500 nm), but rarely in the $4f^2 5d$ configuration, which lies in the vacuum UV (VUV) region (170 nm to 200 nm). Although absorption and emission properties in the VUV region are always difficult to measure due to the spectral limit of many devices, several reports have already investigated the optical properties and fast $4f^2 5d \rightarrow 4f^3$ emission decays of Nd^{3+}-doped scintillator materials. However, most of these host crystals are not suitable for detecting 270 keV fast neutrons because they lack Li or have insufficient ^6Li content making them less sensitive to the neutrons.

The most important property of these glasses is that they exhibit electric-dipole allowed $4f25d \rightarrow 4f3$ ($4I9/2$) broadband emissions with a maximum at 187 nm (VUV) and a decay time of ~5.0 ns. Since these decay times are faster than known Nd^{3+}-doped scintillators as well as Pr^{3+} and Ce^{3+}-doped APLF glasses, the Nd^{3+}-doped APLF glass can be ranked as one of the advanced potential scintillator materials in time-of-flight (TOF) detectors for high-counting-rate fast neutron detection [1].

[1] Investigations on the electric-dipole allowed $4f^2 5d \rightarrow 4f^3$ broadband emission of Nd^{3+}-doped $20Al(PO_3)_3$-$80LiF$ glass for potential VUV scintillator application, Melvin Empizo & al, Journal of Alloys and Compounds, 856 (2021) 158096
https://doi.org/10.1016/j.jallcom.2020.158096

Thursday, November 17th

Morning

Wear and emissions of highly dissipative rubbing systems: how to learn from experiment?

ELyT Global
Transportation
Materials & Structure Design – Surfaces & Interfaces

Anne-Lise Cristol, Yannick Desplanques,

Edouard Davin, Alexandre Mège-Revil, Jean-François Brunel, Philippe Dufrénoy

University of Lille, CNRS, Centrale Lille, UMR 9013-LaMcube, Laboratoire de Mécanique Multiphysique Multiéchelle , Lille, France

Atomic structure of bulk metallic glasses investigated by transmission electron microscopy, synchrotron-radiation X-ray diffraction, scanning tunneling microscopy and ab-initio molecular dynamics simulation

ELyT Global
Theme (Metallic glasses)
Scientific topic (Atomic structure)

Add Picture	**Prof. D.V. Louzguine**

Abstract

The atomic structure of bulk metallic glasses studied by high-resolution transmission electron microscopy and by means of ultra high vacuum scanning tunneling microscopy (STM) will be presented. STM also acts as a spectroscopy giving a chance to resolve local chemistry. Direct atomic structure observation is supported by molecular dynamics (MD) simulation.

Structural changes in a relatively strong Zr-Cu-Ni-Al bulk glass-forming liquid alloy on cooling monitored in-situ by synchrotron radiation X-ray diffraction and supported by the results of first-principles MD simulation will also be shown. Chemical ordering forming extra Zr-(Cu,Ni), Zr-Al and Zr-Zr atomic pairs takes place in the Zr-Cu-Ni-Al supercooled liquid alloy on cooling towards the glass-transition temperature (T_g). Here the change in the ratio of Zr-(Cu,Ni) atomic peak area to other peaks area in the first coordination shell is smaller than that found in case of the Pd-Cu-Ni-P alloy (Cu,Ni-P to other peaks ratio) in accordance with a lower fragility index $m = d\log(\eta)/d(T_g/T)$ (where η is the viscosity) of the Zr-Cu-Ni-Al melt. Atomic redistribution between the first and second coordination shells is also observed.

These findings indicate that fragility is a sign of instability of short and medium range order in fragile liquids.

Skyrmion stabilization by geometric confinement and uniaxial strain

ELyT Global
Confinement of skyrmions
Skyrmion stabilization

Hiroshi Koibuchi

Affiliation

H.Koibuchi*, National Institute of Technology (KOSEN), Ibaraki College, Hitachinaka, Japan

Abstract

We numerically study geometric confinement (GC) of skyrmions and its effect on the stabilization [1,2]. Recent experiments reported that confined SKYs are stabilized in a multilayered nanodomain [3], and the confined SKYs in a nanodomain are further stabilized under the presence of tensile strains [4]. This stabilization mechanism by strains is closely related to GC, and this GC effect is expected to come from the so-called surface effects, which generally increase with reducing size. However, the origin of this GC effect is not always clear in the case of skyrmions. In this study, we compare the results of two different three-dimensional (3D) models, which are different in the definition of discrete energies corresponding to the ferromagnetic interaction (FMI) and Dzyaloshinskii-Moriya interaction (DMI). In one of the models, denoted by model 1, both FMI and DMI energies are defined on edges or bonds of tetrahedrons and almost uniformly distributed independent of the position of bonds. In the other model, denoted by model 2, FMI energy is defined on bonds of tetrahedrons, while DMI energy is zero on the boundary surfaces parallel to the magnetic field. From the numerical data, we find that SKY states are confined (not confined) inside the boundary in model 2 (model 1). Moreover, the confinened skyrmions are stabilized further by tensile strains parallel to the plate, and the skyrmion phase extends to the low-temperature region. This stabilization occurs due to the anisotropic DMI coupling constant induced by the tensile strain caused by lattice deformations. Our simulation data are qualitatively consistent with

experimentally observed and reported stabilization induced by tensile strains applied to the thin plate of the chiral magnet Cu2OSeO3 [5].
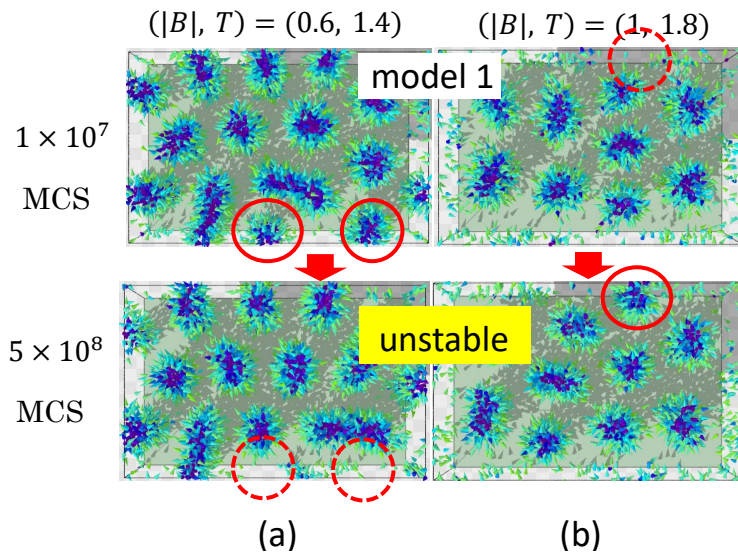
Fig.1 Non-confined skyrmions of model 1 at (a) $(|B|, T) = (0.6, 1.4)$ and (b) $(|B|, T) = (1, 1.8)$, where B and T are magnetic field and temperature. Snapshots on the upper (lower) row are obtained at 1×10^7 (5×10^8) Monte Carlo sweeps (MCS) . Skyrmions enclosed by red circles on disappear or emerge during sufficiently large MCS. This implies that non-confined skyrmions are unstable.

$(|B|, T) = (0.6, 1.4)$ $(|B|, T) = (1, 1.8)$

1×10^7 MCS

model 1

5×10^8 MCS

unstable

(a)   (b)

Fig.2 Confined skyrmions of model 2 at (a) $(|B|, T) = (0.6, 1.4)$ and (b) $(|B|, T) = (1, 1.8)$, where B and T are magnetic field and temperature. Snapshots on the upper (lower) row are obtained at 1×10^7 (5×10^8) MCS . Total number of skyrmions remains unchanged for sufficiently large MCS. This implies that confined skyrmions are stable.

$(|B|, T) = (0.6, 1.4)$ $(|B|, T) = (1, 1.8)$

1×10^7 MCS

model 2

5×10^8 MCS

stable

(a)   (b)
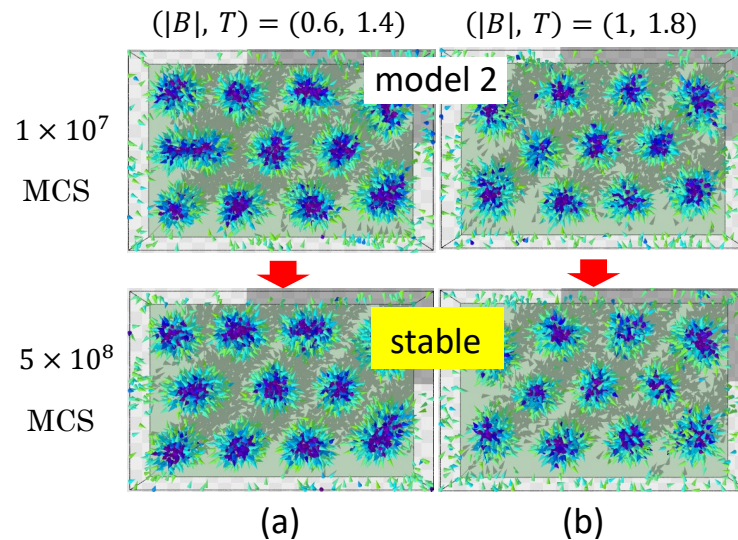
References
[1] H. Koibuchi, F. Kato, S. El Hog, G. Diguet, B. Ducharne, T. Uchimoto, H. T. Diep, Effect of Geometric Confinement on the Stabilization of Skyrmions, http://arxiv.org/abs/2208.03847.
[2] G. Diguet, B. Ducharne, S. El Hog, F. Kato, H. Koibuchi, T. Uchimoto, H. T. Diep, Monte Carlo studies of skyrmion stabilization under geometric confinement and uniaxial strain, http://arxiv.org/abs/2208.07527
[3] P. Ho, A. K.C. Tan, S. G., A.L. G. Oyarce, M. Raju, L.S. Huang, A. Soumyanarayanan, and C. Panagopoulos, Phys. Rev. Appl. 11, 024064, (2019), https://doi.org/10.1103/PhysRevApplied.11.024064.
[4] Y.Wang, L. Wang, J. Xia, Z. Lai, G. T. X. Zhang, Z. Hou, X. Gao, W. Mi, C. Feng, M. Zeng, G. Zhou, G. Yu, G. Wu, Y. Zhou, W. Wang, X.Zhang and J. Liu Nature Comm. 11, 3577 (2020), https://doi.org/10.1038/s41467-020-17354-7.
[5] S. Seki, Y. Okamura, K. Shibata, R. Takagi, N. D. Khanh, F. Kagawa, T. Arima, and Y. Tokura, Phys.Rev. B 96, 220404(R) (2017), https://doi.org/10.1103/PhysRevB.96.220404.

Evaluation of the thermal gradient of in-flight polymer particles during cold spray process

ELyT Global
Resilient polymeric cold spray coating
Particle thermal gradient

C. A. Bernard[1,2,3], H. Takana[4,5], G. Diguet[6], O. Lame[7], K. Ogawa[2,3], J.-Y. Cavaillé[3,5]

[1]*Frontier Research Institute for Interdisciplinary Sciences, Tohoku University, Sendai, Japan*
[2]*Fracture and Reliability Research Institute, Tohoku University, Sendai, Japan*
[3]*ELyTMax, UMI 3757, CNRS—Université de Lyon—Tohoku University International Joint Unit, Tohoku University, Sendai, Japan*
[4]*Institute of Fluid Science, Tohoku University, Sendai*
[5]*Lyon Center, IFS -Tohoku University, Université de Lyon, INSAVALOR, Villeurbanne, 69621, France*
[6]*Micro System Integration Center, Micro/Nano-Machining Research and Education Center, Tohoku University, Sendai, Japan*
[7]*Materials Engineering and Science (MateIS), CNRS, INSA-Lyon, UMR5510, Université de Lyon, Villeurbanne, France*

Abstract

Despite the unprecedented research progress on polymer coatings by cold spray process during the past few years, understanding the high-velocity impact behavior of polymer particles is still in its infancy. The difficulties lie in the knowledge of the high-strain rate deformation of polymer particles at the scale of the microstructure (crystalline lamellae and amorphous chains). Because of that, the influence of the incoming gas on the particle (acceleration and temperature) needs to be considered. If the particle velocity can be determined using a high-speed camera, it is more difficult to obtain the particle temperature experimentally [1], especially for polymers due to their low thermal conductivity.

To evaluate the particle temperature, a solution is to perform computational fluid dynamics (CFD) simulations. However, as particles are considered discrete phase, only an average temperature can be obtained. For a more accurate evaluation of the particle temperature during its flight, it is necessary to consider the particle volume. Our recent study [2] demonstrated the existence of a thermal gradient in micron-sized ultra-high molecular weight polyethylene (UHMPWE) particles.

In this study, a sophisticated model, including gas temperature, pressure, and relative velocity,

has been designed using COMSOL Multiphysics to evaluate the temperature distribution inside a particle. The obtained results show that a large thermal gradient is developed in the particle with a temperature difference reaching 50 K for a 60 μm diameter UHMWPE particle. Only 10 μm diameter particles, showing a negligible temperature difference, are susceptible to melt and clog the nozzle, making them unsuitable for spraying. Such temperature difference influences the mechanical properties of the particle during its flight and, therefore, its impact behavior. The understanding of the particle deformation process with considering the thermal gradient inside the particle and polymer behavior will be further investigated in a future study.

References

[1] A. Nastic, B. Jodoin, Evaluation of Heat Transfer Transport Coefficient for Cold Spray Through Computational Fluid Dynamics and Particle In-Flight Temperature Measurement Using a High-Speed IR Camera, Journal of Thermal Spray Technology. 27 (2018) 1491–1517.

[2] C. Bernard, H. Takana, G. Diguet, K. Ravi, O. Lame, K. Ogawa, J.-Y. Cavaillé, Thermal gradient of in-flight polymer particles during cold spraying, Journal of Materials Processing Technology. 286 (2020) 116805.

EDOT Polymerization in an Emulsion by Plasma Enveloped Bubble

ELyT Global
PEDOT Synthesis
Plasma Material Synthesis

Kazuhiko OTAKE[1,2], Gildas COATIVY[3], Sebastien LIVI[4], Laura COURTY[4], Florent DALMAS[5], Laurence SEVEYRAT[3], Veronique PERRIN[3], Jean Yves CAVAILLE[6], Hidemasa TAKANA[1,2]

[1] Lyon Center, IFS -Tohoku U., Université de Lyon, INSAVALOR, Villeurbanne, 69621, France.

[2] Inst Fluid Sci, Tohoku Univ, Aoba Ku, 2-1-1 Katahira, Sendai, Miyagi 9808577, Japan.

[3] Univ. Lyon, INSA-LYON, LGEF, EA682, F-69621 Villeurbanne, France.

[4] Univ Lyon, CNRS, UMR 5223, Ingénierie des Matériaux Polymères, Université Claude Bernard Lyon 1, INSA Lyon, Université Jean Monnet, F-69623 Villeurbanne Cédex, France.

[5] Univ Lyon, INSA Lyon, UCBL, CNRS, MATEIS, UMR5510, Villeurbanne 69621, France.

[6] ELyTMaX IRL3757, CNRS, Univ Lyon, INSA Lyon, Centrale Lyon, Université Claude Bernard Lyon 1, Tohoku University, Sendai, Japan.

Abstract

   Poly(3,4-ethylenedioxythiophene) (PEDOT) is known as one of the best conducting polymers due to its chemical stability and transparency [1]. PEDOT is already utilized in electronic devices as antistatic agents and transparent circuits, and it has been paid attention widely from industrial fields in these days. PEDOT is typically synthesized by chemical oxidation method and poly(styrenesulfonate) (PSS) is typically doped with PEDOT to enhance the solubility of PEDOT. However, PSS is an insulator and the doping of PSS is the main reason for the relatively low conductivity of the commercial PEDOT:PSS. In addition, the chemical oxidation method requires a cleaning step to take remained oxidation agents away, which makes the process more complicated.

   In this collaborative study, the innovative in-situ plasma polymerization process was

developed utilizing plasma enveloped bubbles. Plasma polymerization is a promising method for PEDOT synthesis without any dopants or oxidation agents. In the plasma polymerization, polymerization is initiated with the hydroxyl or oxygen radicals with high oxidation potential generated by discharge, therefore no agents will be remained in this process [2].

Several studies reported that discharging in small bubbles can be utilized as a process for decomposing persistent organic compounds [3]. The reactive radicals inside small bubbles can also be applied for polymerization of uniformly dispersed EDOT monomer in water (EDOT emulsion). By applying this plasma enveloped bubble technique for the polymerization, the PEDOT synthesis with high water dispersion can be expected without introducing any dopants.

The experimental setup in this study is shown in Figure 1. The reactor mainly consists of a rod electrode inside the plugged glass tube and a mesh electrode wrapped around the reactor. The plasma forming gas (Ar/O_2 mixture) is introduced into a glass tube and bubbles are ejected from the small holes on the glass tube. By applying the pulsed high voltage to the center rod with the mesh electrode grounded, the discharge insider the bubble is generated in the EDOT emulsion at the concentration of 0.3 w%.

Photographs of samples at different processing time are shown in Figure 2. Through this method with plasma enveloped bubble, the samples with high transparency and water dispersibility are successfully obtained. The conductivity of a film made of the processed PEDOT alone was improved with the processing time. In this study, the characteristics of processed samples were experimentally clarified and the effects of oxygen content, input power and processing time, etc. on the synthesized PEDOT properties will be further investigated.
References
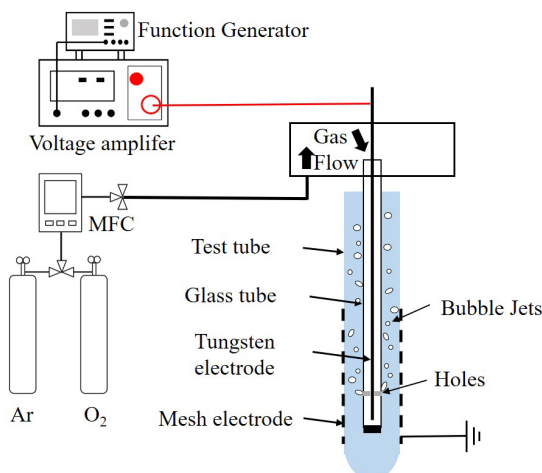
Figure 1 Schematic illustration of experimental setup.

0 min   10 min   20 min   30 min   40 min
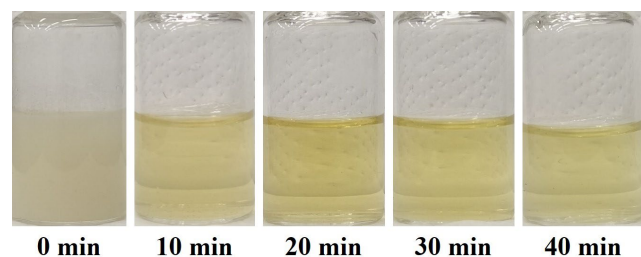
Figure 2 Photographs of samples for each processing time.

(1) Elschner, A., Kirchmeyer, S., et al., "PEDOT Principle and Applications of an Intrinsically Conductive Polymer", New York, CRC Press, (2011).
(2) Pistillo, B.R., Menguelti, K., et al., "One Step Deposition of PEDOT Films by Plasma Radicals Assisted Polymerization via Chemical Vapor Deposition", Journal of Materials Chemistry C, Vol. 4 (2016), pp. 5617-5625.
(3) Nishiyama, H., Takana, H., et al., "Characterization of DBD Multiple Bubble Jets for Methylene Blue Decolorization", Journal of Fluid Science and Technology, Vol. 8, No. 1 (2013), pp. 65-74.

ELyT Global

Electrochemical- and Gaseous Hydrogen Monitoring System for Thermodynamic Equilibrium State using Hydrogen-permeable Pd tubes

	Helmut Takahiro Uchida, Ph.D. [Göttingen U.], Associate Prof. [Tokai U.], Hiratsuka, JAPAN. *helmutuchida@tokai.ac.jp*		*Ayane Ibii, Master Course Student [Tokai U.], Hiratsuka, JAPAN,* *2cemm013@mail.u-tokai.ac.jp*
	Motoko Ishida, Master Course Student [Tokai U.], Hiratsuka, JAPAN, *1cemm004@mail.u-tokai.ac.jp*		*Makoto Ryo Harada, Ph.D. [Tokyo Institute of Technology], Research Fellow [Tokai U.], Research Fellow [AIST], Hiratsuka, JAPAN,* *MRHARADA@tsc.u-tokai.ac.jp*
	Yoshitake Nishi, Eng-Ph.D. (TU), Emeritus Prof. [Tokai U.], MIF-Director Project Researcher (KISTEC), Hiratsuka, JAPAN, west@tsc.u-tokai.ac.jp		

Abstract

Many previous studies have been reported on the reaction of palladium-hydrogen (Pd-H) binary systems using gas-phase hydrogen (H_2) and electrochemical methods ([1-5]). While palladium is expensive industrially and there are aspects that require alternative materials, academically it is one of the most representative reaction systems for understanding the thermodynamic model of metal-hydrogen systems (*i.e.* [6,7]).

Recently, in addition to energy storage using hydrogen from surplus electricity derived from renewable energy sources, energy storage methods have been diversified by utilizing existing infrastructure and technologies, such as reacting with CO_2 to produce methane (CH_4) gas [8] or with nitrogen (N_2) to produce ammonia (NH_3) gas, which is also focused on from the viewpoint of energy security. In solid-solution hydrogen storage metals, hydrogen (H) is dissolved interstitially in atomic state and becomes H_2 gas when released. In other words, there is a high potential to produce CH_4 and NH_3 more efficiently by using the material not only as a purification system for high-purity hydrogen, but also as a membrane reactor on the surface. In this reaction, thermodynamic knowledge as well as reaction kinetics is required to precisely control the hydrogen concentration in the metal.

In this study, we constructed a unique monitoring system based on hydrogen diffusion permeation using a tubular Pd cell, which can bridge both gas-based and electrochemical methods (Fig. 1), to monitor the state of solid solution hydrogen before and after phase transformation of palladium, both in terms of hydrogen gas partial pressure in the gas phase and EMF potential on the solution side. By controlling the temperature conditions, the thermodynamic absorption and desorption characteristics of palladium for hydrogen at each temperature were evaluated.

In the electrochemical monitoring side setup, a mixture of 85 wt.% aqueous H_3PO_4 solution and 85 wt.% Glycerin at a volume ratio of 1:2 [9,10] was used as the electrolyte solution, and a platinum foil (99.95 at.% purity) with an area of 5 cm × 5 cm was used as the counter electrode. An Ag/AgCl saturated electrode was used as the reference electrode, and a galvanostatic DC power supply (Hokuto Electric HA-151) was connected as the power supply. The gas phase side was constructed with a 1/4-inch SUS pipe, and the equilibrium hydrogen pressure inside was monitored by a capacitance manometer manufactured by Inficon Corporation., and the internal gas was evacuated several times before the hydrogen absorption and desorption experiments.

Stepwise electrochemical hydrogen introduction was applied to obtain equilibrium EMF values at each
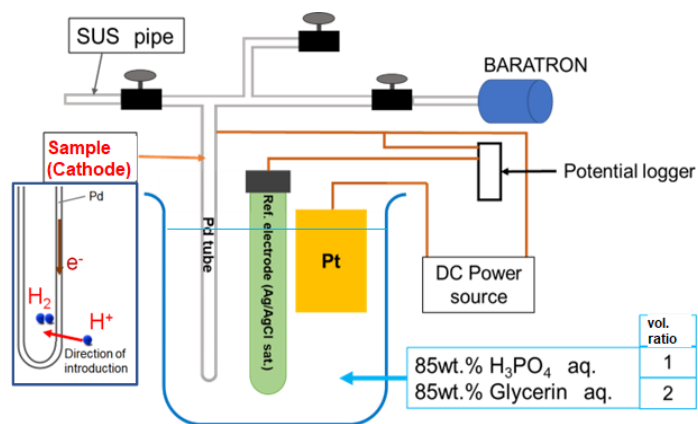
Fig.1 Schematic draw of controlled measurement system for electrochemical and gas-phase hydrogen absorption and desorption at room temperature measurement.
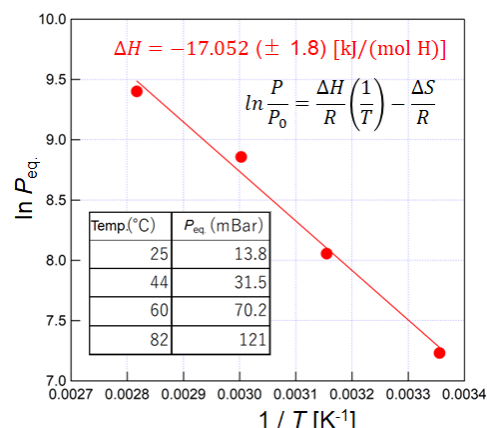

Fig.2 Temperature dependence of equilibrium hydrogen pressure obtained in the palladium hydride formation reaction direction (Van't Hoff plot)

hydrogen concentration c_H at room temperature. The hydrogen content in the samples during the step-by-step loading can be calculated by Faraday's law [11,12]. At each loading step, hydrogen atom produced at the sample surface diffuses in and the process is observed as a change of electromotorical force (EMF) until it equilibrates. The EMF value at equilibrium as a measure of the chemical potential of hydrogen is directly translated into hydrogen partial pressure p_{H2} by the Nernst equation [13,14].

$$p_{H_2} = p_0 \cdot \exp\left(\frac{(U - U_0)nF}{RT}\right)$$

Here, p_0 is the standard pressure of hydrogen, U is the measured EMF value, U_0 is the standard potential of reference electrode ($U_0 \approx 0.195$ V for the Ag/AgCl$_{sat}$ saturated electrode with 3M KCl solution at 298 K [15,16], calibrated to be 0.197 V for this work), n is the number of electrons related to the reaction ($n = 2$ for hydrogen), $F = 96500$ [C/mol]is the Faraday constant, R is the gas constant and T is absolute temperature.

With respect to the total amount of hydrogen loaded into the specimen was calculation by Faraday's law [12], assuming that all the hydrogen ions were loaded into the specimen.

The hydrogen concentration in palladium was evaluated from the hydrogen introduction conditions using Faraday's equation [12]. Furthermore, $\Delta H = -17.05 \pm 1.8$ kJ/mol H was obtained as the enthalpy of the two-phase plateau region of Pd-H in the temperature range 298-360 K. This value was comparable to many values reported in previous studies[17] and was confirmed with good reproducibility. In conclusion, we have successfully fabricated an evaluation system for direct observation of the amount of hydrogen introduced in the Pd-H reaction, both electrochemically and at gas pressure, and confirmed the reliability of the system. Furthermore, it was experimentally confirmed that the thermodynamic equation between equilibrium potential and equilibrium hydrogen pressure is valid for the reaction in the Pd-H system.

References:
[1] G. Alefeld *et al.*, "*Hydrogen in Metals I*", (1978), Springer-Verlag, ISBN: 9783540087052.
[2] G. Alefeld *et al.*, "*Hydrogen in Metals II*", (1978), Springer-Verlag, ISBN: 9780387088839.
[3] T. B. Flanagan and W.A. Oates, *Annu. Rev. Mater. Sci.*, **21**, (1991), 269-304.
[4] M. Devanathan and Z. Stachurski, *Proc. R. Soc. Lond. A*, **270**, (1962), 90-102.
[5] H. Frieske, E. Wicke, *Ber. Bunsenges. Physik. Chem.*, **77**, (1973), 48-52.
[6] R. Schwarz and A. Khachaturyan, *Acta Mater.*, **54**, (2006), 313-323.
[7] S. Wagner *et al.*, *Script. Mater*., **64**, (2011), 978-981.
[8] K. Sawahara *et al.*, *Int. J. Hydrogen Energy*, **47**, (2022), 19051-19061.
[9] H.T. Uchida, R. Kirchheim, and A. Pundt, *Script. Mater*., **64**, (2011), 935-937.
[10] R. Kirchheim and A. Pundt, "*Hydrogen in Metals*", Ch.25 in book: D.E. Laughlin and K. Hono (ed.), "*Physical Metallurgy, Fifth Edition: 3-Volume Set*", (2014), Elsevier, ISBN: 9780444537706
[11] H.T. Uchida *et al.*, *Acta Mater.*, **85**, (2015), 279-289.
[12] R. Kirchheim, *Prog. Mater. Sci.*, **32**, (1988), 261-325.
[13] P.W. Atkins and M.J. Clugston, "*Principles of physical chemistry*", (1982), Pitman Books.
[14] ASM Intl., "*Corrosion: ASM Metals Handbook, 9th ed. (Vol.13)*", (1987), Gulf Professional Publishing.
[15] P. Rieger, "*Electrochemistry - Second Edition*", (1993), Springer Verlag, p.32.
[16] E. Ghali, "*Corrosion Resistance of Aluminum and Magnesium Alloys: Understanding, Performance, and Testing*", (2010), Wiley, ISBN: 9780471715764.
[17] H. Frieske and E. Wicke, *Ber. Bunsenges. phys. Chem.*, **77**, (1973), 48-52.

Diffusion of Water in Epoxy Ionic Liquid Composite Polymer cured and its Effect on Dielectric and Mechanical Properties

ELyT Global

POMAD project

OLLIVIER-LAMARQUE Lucas, IFS – ELyTMaX UMI 3757

UCHIMOTO Tetsuya, IFS – ElyTMaX UMI 3757
MARY Nicolas, MATeIS UMR 5510
LIVI Sébastien, IMP@INSA UMR 5223

Abstract

Due to their high surface coverage, good adhesion to metal surfaces and their excellent corrosion resistance, epoxy thermosets are widely used as protective coatings. However, anticorrosion protection of these coatings can be improved against water uptake and can be tuned by changing the chemical nature of the curing agents.

In this work, a comparative study has been performed on the water uptake of an epoxy-amine based on bisphenol A diglycidyl ether (BADGE) cured with an aliphatic amine and the same epoxy initiated with a phosphonium ionic liquid (IL). Thus, the epoxy networks were immersed in saline water solution in a controlled temperature environment. Gravimetric and electric impedance measurements were carried out for a maximum of 3 months.

Tensile tests and dynamic mechanical analysis were carried out before and after the immersion to estimate the degradation of the polymer matrix. The variation of glass transition temperature is used as indicator of degradation.

Results were analyzed to assess the water diffusion coefficients and water saturation limits. Two models, the Brasher-Kingsbury and a novel mixing rule were applied on permittivity values. Results highlighted that epoxy-ionic liquid system are less sensitive to water uptake than conventional epoxy- amine network. Due to their higher hydrophobic properties the water saturation limit is more than four time less. Beside the analysis show that the mixing rule model proposed here is prone to estimate the water uptake with accuracy from electrical impedance measurements.

Mechanical measurements show the glass transition temperature is decreasing by 20ºC with the water uptake for conventional epoxy-amine network. In the case of epoxy-IL network, the glass transition temperature is not affected by the water uptake.

Thursday, November 17th

Afternoon

Flow Structure Extraction Related to the Noise Generation in A Subsonic Free Jet by Using Mode Decomposition Methods

ELyT Global
Aeroacoustics
Subsonic jet, CFD, data mining

Shota MORITA

D2 Student
Aerospace Fluid Engineering Lab.

IFS/Tohoku Univ. JAPAN

Aiko YAKENO, Ph. D.

Assistant Professor
Aerospace Fluid Engineering Lab.

IFS/Tohoku Univ. JAPAN

Christophe Bogey, Ph. D.

Directeur de Recherche CNRS
Laboratoire de Mécanique des Fluides et d'Acoustique

Ecole Centrale de Lyon, France

Shigeru OBAYASHI, Ph. D.

Professor
Aerospace Fluid Engineering Lab.

IFS/Tohoku Univ. JAPAN

Abstract
1. Intoroduction

The noise generated by the jet engine exhaust of jet airliners with about M = 0.9 is the main source of noise during takeoff and has been a major problem since the jet airliners has been in service in 1952. This noise is "vortex noise" caused by the unsteady motion of vortices due to turbulence in the jet [1], and is known to occur at the transition to turbulence in the jet (The end of the potential core). However, since the vortex sound is caused by complex motions of vortices of various scales, The mechanism of vortex structures leading to noise generation is still under discussion. As a fine explanation to this mechanism, a recent study proposed that pressure waves propagating upstream along the jet axis interact with Kelvin-Helmholtz (K-H) instability possibly forming a feedback loop that intensifies (Bogey, 2021) [2].

In this study, to verify whether feedback loop phenomena occur in subsonic free jets, Dynamic Mode Decomposition (DMD) [3], which is a kind of method that can extract specific periodic structures from flow data, and a method called Spatial-Temporal Fourier analysis are applied to the direct numerical results computed by Bogey [4].

2. Method

To clarify the flow structures around the trigger of the vortex generation, which is called the Kelvin Helmholtz instability, we first extract the flow structures near the jet exit by applying

DMD to time-series data of pressure fluctuation and selecting DMD mode (periodic characteristic structure) at a Strauhal number St_D corresponding to the frequency peaks including K-H instability identified by frequency analysis. Then, spatio-temporal Fourier analysis is performed on the extracted DMD modes to extract pressure waves propagating to upstream direction in the DMD modes, and how these waves affect the flow is discussed.

Regarding the data under study, these methods are applied to the sectional pressure time-series data (Fig.1) in the two-dimensional (x, z) plane at azimuthal angle $\theta = 0$ which have been recently obtained for a axisymmetric free jet of M = 0.9 and Re = 3125 by Dierect Numerical Simulation (DNS).

3. Result

As a result of the DMD, the DMD mode at the frequency which K-H instability was extracted and visualized (Fig.2). This frequency is also the dominant frequency peak near the nozzle exit. From Fig.2, we could see that this DMD mode describes not only the K-H instability wave propagated to the downstream on the shear layer but also pressure waves propagating upstream along the center axis. Based on this result, Spatial-temporal Fourier analysis is applied to the above DMD mode and extract the waves propagating upstream direction (Fig.3).From Fig.3, we confirmed that they originate from the end of the potential core. This result suggests that the acoustic waves generated at the end of the potential core are likely to be observed near the jet exit and induce K-H instability. Then, our results support the presence of a feedback mechanism in a subsonic free jet.

Fig.1 The instantaneous pressure field visualization result used in this study.	Fig.2 The DMD mode of St_D~0.47(K-H instability frequency) visualization result.

Fig.3 The Spatio-Temporal Fourier analysis result of DMD mode.
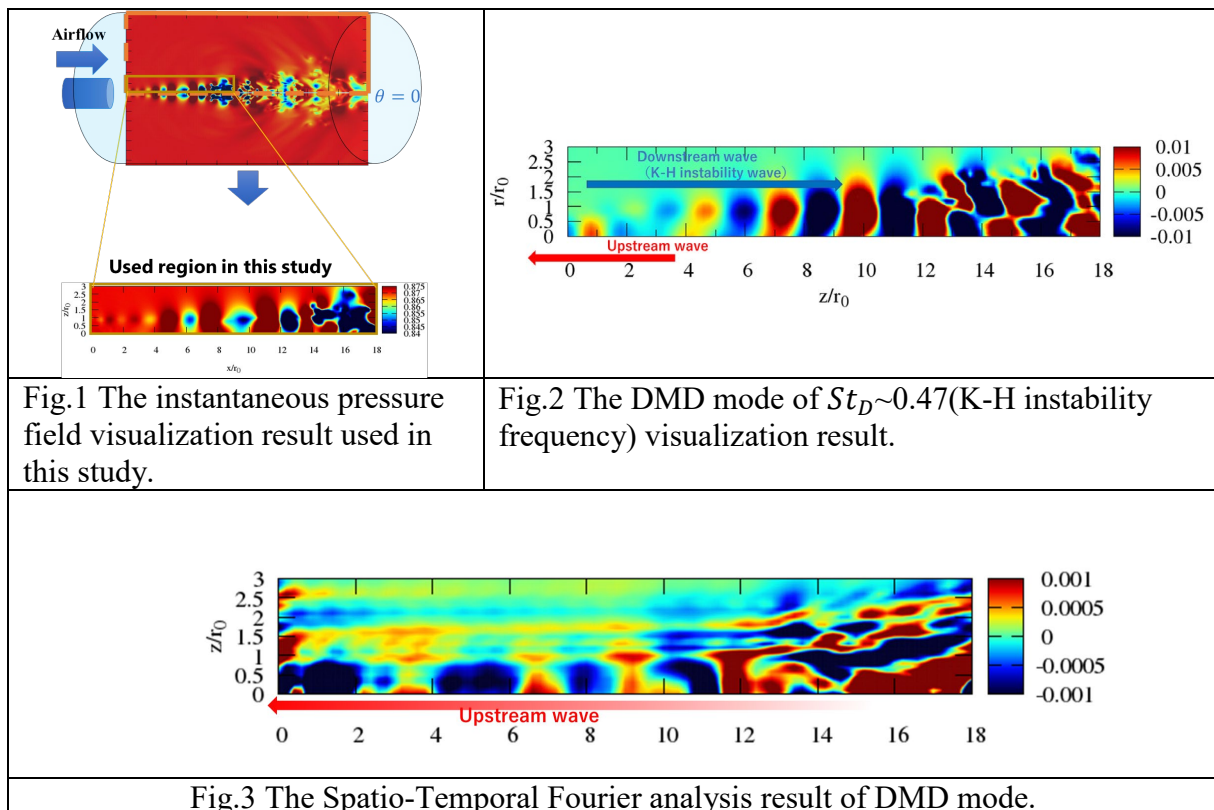
References

[1] Powell, Alan. "Theory of vortex sound." *The journal of the acoustical society of America* 36.1(177-195), 1964.
[2] Bogey, C. Acoustic tones in the near-nozzle region of jets: characteristics and variations between Mach numbers 0.5 and 2, J. Fluid Mech. (2021) 921: A3.
[3] P. Schmid, "Dynamic mode decomposition of numerical and experimental data", *Journal of Fluid Mechanics*, 656(5-28), 2010.
[4] C. Bogey, "Two-dimensional features of correlations in the flow and near pressure fields of Mach number 0.9 jets", AIAA SciTech Forum (2019-0806), 2019.

Sensitivity Analysis to Investigate the Secondary Structure from Atmospheric Shear Flow

ELyT Global

Ryoichi Yoshimura *D3 Student* *Aerospace Fluid Engineering Lab.* *IFS/Tohoku Univ. JAPAN*	*Aiko YAKENO, Ph. D.* *Assistant Professor* *Aerospace Fluid Engineering Lab.* *IFS/Tohoku Univ. JAPAN*
Benoît Pier, Ph. D. *Research Director* *Laboratoire de mécanique des fluides et d'acoustique (LMFA)* *Ecole Centrale de Lyon, France*	*Shigeru OBAYASHI, Ph. D.* *Professor* *Aerospace Fluid Engineering Lab.* *IFS/Tohoku Univ. JAPAN*

Abstract

1. Introduction

Atmospheric Turbulence in one of the causes of airborne accidents. Especially, turbulence, which appears without any clouds, is called CAT (Clear Air Turbulence) and known that CAT is caused by Kelvin-Helmholtz instability. Breaking of KH waves generates vortices that shake aircraft large. Secondary structures such as rib-structure and vortex-core instability are thought to be mainly responsible to the breaking of KH waves.

The secondary structures have been investigated in idealized conditions. Linear stability analysis and direct numerical simulation investigated what grow on KH waves [1-3]. However, almost no similar analyses have been done for vertical wind shears in the 3D atmosphere, which generally do not have ideal hyperbolic tangent profiles.

In addition, this study investigates the rib-structure, one of the secondary structures, using sensitivity analysis. Sensitivity analysis allows us to observe response of structures intrinsically unstable to given perturbation on the baseflow. We investigate characteristic of the secondary structures by performing the sensitivity analysis on KH waves (the baseflow) simulated by an atmospheric model. Additionally, we check if the results from the sensitivity

analysis correspond to findings obtained in the previous studies using traditional stability analysis methods.

2. Method

KH instability waves were simulated in the atmospheric field obtained by a weather simulation model and used the field as the baseflow. The baseflow perturbed with disturbance was time integrated in a Euler solver to see its response. We used rankine vortex-like disturbance that imitate rib-structure. The computational domain for the Eular solver is set so that its width is equivalent to 4 KH waves. The horizontal grid interval is 150 times smaller than the period of KH waves.

3. Results

As a result, the growth of rib-like vortices on the baseflow KH waves can be discussed using $\overline{w_i w_j S_{ij}}$. Figure 1 (left) shows that stretching of rib-like vortices as disturbance (gray, $\overline{w_i w_j S_{ij}}$) becomes large where the baseflow strain (red, S_{ij}) is large. The red region is called "braid", which is oblique region with large strain appearing between two KH vortices (Figure 1 right). In addition, $\overline{w_i w_j S_{ij}}$ also becomes large when the vorticity of the disturbance vortices is large (figures not shown). Therefore, the magnitude of the growth can be quantified by $\overline{w_i w_j S_{ij}}$. The results showing vortices growing in the region with large baseflow strain corresponds to the findings shown in the previous studies [1-3].
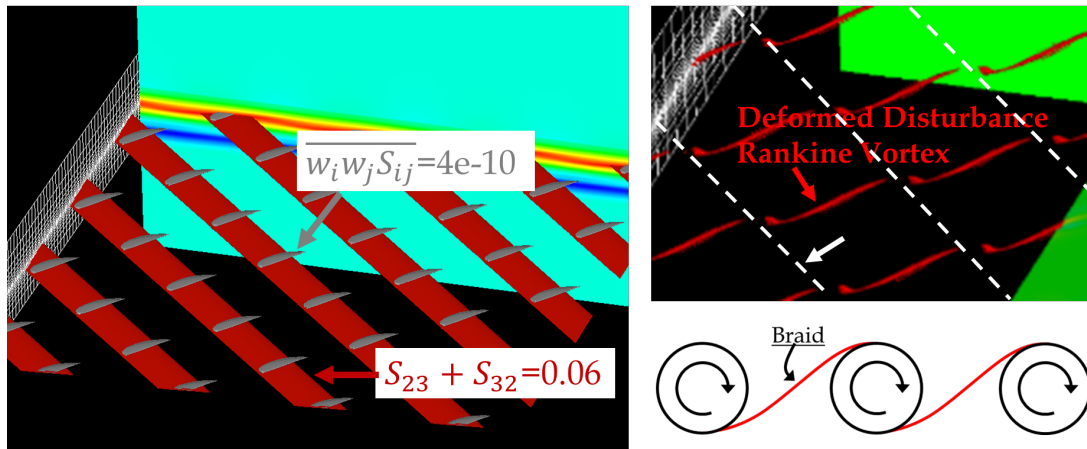
Figure 1 (left) Large baseflow strain ($S_{23} + S_{32}$) (red) and the region where vortex disturbance is stretched. (right top) Vortex disturbance converging into the shape of the braid. (right bottom) Illustration of braid.

References

[1] Pierrehumbert, R. T. & Widnall, S. E. (1982). The two- and three-dimensional instabilities of a spatially periodic shear layer. Journal of Fluid Mechanics 114, 59–82.
[2] Metcalfe, R., Orszag, S., Brachet, M., Menon, S., & Riley, J. (1987). Secondary instability of a temporally growing mixing layer. Journal of Fluid Mechanics, 184, 207-243.
[3] C.P. Caulfield and W.R. Peltier, (2000). The Anatomy of the Mixing Transition in Homogeneous and Stratified Free Shear Layers, J. Fluid Mech., 413, 1-47.

Superlubricity of a-C/Si$_3$N$_4$ contact in presence of castor oil

ELyT Global   Theme: T2 TRIBOCHEM

Momoji Kubo
IMR
Tohoku University
2-1-1 Katahira, Aoba-ku
Sendai 980-8577, Japan

Yang Wang
Research Institute of
Frontier Science,
Southwest Jiaotong
University, 610031,
Chengdu, China

Maria Isabel De Barros Bouchet
LTDS
Ecole Centrale de Lyon
69134, Ecully, France

Jean Michel Martin
LTDS
Ecole Centrale de
Lyon
69134, Ecully, France

Abstract

To meet the surging needs in energy efficiency and eco-friendly lubricants, a novel superlubricious technology using an unsaturated fatty acid and ceramic materials is proposed. By using amorphous carbon coatings with a selected fraction of sp^2 and sp^3 hybridized carbon in presence of a commercially available silicon nitride bulk ceramic, castor oil provides superlubricity although the liquid oil film in the contact is at the nanometer scale. (Figure 1) Local tribochemical reactions between contacting asperities are essential to maintain superlubricity at low speeds. High local pressure and shear activate chemical degradation of castor oil generating graphitic/graphenic-like species on top of asperities, thus helping both the chemical polishing of surface and its chemical passivation by H and/or OH species. For the first time, formation of alkane and alkene surface oligomers have been evidenced to play a major role in the friction reduction in the superlow regime (Figure 2). Computer simulation unveils that formation of chemical degradation products of castor oil on friction surfaces are favored by the quantity of sp^2-hybridized carbon atoms in the amorphous carbon structure. Moreover, short alkene chains are found to terminate the tribofilm on Si$_3$N$_4$ (Figure 2). Hence, tuning sp^2-carbon content in hydrogen-free amorphous carbon, in particular, on the top layers of the coating, provides an alternative way to control superlubricity achieved with unsaturated fatty acids.

Results
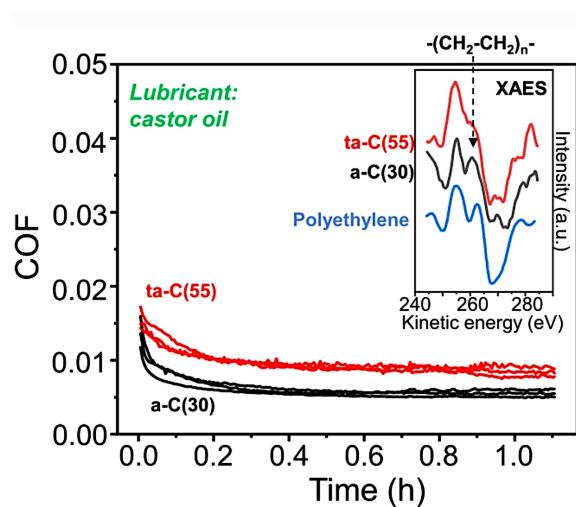
Figure 1 shows the evolution of friction coefficient against time for two a-C/Si$_3$N$_4$ tribopairs. It is shown that a-C (hardness 30 GPa) gives better results than ta-C (55 GPa). Figure 1 also shows Auger analyses (XAES technique) performed at the C KLL transition inside wear scar. The presence of alkanes and alkenes oligomers at the extreme surface is clearly evidenced by comparison with polyethylene (PE) as well as more sp2 carbon inside the wear scar (D parameter, not shown here).
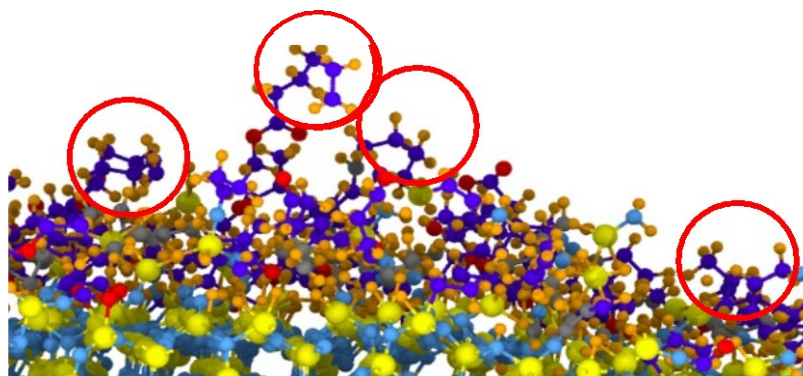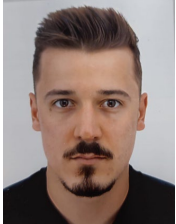
Figure 2 shows computer simulation results of tribochemical reactions between a-C and Si$_3$N$_4$ nano asperities in presence of ricinoleic acid (a selected degradation product of castor oil). The formation of alkane/alkene chains is well visible inside red circles.

To conclude, we show here that superlubricity of a-C/Si$_3$N$_4$ contact in presence of castor oil is attributed to a novel mechanism featuring the role of ricinoleic acid molecules in generating top surface oligomerization.

[1] Y. Long, Y. Wang *et al.* ***Friction* (2022).** https://doi.org/10.1007/s40544-022-0601-1

Multi-scale elucidation of friction mechanisms in ice-rubber interfaces

ELyT Global
**Theme (Transportation)
Scientific topic (Surfaces & Interfaces)**
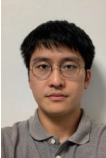
| | **PhD Student**

Anderson DALAVALE KAISER PINTO | | **CNRS Director of Research LTDS**

Juliette Cayer-Barrioz | | **Prof ECL**

Denis Mazuyer |

Abstract

In the context of improving icy road safety, this work aims at analyzing and understanding the interfacial friction response of an ice-rubber contact, in a large range of environmental temperature, going down to -20°C and sliding velocity, ranging from 50µm/s to 1m/s. The material properties of the rubber samples provided by Michelin varied in terms of composition (presence or not of carbon black), surface texturing (smooth, intermediate and rough), elastic modulus and the glassy temperature transition. In-situ contact area measurement was developed during sliding experiments and also during loading and unloading, allowing to identify the relative influence of adhesion and viscoelastic contributions. Sliding experiments, with the rubber sample kept still/block and the ice disc put in rotation, were performed. As the temperature was set close to 0°C, presence of water was identified during the experiment and it increased as time progressed and speed increased, due to the local heating. At lower temperature, the bell-shape friction-velocity curve was obtained, confirming previous work [1]. However, the curve shape was impacted by the increase of the environment temperature to values close to the melting point. A simple analytical model of friction, where adhesion-viscoelasticity and thermal dissipation are both integrated as multiplicative contributions [1], allowed us to discuss the friction mechanisms.

[1] S. Hemette. Rubber-Ice Friction: A multi-scale and multi-physical approach. PhD thesis, 2019

Introduction of Synthetic Artery Data
ELyT Global
Engineering for Health
Simulation & Modeling

	Kazuyoshi Jin Graduate School of Biomedical Engineering, Tohoku Univerisity	Keiichiro Shiraishi Graduate School of Biomedical Engineering, Tohoku Univerisity	Ko Kitamura Graduate School of Biomedical Engineering, Tohoku Univeristy	Prof. Shunji Mugikura Tohoku University Hospital
Prof. Naoko Mori Tohoku University Hospital	Prof. Makoto Ohta Insitute of Fluid Science, Tohoku University	Prof. Hitomi Anzai Insitute of Fluid Science, Tohoku University	

Abstract

1. Background

Collecting large amounts of data for vascular disease is the essential requirement for Healthcare AI. Synthetic data generation is one of the solution, however the synthetic data frequently generated "unrealistic" shape. Recently, statistical shape model (SSM) has attracted attention for generating synthetic data of patient. As a major strategy in SSM, synthetic geometry was generated based on principal component analysis (PCA) of real patient. However, the conventional PCA-SSMs have difficulty in maintaining the continuity of the geometry and controlling the geometrical parameters [1,2]. For these reasons, conventional PCA-SSMs are difficult to be applied to the complex artery shapes and to reproduce individual differences. In this study, we introduce two new SSM strategy: The use of relative coordinate vector and the use of multivariate normal distribution (MVND). These methods aim to create SSMs with natural shapes, continuity of arteries, and reproductivity of individual differences.

2. Material & Method
2.1 Relative Coordinates Method

The first approach introduces a relative representation of the centerline coordinate to emphasize the continuity of the arterial geometry. 3D shape of aorta was reconstructed from CT images data of five patients on The Cancer Imaging Archive [3], and the centerline position and radius of each point was extracted. To unify the number of points in the centerline among patients, aorta part was uniformly resampled into 30 points. Then, the points of centerline was expressed in a new relative coordinate. Our new relative coordinates use a vector from the previous point to next point as the coordinate value. To investigate the change in continuity due to the use of relative coordinates, the angle between the front and back points was calculated.

The mean angle and standard deviation (SD) were compared for the synthetic aorta using conventional absolute coordinates and the synthetic aorta using our new relative coordinates.

2.2 MVND method

The second approach to maintain the continuity of artery geometry is to introduce the correlation between centerline points. The position and diameter of the centerline of basilar artery (BA) was extracted from the head MRA data of 46 patients. The centerline was divided evenly; the number of landmark points was set from 3 to 30. Assuming the position of the landmark points (x,y,z) and the corresponding inner diameters (d) follows MVND, the covariance matrix was calculated from (x,y,z,d) of 46 patients. Next, landmark point groups and corresponding inner diameters were generated for 100 patients according to MVND equation calculated from the covariance matrix. B-spline interpolation was performed with landmark point groups. Finally, the distributions of geometric features of the synthetic artery dataset were compared with those of real patient dataset.

3. Results & Discussion
3.1 Relative Coordinates Method

The mean and SD of the angle between each point and the front and back points was 2.42±0.49 [rad] in absolute SSM and 2.73±0.16 [rad] in relative coordinate. The value of the SD indicates that the absolute coordinate SSM has a larger angle variation. This suggest that using the relative coordinates prevents the continuity of the model and represent a smooth shape closer to actual arteries.

3.2 MVND method

The generated shapes show a natural running of arteries. Moreover, the distributions of length, tortuosity, and curvature of the synthetic artery dataset generally agreed to those of the real patient database. However, when the number of landmark points is small, the BA curvature distribution of the synthetic artery dataset did not fit that of the real artery database. Therefore, synthetic artery dataset using MVND may represent the real dataset with the complexity of cerebral arteries' bent if enough landmark points number are selected.

4. Conclusion

To overcome the limitation of geoemtric discontinuity in conventional PCA-SSM, we proposed two new SSM approaches, relative coordinate method and MVND method. Two methods enable to preserve the continuity of the model and to create a smooth shape closer to actual aorta and BA, respectively. And MVND method could generate the similar distributions of the geometric features in synthetic geometry compared to those in the real artery dataset. These results suggests that our two approach works to improve the smoothness of shape. And MVND works to reproduce the distribution of geometric features similar to that of real artery. By using our SSM approaches as training data for deep learning, it is expected that the accuracy of prediction using deep learning for Healthcare AI will be improved.

5. Acknowledgement
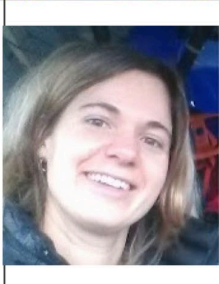
6. References
[1] L.Liang., et al., Biomech Model Mechanobiol.16(5):1519–1533. 2018.
[2] B. Thamsen., et al., IEEE TRANS MED IMG. 40:5. 2021.
[3] Clark K. et al., J Dig Img. 26(6):1045-1057. 2013

Blood flow simulations in cerebrovascular models from BraVa database

ELyT Global
Medical Applications Simulation

D.D. student Yutaro KOHATA *1,2,3	Assistant Prof. Hitomi ANZAI *1	Prof. Makoto OHTA *1,4
D.D. student Méghane DECROOCQ *1,2,3,4	Associate Prof. Carole FRINDEL *1,3	

Affiliation:
1. Institute of Fluid Science, Tohoku University
2. Graduate School of Biomedical Engineering, Tohoku University
3. CREATIS, INSA Lyon
4. ELyTMax UMI3757

Abstract

Introduction

Cerebrovascular abnormalities contribute to the pathophysiology of several neurological conditions (1). Some patients show a lack of arteries in the circle of Willis (CoW), the primary collateral blood flow pathway between the anterior and posterior circulations of the brain (2), and which leads lacks of blood flow communication. Tanaka et al. investigated 125 healthy volunteers with magnetic resonance (MR) imaging, classified the variations of CoW vasculatures into three types (complete CoW, or being lack of one anterior or posterior artery either at right or left), and also reported the differences in the flow conditions at the input vessels (internal carotid and basilar arteries) between CoW vascular types (3). However, quantitative flow conditions by MR imaging measurements were limited in spatial and temporal

resolution. Cerebrovascular hemodynamics with CoW variations and in higher resolution were still not available.

Gaidzik et al. exhibited CoW hemodynamics in high resolution for one case using a CFD simulation. Based on his knowledge, cerebrovascular hemodynamics with CoW variations and in higher resolution can be achieved using CFD simulation.

Therefore, the purpose of our study is to demonstrate the variations in cerebrovascular hemodynamics with CoW and in higher resolution using CFD simulations.

Method

The vascular models were referred form from an open database, the Brain Vasculature (BraVa) database (5) which contains centerlines of the vessels. The 3D vascular models for CFD simulations were reconstructed from the vascular centerlines of BraVa database using a reconstruction method from Decroocq *et al.* (5). The reconstruction method not only provide volume meshes but also able to edit the cerebrovascular models, such as cutting off one communicating artery, so that we can prepare the models with anatomical variations.

CFD simulations were performed on the volume meshes using a CFD software, ANSYS CFX. The flow conditions at the model boundaries (boundary conditions; BC) were referred from Tanaka *et al.* and applied as volume flow rate condition.

The results of CFD simulations were analyzed with respect to vascular variations and hemodynamics. The vascular variations were investigated in terms of both geometrical and topological characteristic, then their effect on hemodynamics were analyzed by comparing with the hemodynamics in the other models.

Acknowledgements

References

1. Fan JL, Nogueira RC, Brassard P, Rickards CA, Page M, Nasr N, et al. Integrative physiological assessment of cerebral hemodynamics and metabolism in acute ischemic stroke. J Cereb Blood Flow Metab. 2022 Mar;42(3):454–70.
2. Lee MKW. MORPHOLOGY OF CEREBRAL ARTERIES. Pharmacol Ther. 1995;66:149–73.
3. Tanaka H, Fujita N, Enoki T, Matsumoto K, Watanabe Y, Murase K, et al. Relationship between Variations in the Circle of Willis and Flow Rates in Internal Carotid and Basilar Arteries Determined by Means of Magnetic Resonance Imaging with Semiautomated Lumen Segmentation: Reference Data from 125 Healthy Volunteers. 2006;
4. Li Y, Anzai H, Nakayama T, Shimizu Y, Miura Y, Qiao A, et al. Simulation of hemodynamics in artery with aneurysm and stenosis with different geometric configuration. Journal of Biomechanical Science and Engineering. 2014;9(1).
5. Decroocq M, Frindel C, Ohta M, Lavoué G. Modeling and hexahedral meshing of arterial networks from centerlines [Internet]. arXiv; 2022 [cited 2022 Oct 3]. Available from: http://arxiv.org/abs/2201.08279

Robust shape optimization of a disc-brake system under dynamical criterion

ELyT Global
Project ELyT lab : R7 – Robust Multi Objective optimization design approaches

Koji SHIMOYAMA[1]

Frédéric GILLOT[2]

Achille JACQUEMOND[2]

Sébastien BESSET[2]

[1]*Tohoku University, IFS*

[2]*Ecole Centrale de Lyon, LTDS DySCo Team*

Abstract

Framework of our collaborative research studies concerns robust shape optimization of structures and systems under extremes conditions. Load involves in such conditions usually leads to non-linear behavior of structures, making figure of merits computationally costly and without accessible derivatives.

As an applicative example, we are working since 5 years on a disc-pad system exhibiting vibro-acoustic properties arising from friction-induced vibration, commonly known as squeal noise. The complex nature of the problem demands an efficient optimization strategy considering the computation cost.

This problem is addressed through defining the expensive evaluation of the Stability criteria (representing the magnitude of the squeal noise) with the meta-model and using the Efficient Global Optimization (EGO) search algorithms. The multi-objective definition of the optimization results in pareto-optimal solutions obtained through genetic algorithm for the considered shape parameters.

1. Context

The brake squeal noise is considered to be a very challenging problem since there is no stand-alone mechanism to explain the behavior, though there are many mechanisms which explains in their own respective sense. This makes it hard to define a criteria for the squeal noise to be considered for optimization. But one of the methods which has proven to be efficient is complex eigenvalue analysis which gives a measure of instability. Combined with an isogeometric formulation of the system, an EGO scheme is set-up to generate pareto-optimal solutions in an effective yet realistic computational time. Such generation is made possible with a dedicated algorithm

2. Achieved results

The deterministic optimization loop has been addressed during Pradeep Mohanasundaram Ph.D. as a double diploma student (ECL / TU – 2017-2021). Results have been published [1,2,3] and his work is now a strong basis for the starting Ph.D. of Achille Jacquemond, since October 2021. We are now focusing on uncertainties quantifications within the optimization loop, and preliminary results have been presented in an international conference (WCCM 2022, Yokohama, Japan). Achille has stayed three months within Pr. Shimoyama Lab. Under a JSPS Summer Grant (June-August 2022) to develop a noisy Kriging for robustness criteria building.
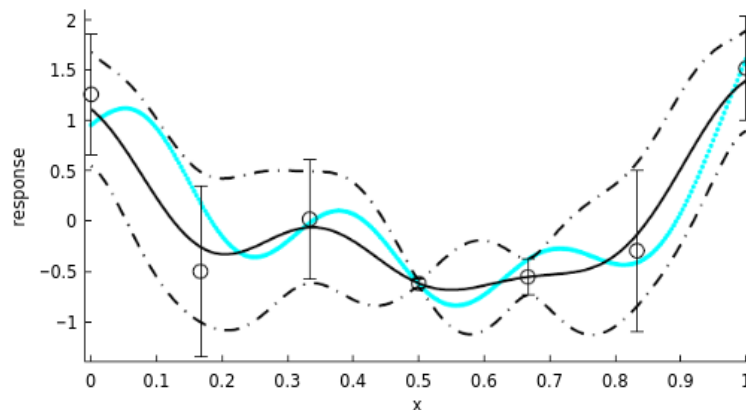
Figure 1: Example of Noisy Kriging, real function in green, observations and their standard deviation in circle, mean in black and 2 sigma interval in dotted line [4]

References :

[1] Mohanasundaram, P., Gillot, F., Besset, S., Shimoyama, K., *Modelling friction-induced dynamic instability dedicated for Isogeometric formulation,* Shock and Vibration, Accepted, 2022
[2] Mohanasundaram, P., Gillot, F., Besset, S., Shimoyama, K., *Multi-references acquisition strategy for shape optimization of disc-pad-like mechanical systems,* Structural and Multidisciplinary Optimization, Volume 64 Issue 4 Oct 2021 pp 1863–1885 https://doi.org/10.1007/s00158-021-02947-7
[3] Mohanasundaram, P., Gillot, F., Shimoyama, K., Besset, S., *Shape optimization of a disc-pad system under squeal noise criteria.* *SN Appl. Sci.* **2,** 547 (2020). https://doi.org/10.1007/s42452-020-2175-8
[4] Picheny, V., Wagner, T. & Ginsbourger, D. A benchmark of kriging-based infill criteria for noisy optimization. Struct Multidisc Optim 48, 607–626 (2013). https://doi.org/10.1007/s00158-013-0919-4

Friday, November 18th

Afternoon

Recent advances in the study of magnetorheological elastomers (MREs)

ELyT Global
**Energy – Engineering for Health
Materials & Structure Design – Simulation & Modeling**

Prof. Kostas Danas	Prof. Laurence Bodelot
Dr. Dipayan Mukherjee	Dr. Matthias Rambausek

Abstract

Most current magnetorheological elastomers (MREs) are broadly categorized into hard(h-MREs) and soft(s-MREs) [1] depending on the magnetic properties of the underlying particles. The former consist of particles exhibiting strong magnetic dissipation (e.g., NdFeB), while the later are purely energetic (e.g., carbonyl iron). In this work, we present a unified modeling framework for h-MREs [2] including the response of the s−MREs as a limiting case when the dissipation is set to zero. In addition, the proposed framework is dual in the sense of a partial Legendre-Fenchel transform of the magnetic part, i.e., we propose exactly equivalent models in the F−H and F−B variable spaces. Specifically, the models are capable of modeling the magnetic and the induced mechanical dissipation in the h-MREs, resulting from the ferromagnetic hysteresis of the underlying particles. In the limit of vanishingly small magnetic coercivity, both models yield a purely energetic response relevant for the s−MREs. The proposed dual models mostly involve the matrix and the particle material parameters except the particle volume fraction of the composite and a coupling coefficient, which is obtained via calibration with available full-field numerical homogenization estimates. Efficient finite element, numerical solutions for various boundary value problems (BVPs) involving h- and s-MREs are obtained via incremental variational principles. The calculations for the end-tip deflection of a uniformly pre-magnetized cantilever exhibit excellent agreement with the experimental data. The investigations on the remanent fields and the magnetic actuation performance of

hybrid h-/s-MRE rank-1 laminated cantilevers and non-uniformly pre-magnetized, functionally graded beams are also carried out. The analysis shows that the profiling of the h-MRE beams plays a crucial role in their deflection patterns and magnitudes depending on the actuation field direction. Moreover, the analysis reveals that concentrating the hard-magnetic particles near the beam flanks reduces the actuation field considerably without altering substantially the deflection patterns.

References

[1] Mukherjee, D., Bodelot, L., Danas, K. (2020). Microstructurally-guided explicit continuum models for isotropic magnetorheological elastomers with iron particles, Int. J. Non-Linear Mechanics, 120, 103380.

[2] Mukherjee, D., Rambausek, M., Danas K. (2021). An explicit dissipative model for isotropic hard magnetorheological elastomers, J. Mech. Phys. Solids, 151, 104361.

Material design for corrosion and stress corrosion cracking management in nuclear applications

ELyT Global
Energy
Materials & Structure design

Surfaces & Interfaces

H. Abe[1]
T. Miyazaki[1]
Y. Watanabe[1,2]

B. Ter-Ovanessian[3]
N. Mary[3]
B. Normand[3]
K. Jaffre[2,3]

**Affiliation**

[1] _Graduate School of Engineering, Tohoku University, 6-6-01-2 Aoba, Aramaki, Aoba-Ku, Sendai, Japan_
[2] _ELyTMaX UMI 3757, CNRS–Université de Lyon–Tohoku University, International Joint Unit, Sendai, Japan_
[3] _Université de Lyon, INSA-Lyon-UCBL-CNRS, UMR CNRS 5510 MATEIS, Villeurbanne Cedex, France_

Abstract
1. Introduction

One of the major problems of the nuclear industry is the management of the sustainability and safety of installations. Recently, in France, corrosion problems have been detected in several nuclear power plants, resulting in longer maintenance times. This recent news illustrates the need for understanding, prevention and mitigation of corrosion and stress corrosion cracking (SCC). The latter generally results from detrimental synergistic effects, activated between the material metallurgy, the environment and mechanical stresses. For nuclear power plant, this phenomenon could be severe due to specific conditions: high temperature, high pressure and irradiation.

Within the framework of ElytLab and ElytGlobal, several collaborative projects between INSA and Tohoku University have been carried in order to identify the discriminating factors regarding the material (chemical composition, microstructure, residual strains or stresses) leading to a reduction of the SCC risks. At least, two ways were investigated the optimization of the Cr content in Ni-based alloys (double diploma Ph'D F. Hamdani, 2011-2015) [1-2] and the effect of surface machining (double diploma Ph'D K. Jaffré, 2017-2021) [3-5].

2. Striking Results

The main goals of the Ph'D of F. Hamdani were to investigate: i) the influence of chromium content, ii) impact of iron addition on the corrosion and oxidation resistance of Ni-based alloys in primary water and superheated steam at 700°C (future applications). For this purpose, Ni-xCr ($14 \leq x \leq 30$ wt.%), Ni-xCr-8Fe (x=14,22 and 30 wt.%) model alloys and industrial material Alloy600 have been studied.

Various experimental technics were used to establish a relationship between alloying elements and physical properties of the oxide layers and oxidation kinetics. To uncouple the effect of surface cold-work and the chemical composition of the base metal, mirror and electropolishing were carried out. In primary water, critical chromium content of 20 wt.%, which corresponds to the minimum amount of chromium required to the transition from non-protective to protective and compact Cr-oxide layer, is determined. In superheated steam, oxidation kinetics and oxide scale characteristics showed the existence of optimum chromium content around 24 wt.%. In both cases, corrosion and oxidation resistance is degraded as chromium content was increased more than optimal amount. Iron addition (8 wt.%) had a detrimental effect on the protectiveness of the resulting oxide scales. This work also showed that even slight cold work introduced with fine emery finish has significant impact on oxidation properties and cracking susceptibility of Ni base alloys in superheated steam.

The latter finding motivated the work of K. Jaffré who studied the effect of surface finishing process on the corrosion behaviour of 304L Stainless Steel (SS). This work was also triggered by the need to understand the impact of some of the maintenance and repair procedures. The main objectives of this project were: (i) to establish the correlation between surface modifications (macroscopic defects, roughness, residual stresses, chemical, and microstructural alterations) and the properties of passive films (room temperature); (ii) to understand how these modifications affect the properties of oxides at high-temperature water (BWR, PWR). To highlight the influence of surface finishing process used in maintenance, the corrosion and oxidation behaviour of grinded and mechanically polished samples (2400-SiC, diamond paste 1µm and colloidal silica polishing) of 304L SS have been studied. After the detailed characterization of the features of material modifications at the subsurface related to surface treatments, their influences on the corrosion and oxide behaviour were investigated at room and high temperatures. If the overall passive behaviour in borate buffer solution was similar for all the samples, the number of doping species, the capacitance value, and the thickness of the passive film were influenced by the roughness, the defects on the surface, and also by the residual compressive stresses. Consequently, the passive film formed on the more disordered and reactive surface was the thinnest and the less stable. After exposure in simulated primary water of nuclear power plant, the main conclusions drawn by this study was that the surface treatment only impacts the oxidation kinetics, the oxidation features were quite identical for a given environment and finally that the environment chemistry play a major role on the oxidation behaviour of a mechanically modified surface.

3. Future plan

As mentioned above, our collaboration aimed at determining the fundamental effects of alloy composition and surface finish on corrosion resistance has been successful. On the other hand, corrosion or SCC problems in structural materials of nuclear power plants are often observed at weld parts, however, knowledge of the detailed mechanisms of that is very limited. Therefore, it is useful to extend the research approach we have developed to the degradation issues at weld parts. There is much to be noted in terms of characteristic metallurgical structure, compositional deviations, residual stresses, and thermal aging degradation in welds, but it is considered a challenging issue to be solved.

References :

[1] F. Hamdani, H. Abe, B. Ter-Ovanessian, B. Normand, Y. Watanabe, Effect of Chromium Content on the Oxidation Behavior of Ni-Cr Model Alloys in Superheated Steam, Metall. Mater. Trans. A. 46 (2015) 2285–2293. doi:10.1007/s11661-015-2786-7.
[2] F. Hamdani, Ph'D Thesis, 2015
[3] K. Jaffré, B. Ter-Ovanessian, H. Abe, N. Mary, B. Normand, Y. Watanabe, Effect of Mechanical Surface Treatments on the Surface State and Passive Behavior of 304L Stainless Steel, Metals 2021, 11(1), 135; doi:10.3390/met11010135
[4] K. Jaffré, H. Abe, B. Ter-Ovanessian, N. Mary, B. Normand, Y. Watanabe, Influence of Mechanical Surface Treatments on Oxide Properties Formed on 304L Stainless Steel in Simulated BWR and PWR Primary Water, J. Nuc. Mat., 556 (2021) #153258, https://doi.org/10.1016/j.jnucmat.2021.153258
[5] K. Jaffré, Ph'D Thesis, 2021

Hypoxia triggers collective aerotactic spreading of eukaryotic cells

ELyT Global
Theme: Engineering for Health
Scientific topic: Microsystems for cell Engineering

M. Nasser GHAZI

Ms. Satomi HIROSE

Prof. Jean-Paul RIEU

Prof. Christophe ANJARD

Assoc. Prof. Kenichi FUNAMOTO

Authors :
N. Ghazi[1], A. Chauviat[4], S. Fabre[4], O. Cochet-Escartin[1], M. Demircigil[2], S. Hirose[3], V. Calvez[2], K. Funamoto[3], C. Anjard[1], J.-P. Rieu[1]

Affiliations :
1-Institut Lumière Matière, Université Claude Bernard Lyon 1, Villeurbanne, France
2- Institut Camille Jordan, Université Claude Bernard Lyon 1, - Villeurbanne, France
3- Institute of Fluid Science, Tohoku University, Sendai, Japan
4- UMR5557, INRA-Université Claude Bernard Lyon 1, Villeurbanne, France

Abstract

A state of low oxygen occurs frequently in soil, water and multicellular tissues and has played a pivotal evolutionary role in shaping multicellularity. While both the social amoeba *Dictyostelium discoideum* (*Dd*) and the asocial amoeba *Acanthamoeba castellani* (*Ac*) are obligatory aerobic organisms, their ecological niche in the soil expose them to reduced oxygen availability in particular due to competition with bacteria.

We have recently observed that vertically confining a micro-colony of *Dd* cells in a growth medium triggers cells to move quickly outward of the self-generated central hypoxia area and thus form an expanding ring propagating for days [1]. The analysis of the cells' behavior within the micro-colony reveals a complex response to hypoxia depending upon their position:
- Cells closer to the ring present a clear outward directionality and are capable of dividing.
- Inner cells are not dividing, very motile but with limited outward directionality.
Using both oxygen sensors and microfluidic devices, we confirmed that *Dd* cells are aerotactic within 1-2% of $d\nabla C/C$ where C is the oxygen level and d is the cell size [2].

The variety of cell behaviors within the micro-colony were mimicked using a mean field PDE model that includes the cell division rate r, the motility D (diffusion constant) and a positive aerotactic bias a_0 where each quantity may depend on C. This model predicts that under hypoxia a ring may appear and persist yet that if D and/or r are too large, then the ring may disband [1].

We are testing this model with new data from the asocial amoeba Ac using the spot assay, microfluidic devices, growth and random motility experiments. These amoebae are fast moving ($D(Ac) \geq 20\ D(Dd)$) with a faster aerotactic bias as well but slowly dividing ($r^{-1}(Ac) \leq 3\ r^{-1}(Dd)$). Interestingly, upon spreading, ring formation occurs yet quickly dissipates unlike Dd (Figure 1). With the main differences being D and r, this quick dissipation of the Ac ring is accounted for in our model.
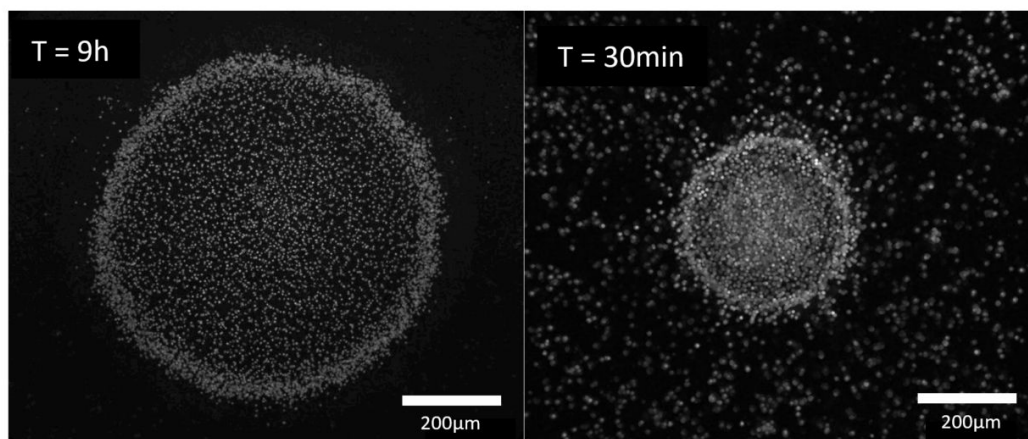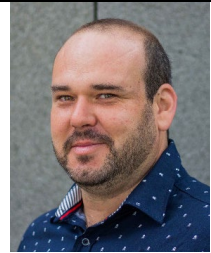
Figure 1: Self-generated O_2 gradients. On the left, Dd cells maintain a robust ring after 9 hours. On the right, Ac cells with a short-lived ring dissipating after 30 minutes.

[1] O. Cochet-Escartin, M. Demircigil, S. Hirose, B. Allais, P. Gonzalo, I. Mikaelian, K. Funamoto, C. Anjard, V. Calvez, J.-P. Rieu. Hypoxia triggers collective aerotactic migration in *Dictyostelium discoideum*. 2021. *eLife* (2021) 10:e64731 doi: 10.7554/eLife.64731

[2] S. Hirose, J.-P. Rieu, C. Anjard, O. Cochet-Escartin, K. Funamoto. "The Oxygen Gradient in Hypoxic Conditions Enhances and Guides Dictyostelium discoideum Migration". *Processes*. 2022, 10(2), 318; https://doi.org/10.3390/pr10020318

Cancer cell migration under oxygen concentration gradients

ELyT Global
**Theme: Engineering for Health
Scientific topic: Microsystems for Cell Engineering**

Mr. Satoshi ARATAKE	**Ms. Zhouxing SU**	**Prof. Jean-Paul RIEU**	**Assoc. Prof. Nicolas AZNAR**	**Assoc. Prof. Kenichi FUNAMOTO**
Tohoku University	Cancer Research Centre of Lyon	Université Claude Bernard Lyon 1	Cancer Research Centre of Lyon	Tohoku University

Abstract

Oxygen concentration *in vivo* is lower than that in the atmosphere (21% O_2) even under physiologically healthy conditions because cellular activities consume oxygen. It possibly further decreases under pathological conditions. In a microenvironment in cancer tissue (cancer microenvironment), spatial and temporal variations of oxygen concentration can be found because of an excessive cell proliferation and a formation of immature vascular networks. Such heterogeneous oxygen concentration affects cell dynamics.

The authors have developed microfluidic devices to investigate cell dynamics while controlling oxygen concentration [1]. The oxygen concentration in the microfluidic devices is controlled by gas exchange between the cell-cultured channels and gas channels into which gas mixtures at predefined oxygen concentrations are supplied. The controllability of oxygen concentration was improved by a double-layer device in which the gas channels above the cell-cultured channels (see details in Fig. 1(a)) [2]. The microfluidic device was fabricated from gas-permeable poly(dimethylsiloxane) (PDMS) and a glass cover slip. In addition, a polycarbonate film is embedded inside the device at a height of 1 mm to prevent oxygen diffusion from the atmosphere. Oxygen concentration profile across the cell culture channel was investigated computationally by using commercial finite element software (COMSOL Multiphysics 5.4; COMSOL, USA), and then validated by using oxygen-sensitive nanoparticles embedded in the gel channel (Fig. 1(b)). Uniform hypoxic oxygen conditions H0 and H5 were generated by supplying gas mixtures at 0 and 5% O_2 to the both gas channels, respectively, and a uniform normoxic condition N was generated by supplying gas mixture at 21% O_2. Moreover, linear oxygen concentration gradients G(0-10) or G(0-21) were generated by supplying gas mixture at 10% or 21% O_2 to the right gas channel, while supplying the gas mixture without oxygen (0% O_2) to the left gas channel.

Human breast cancer cells (MDA-MB-231 cell line) were mixed with the type I collagen gel

(1.5 mg/ml at pH 7.4) at 2×10^5 cells/ml, and seeded in the gel channel. The cell distribution was then observed under each oxygen condition (Fig. 1(c)). The increase in cell number was measured over the 24 h period by counting the number of cells before and after the experiment (Fig. 1(d)). As the results, it was higher in regions L and R than in region M under uniform oxygen conditions H0, H5 and N. In contrast, under oxygen concentration gradients, it was higher in regions M and R in the condition G(0-10), and lower in region R and highest in region M in the condition G(0-21). Thus, the cells were activated after hypoxic exposure, promoting their migration and proliferation. Moreover, the cells tend to migrate toward an area of mild hypoxia when cultured under an oxygen gradient.
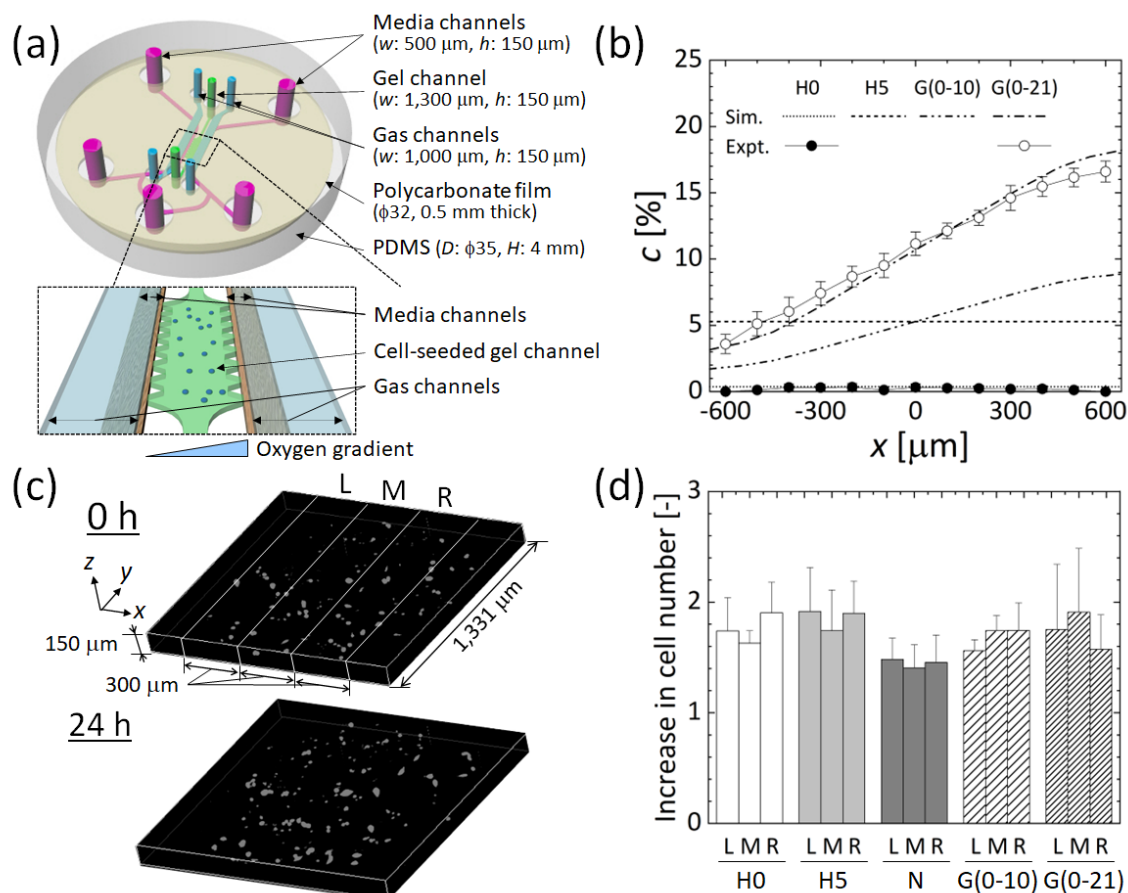
Fig. 1 Cellular experiment with human breast cancer cell line (MDA-MB-231 cells) by using microfluidic devices: (a) design of the microfluidic device. (b) Computational and experimental results of steady oxygen concentration profiles across the media and gel channels under the uniform hypoxic conditions H0 and H5, and the oxygen concentration gradients G(0-10) and G(0-21). (c) Representative 3D distributions of the cells in the collagen gel before and after 24-h exposure to the normoxic condition N. (d) Increase in cell number in the three equivalent regions L, M, and R (shown in (c)) of the gel channel after 24 h under each oxygen condition. Error bars represent standard deviation.

References

[1] K. Funamoto, I.K. Zervantonakis, Y. Liu, C.J. Ochs, C. Kim, R.D. Kamm, A novel microfluidic platform for high-resolution imaging of a three-dimensional cell culture under a controlled hypoxic environment, *Lab Chip*, Vol. 12, No. 22, (2012), 4855-4863.

[2] R. Koens, Y. Tabata, J.C. Serrano, S. Aratake, D. Yoshino, R.D. Kamm, K. Funamoto, Microfluidic platform for three-dimensional cell culture under spatiotemporal heterogeneity of oxygen tension, *APL Bioeng.*, Vol. 4, Issue 1, (2020), 016106-1-11.

Effect of wall elasticity on flow instability and wall shear stress of a full-scale, patient-specific phantom in middle cerebral artery

ELyT Global
Medical Applications
Flow Behavior/ Material Selection

Ryuhei Yamaguchi

Academic Researcher in IFS Tohoku University

Atsushi Totsuka

Technical Staff In IFS Tohoku University

Makoto Ohta

Professor, In IFS Tohoku University

Abstract

The mechanisms underlying the growth and rupture of aneurysms are poorly understood. Although the wall shear stress (WSS) in elastic wall aneurysm is examined using fluid–structure interaction (FSI) simulations, it has not been sufficiently validated using experimental modalities, such as particle image velocimetry (PIV). In this study, I investigated pulsatile flow in an elastic, image-based, patient-specific cerebral aneurysm model using PIV including phantom material [1-2].

1. Introduction

I explored the hemodynamics of the WSS and the kinetic energy cascade (KEC) in the elastic phantom compared with a rigid model, at the apex of the bifurcation of the middle cerebral artery (MCA) in vitro. The effects of elasticity on the WSS, gradient of WSS (WSSG), and tensile strength of the aneurysm wall were also investigated, in addition to the effect of wall elasticity on the KEC compared to a rigid wall. The WSSG around the stagnation point was large. In particular, the wall elasticity suppressed the WSS magnitude around the stagnation point and attenuated the KEC (Kinetic Energy Cascade, i.e., flow instability). And I have bee trying to fabricate phantom in silicone elastomer. Future studies examining KEC frequency and WSS characteristics in a phantom should consider assessing elasticity.

2. Morphology

In this study, two pacient-specific phantoms in MCA are shown in Figs.1 and 2. For both phantoms, I examined the suppreession of WSS. In Fig.1, the elastic phantom was fabricated using photo stereolithographic technology as follows. According to stl (stereolithography) data, the (inner) body of the aneurysm model was enclosed by the outer wall with a space (gap) of 1.2 mm similar to that of Guillaume. Silicone elastomer was injected into this space. After the silicone elastomer hardened, the inner and the outer bodies enclosing this space were removed.

The second phantom is a full-scale patient-specific model was fabricated using dipping by myself. The thickness of dome is 0.37 ± 0.15 mm. Sylgard 184 (Dow Chemical) is the most popular as the phantom material why we can choose given elasticity from 0.6 to 3.0 MPa and could adjust arbitrary thickness above 0.4 mm. Unfortunately, in dipping the neck and bifurcatin parts are thicker than that of dome.

3. Method

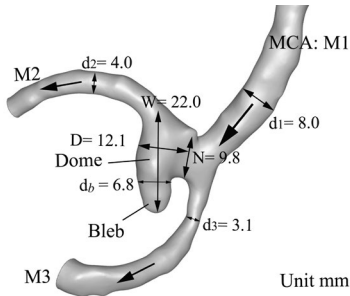The working fluid was used the aqueous glycerol with sodium iodide (47.38% water, 36.94% glycerol, 15.68%
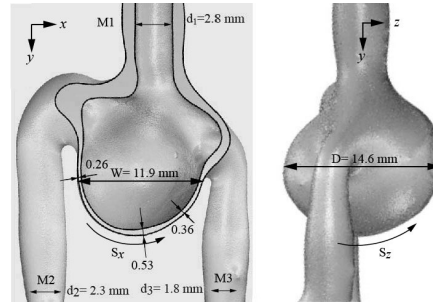
Fig.1 3.25-fold scaled-up Phanrom 03 in MCA.

Fig.2 Morphology of full-scale phantom 02 (left and right panels show front and side views.

sodium iodide). The physical properties were as follows: density $\rho = 1188$ kg/m^3, kinematic viscosity $\nu = 3.57 \times 10^{-6}$ m^2/s same as blood, and refractive index n = 1.411 which is the same as the current silicon elastomer.

4. Results

The comparison of flow patterrn in elastic and rigid model03 is shown in Fig.3. The velocity of inlet velocity in elastic is a little smaller than that in rigid models owing to elastic expansion. As shown in Fig.4 at t/T= 0.125, the magnitude of WSS in rigid is little larger than that in elasstic model, i.e., elasticity suppresses the WSS. At stagnation point, WSSG indicates positive and negative, i.e., stretching and compression for aneurysm wall, respectively.
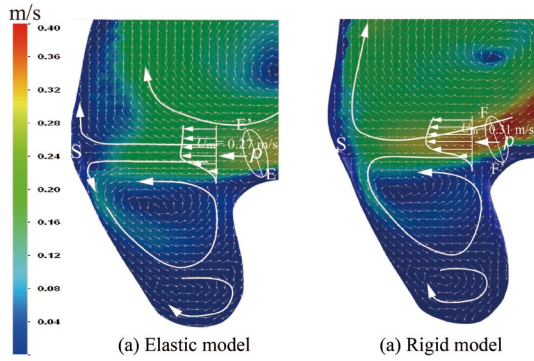
Fig.3 Velocity contour of elastic and rigid models03 at t/T= 0.125.

Fig.4 WSS at mid-systole in model03 at t/T= 0.125.
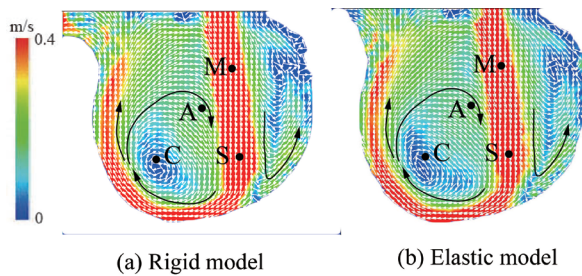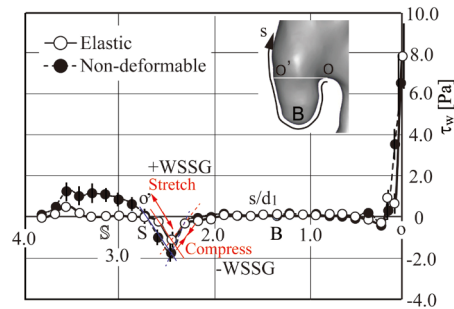
Fig.5 Velocity in rigid and elastic models02 (t/T= 0.28)
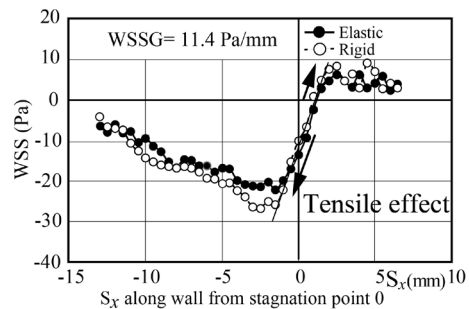
Fig.6 WSS and WSSG at xy plane in both model02s at t/T=0.280.

Although the velocity pattern within aneurysm model02 is shown in Fig.5 at peak systoke, the flow patterns are similar in both models, the velocity in rigid is a little lager than in elastic models. The WSS at peak systoke is shown in Fig. 6. WSS in elastic is slightly lower than that in rigid models owing to wall compliance. I insist the elasticity suppress by approximately 3~5%. the WSS in rigid model.

The comparison of kinetic energy cascade in elastic, i.e., flow instability, with that in rigid models is shown in Fig. 7. From 1 to 10^2 Hz, the KEC steeply decreases, and over 10^2 Hz KEC reaches 10^{-7} in rigid and 10^{-8} in elastic models. Clearly, the elasticity attenuates flow instability.
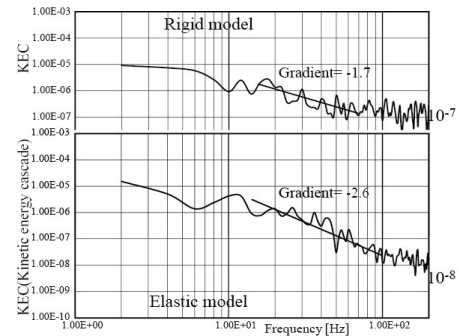
Fig.7 KEC in rigid and elastic models at point C.

References [1] Yamaguch, et al, (2022) Characteristic effect of wall elasticity on flow instability and WSS of a full-scale, patient-specific aneurysm in MCA. J. Appl. Phys. 131. [2] Yamaguchi et al, (2008) Velocity profile and WSS of saccular aneurysms at ACoA. Heart Vessels, 23.

Effect of difference wall stiffness between single-segment models and two-segments models on velocity map

ELyT Global
Engineering for Health
Simulation & Modeling

Kotaro Daibo Institute of Fluid Science, Tohoku University Gradute Biomedical Engineering Tohoku University

Muhammad shiddiq sayyid hashuro Institute of Fluid Science, Tohoku University Gradute Mechanical Engineering Tohoku University

Hiroyuki Kosukegawa Institute of Fluid Science, Tohoku University Blue Practice Co.Ltd

Kaihong Yu Institute of Fluid Science, Tohoku University Blue Practice Co.Ltd

Makoto Ohta Institute of Fluid Science, Tohoku University

Abstract

1.Introduction

Blood vessel models are frequently used for evaluation system of medical device and training system for clinicians. Blood vessels have relatively low friction, and their stiffness are partially different; healthy part is relatively softer, whereas diseased part is stiffer [1]. PVA-H (Polyvinyl alcohol hydrogel) is used as a material for blood vessel models as it offers many advantages

such as transparency, low friction, deformability for any shapes and controllable thickness and stiffness by changing the concentration of PVA.

The purpose of this study is to make blood vessel models with segments of different stiffness. By using the different concentrations of PVA, we fabricated a tubular model with segments of different stiffness. Particle Image Velocity (PIV) experiments were conducted in order to check the change of flow pattern due to the different stiffness. This research will produce a model which mimic pathologies that impact the local stiffness of the vessel wall, such as arteriosclerosis.

2.Method

A straight tube made from PVA-H (internal diameter: 4.0 mm, outer diameter: 6.0 mm, wall thickness: 1.0 mm) was molded. Three models were prepared; two were molded with a uniform PVA-H concentration (12 wt% and 15 wt%) as conventional single-segment models. The other one was a two-segment model with 12 wt% and 15 wt% PVA-H.

The tubes were fixed in an acrylic box and 5 wt% PVA-H solution was poured into the box to mimic surrounding tissues.

To obtain velocity map, PIV (particle image velocity) was conducted. Pulsatile pump (Alpha Flow EC-1, Fuyo Corporation, Japan) flowed the working fluid in a circulation system. Working fluid (density: 1418 kg/m^3, viscosity: 7.37 mPa·s) was prepared with a mixture of glycerol, water and sodium iodide to mimic the human blood. The fluid has similar reflective index to the manufactured PVA-H. Pressures and flow rates before and after the models were obtained using pressure sensors (AP-12S, Keyence, Japan) and flow sensors (FD-SS2A, Keyence, Japan). Pulsatile flow between 80 mmHg and 120 mmHg [2], waveform period 1.0 s were used. PIVlab toolbox [3] on Matlab was used for velocity map.

3.Results and Discussion

The pressure ratio between inlet and outlet was almost constant, whereas the flow rate ratio was changed depending on the time. The flow rate ratio was increased at the systole period and decreased at the diastole. It is confirmed that the compliance of the PVA-H model changes. The PIV results show the difference of flow speed distribution on the longitudinal plane depends on the models.

5.Reference

[1] Noriyoshi Chubachi, Hiroshi Kanai, Ryoji Murata *et al*: Measurement of Local Pulse Wave Velocity in Arteriosclerosis by Ultrasonic Doppler Method. 1750 - 1994 ULTRASONICS SYMPOSIUM

[2] American Heart Association :

[3] Thielicke, W., Sonntag, R. (2021) Particle Image Velocimetry for MATLAB: Accuracy and enhanced algorithms in PIVlab. Journal of Open Research Software, 9: 12. DOI: https://doi.org/10.5334/jors.334

Modeling of Olsen cycle for pyroelectric energy harvesting and assessment of abnormal electrocaloric effect in ferroelectric single crystals

ELyT Global

Theme: Energy
Scientific topic: - Simulation and modeling

Gaspard Taxil[1,2,3,4]	**Mickaël Lallart**[1,*]	**Gaël Sebald**[2]	**Benjamin Ducharne**[1,2]	**Tung Thanh Nguyen**[2,4]	**Takahito Ono**[3]	**Hiroki Kuwano**[2,4]

[1] *Univ. Lyon, INSA-Lyon, LGEF EA682, F-69621, France*
[2] *ELyTMaX IRL 3757, CNRS, Univ. Lyon, INSA Lyon, Centrale Lyon, Université Claude Bernard Lyon*
[3] *Graduate School of Engineering, Tohoku University, Sendai 9808579, Japan*
[4] *New Industry Creation Hatchery Center (NICHe), Tohoku University, 6-6-10 Aramaki-Aoba, Aoba-ku Sendai, Miyagi 980-8579, Japan*
[*] *Mickael.lallart@insa-lyon.fr*

Abstract

Energy harvesting from residual energy in the environment is a promising way to power wireless sensors or other low-power devices in harsh or remote conditions. Pyroelectric energy harvesting consists in directly converting thermal energy into electrical one. Waste heat is an underestimated energy source seldomly exploited. The energy challenges of the next decades have increased the interest in waste-heat energy harvesting and different approaches have been developed to take advantage of these energy losses with pyroelectric materials [1]. One of the promising features of ferroelectric materials is the possible enhancement of energy conversion by using their phase transitions in particular temperature ranges and electric field [2]. The advantage of using phase transitions in ferroelectric materials is to take benefit of the non-linear response of the polarization close to the transition and thus, increase the polarization variation. Due to its high energy conversion potential, the Olsen cycle has been established to be the most favorable for pyroelectric energy harvesting [3]. The Olsen cycle consists of starting from a low temperature T_l and an initial electric field $\mathbf{E_i}$. An electric field is applied until a final value $\mathbf{E_f}$. (A-B path on Figure. 1(a)). Then, the temperature is increased to a higher value T_h (B-C path). Afterwards, the electric field is decreased to its initial value $\mathbf{E_i}$ (C-D path). Finally, the temperature is decreased down to the initial T_l value (D-A path). An illustration of such P-E (Polarization-Electric field) cycle is given in Figure 1(a). Previous works used a laser-based pyroelectric harvester with a square temperature variation and a triangle function evolution of the electric field [4]. We employed this temporal profile in our simulation for preliminary comparison and model assessment. An illustration of the evolution of the temperature and the electric field in our theoretical approach is given in Fig. 4(b).
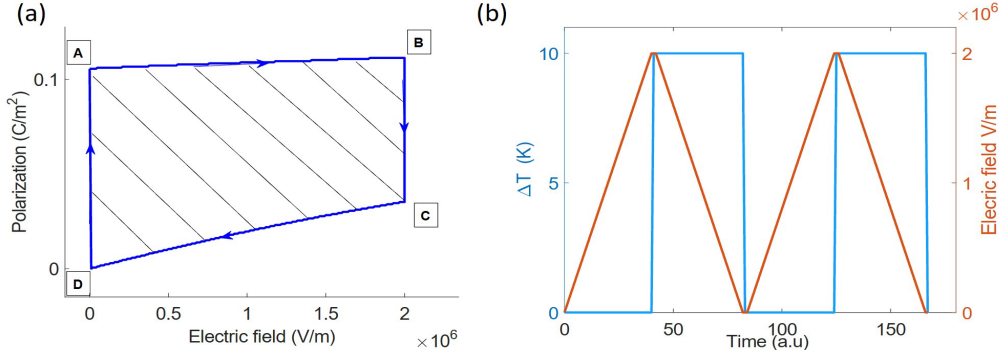
Figure 1 (a) Representation of an Olsen cycle in the P-E space; (b) Evolution of the temperature and the electric field in function of time for two consecutive Olsen cycles

In order to assess the energy conversion ability, a theoretical approach was proposed here based on the Landau-Devonshire theory and consists in modeling such cycles. The thermodynamic stable ferroelectric phase with associated polarization was obtained via minimizing Landau free enthalpy. The Landau free enthalpy is expressed as [5]:

$$\Delta G = \alpha_1(P_1^2 + P_2^2 + P_3^2) + \alpha_{11}(P_1^4 + P_1^4 + P_1^4) + \alpha_{12}(P_1^2 P_2^2 + P_1^2 P_3^2 + P_2^2 P_3^2) + \alpha_{123}P_1^2 P_2^2 P_3^2 + \alpha_{111}(P_1^6 + P_2^6 + P_3^6) + \alpha_{112}\big(P_1^2(P_2^4 + P_3^4) + P_2^2(P_1^4 + P_3^4) + P_3^2(P_2^4 + P_1^4)\big) + \alpha_{1111}(P_1^8 + P_2^8 + P_3^8) + \alpha_{1122}(P_1^4 P_2^4 + P_1^4 P_3^4 + P_2^4 P_3^4) + \alpha_{1112}\big(P_1^6(P_2^2 + P_3^2) + P_2^6(P_1^2 + P_3^2) + P_3^6(P_1^2 + P_2^2)\big) + \alpha_{1123}(P_1^4\ P_2^2\ P_3^2 + P_1^2\ P_2^4\ P_3^2 + P_1^2 P_2^2 P_3^4) - E_1 P_1 - E_2 P_2 - E_3 P_3$$

(1)

where P_i and E_i are respectively the components of polarization and electric field in the cubic basis; α_i, α_{ij}, α_{ijk} and α_{ijkl} are tensors which represent the different orders of the dielectric stiffness. By minimizing the Landau free energy with respect to polarization, we can find for each value of temperature and electric field the stable phase of ferroelectric materials with the associated polarizations.
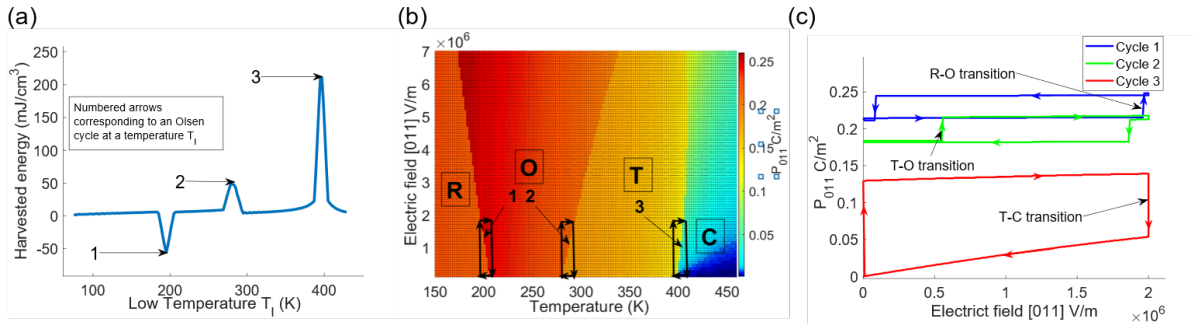
Figure 2 (a) A plot of the harvested energy in function of the working temperature T_l for $BaTiO_3$; (b) T-E phase diagram versus polarization with different cycles denoted; (c) A plot of the associated P(E) cycles.

This allowed identifying phase transitions of interest in ferroelectric materials for pyroelectric energy harvesting depending on both low temperature (T_l) of the cycle and crystal orientation. We chose to model the harvested energy as a function of the low temperature T_l while keeping a temperature span of $\Delta T = T_h - T_l = 10K$, $\mathbf{E}_i$=0kV/cm and $\mathbf{E}_f$=2kV/mm. Particular T_l values have been identified and denoted with numbers (Figure. 2(a)). The corresponding cycles are represented in a T-E phase diagram (Figure. 2(b)) and in the P-E space (Figure. 2(c)). This work allowed us to obtain which phase transitions and in which thermodynamic conditions operated Olsen cycles to optimize pyroelectric energy harvesting for different single crystal orientations.

References:

[1] S. Pandya, G. Velarde and L. Martin: NPG Asia Materials., Vol. 11(2019)
[2] A. Khodayari, S. Pruvost and S. Mohammadi: IEEE Trans Ultrason Ferroelectr Freq Control, Vol. 56, 693 (2009)
[3] Randall B. Olsen, David A. Bruno and J. Merv Briscoe: J. Appl. Phys., Vol. 58 (1985)
[4] B. Hanrahan, C. Mart and A. Smith, Energy Technology 7. 1900515 (2019)
[5] J; J. Wang, P. P. Wu and L. Q. Chen : J. Appl. Phys, Vol 108, 114105 (2010)

Thermal processes in thermomagnetic energy generators

ELyT Global
**Theme: Energy
Scientific topic -Materials and structure design
- Simulation and modeling**

JOSEPH, Joel LALLART, Mickael MIKI, Hiroyuki KOHL, Manfred
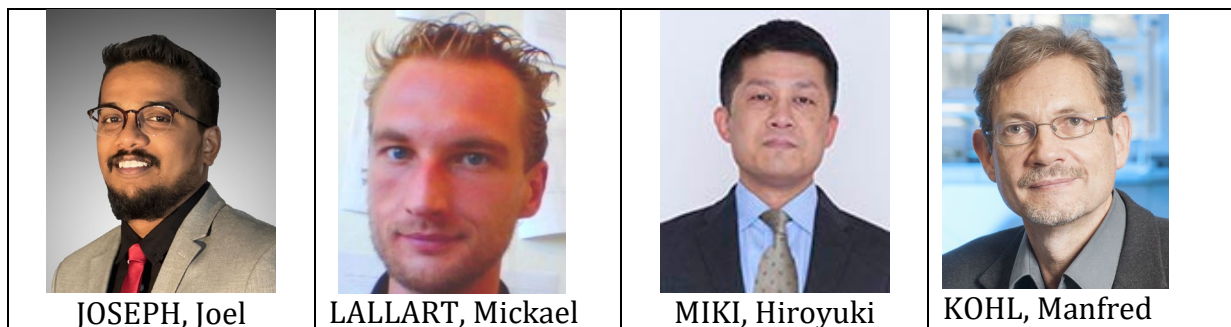
Abstract

The MISTRAL project examines thermomagnetic generators (TMGs) based on magnetic shape memory alloys (MSMAs) as they have potentially high efficiency and favorable scaling behavior. A permanent magnet and an oscillating bending beam that is self-actuated by a thermal gradient have been developed into micro-scale energy generators. By moving a pick-up coil in the external magnetic field, resonant oscillations are generated and converted efficiently to electrical power. Here, we present a study on the thermal processes involved in the thermomagnetic generators that reveal critical limits in temperature change within the thermomagnetic material.

1. Introduction

In an increasingly interconnected world, the demand for compact, dependable power sources for wireless sensors has prompted investigation into micro energy harvesting systems. Technologies that collect tiny amounts of energy from the environment, such as light and vibrations, and transform them into electrical energy are referred to as energy harvesters. Thermoelectric modules are the technology that has received the most attention for thermal energy harvesting. However, thermoelectric devices exhibit poor conversion efficiency and demand a heat sink. These restrictions can be removed by utilizing the multiferroic capabilities of magnetic shape memory alloys (such as Ni-Co-Mn-In and Ni-Mn-Ga) in a TMG. Figure 1 shows the schematic of the TMG design which includes a brass cantilever attached to a substrate on the tip of which a film of Ni-Mn-Ga is placed. The assembly is then placed under a permanent magnet that provides the magnetic field to magnetize Ni-Mn-Ga film and the magnetic field gradient required for the magnetic force. The device is attracted to the surface of the magnet, which at the same time is the heat source. Heat transfer from magnet causes the Ni-Mn-Ga film to demagnetize and thus the cantilever resets to its initial position. This cycle is repeated, and optimized heat intake and heat dissipation enables resonant self-actuation. The previous work in the topic includes development of concept of resonant self-actuation,[1]

upscaling of the device for increased power output of up to 50μW/cm^2,[2] study on coupling effects of TMGs operating in parallel, and development of a lumped element model to optimize the design.[3]

a) Heating at contact with heated permanent magnet.
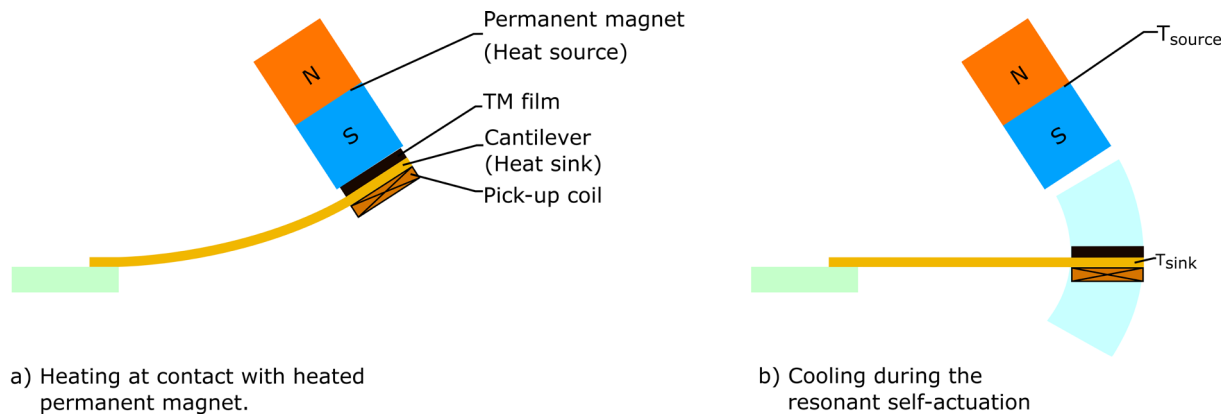
b) Cooling during the resonant self-actuation

Figure 1. Schematic view of principle of thermomagnetic generator

2. Thermal processes

Optimization of heat intake and heat dissipation is key in sustaining resonant self-actuation of TMGs and for maximizing the power outputs. In the current study the impact of heat transfer coefficient at contact (κ) and thermal resistance of the bonding layer (R_b) between the Ni-Mn-Ga film and the cantilever on the performance is investigated in detail. The aim is to identify the critical limits at which the TMG fails to achieve resonant self-actuation. A validated LEM simulation model presented in Joseph et al.[3] is used to vary the parameters κ and R_b.

3. Results

The results reveal the critical limits of the TMG with 10μm Ni$_{53.5}$Mn$_{23.8}$Ga$_{22.7}$ film. The value of κ is varied from a value of 5 kW/m^{2}K to 12 kW/m^{2}K and the value of R_b is varied between 1 K/W and 55 K/W and the effect on performance parameters like stroke, frequency and power output are looked at in detail. The performance parameters are governed by the internal thermal processes of heat intake and heat dissipation. As long as the temperature change (ΔT) during the mechanical cycle is sufficiently large, resonance self-actuation is stable. ΔT limit for the studied device is approximately 6°C, which is met for a heat transfer coefficient $\kappa > 8$ kW/m^{2}K, above which stable resonant operation is observed. Performance grows steadily as κ increases at all source temperatures. Stable performance occurs in terms of oscillation stroke, frequency, and power for all heat source temperatures with sufficiently large value of R_b over 10 K/W. Heat dissipation via conductive heat loss and heat intake are out of balance for low values of $R_b < 10$ K/W. As a result, there is a significant reduction in ΔT, which has a negative impact on oscillation stroke and power output at all source temperatures. At high source temperatures exceeding 150°C, the device ceases operating in resonant self-actuation mode when R_b falls below 5 K/W. In this instance, the cantilever and Ni-Mn-Ga film become thermally coupled. Thus, at higher source temperatures the cantilever temperature rises above the threshold causing significant reduction in heat dissipation and ΔT, causing the device to stop operation. In summary, we show that device performance can be further enhanced in terms of heat intake and dissipation during resonant self-actuation leading to an increase in power generation.

References

1. Gueltig, M., Wendler, F., Ossmer, H., Ohtsuka, M., Miki, H., Takagi, T., and Kohl, M. (2017). Adv Energy Mater *7* (5)
2. Joseph, J., Ohtsuka, M., Miki, H., and Kohl, M. (2020). Joule *4 (12)*, 2718–2732
3. Joseph, J., Ohtsuka, M., Miki, H., and Kohl, M. (2021). Materials *14 (5)*, 1234
4. Joseph, J., Wehr, M., Ohtsuka, M., Miki, H., and Kohl, M. (2021). 21st International Conference on Solid-State Sensors, Actuators and Microsystems (Transducers), 463-466

Radiative cooling of solar cells: detailed opto-electro-thermal modeling and influence of surface structuring

J. Dumoulin[1], E. Drouard[2], M. Amara[1]

1INL UMR5270, Univ. Lyon, INSA-Lyon, CNRS, Villeurbanne France

2 INL UMR5270, Univ. Lyon, Ecole Centrale de Lyon, Ecully France

ELyT Global
Energy

Abstract

Silicon solar cells are designed to efficiently absorb solar photons but convert only a limited proportion of the incoming energy into electricity. In real operating conditions, the cells therefore operate at much higher temperatures than in standard test conditions [1]. This heating is detrimental to their energy conversion efficiency and lifetime. Several cooling strategies are therefore being studied to reduce the cell temperature [2]. In recent years, there has been a growing interest in the so-called radiative sky cooling (RSC) strategy. This approach consists in optimising the thermal radiation of cells or modules by taking advantage of the atmospheric transparency in the 8-13 μm range [3]. Although some preliminary studies on the topic predict cooling of more than 13 °C on silicon wafers [4], they remain insufficient to fully assess the potential of this technique for various technologies.

In this work, we first give the big picture of radiative sky cooling and discuss some peculiarities when applied to photovoltaic devices. Using a fundamental modelling framework developed during the thesis [5], we then show the great benefit of enhanced RSC. Furthermore, we unveil the ideal thermal emissivity profile needed to achieve the best cooling performance. In a second step, we make a focus on photonic improvement pathways. Using a transfer matrix method, we simulate the thermal emissivity of a silicon module from the visible to the mid-infrared range. This allows us to investigate practical pathways for improved RSC.

References

[1] Weiss, L. et al. "Impact of radiative-heat transfer on photovoltaic module temperature. Progress in Photovoltaics: Research and Applications". 2016.

[2] Granqvist, C. G. et al. "Radiative cooling to low temperatures: General considerations and application to selectively emitting SiO films". Journal of Applied Physics. 1981.

[3] Chen, Z. et al. "Radiative cooling to deep sub-freezing temperatures through a 24-h day-night cycle". Nature Communications. 2016.

[4] Zhu, L. et al. "Radiative cooling of solar absorbers using a visibly transparent photonic crystal thermal blackbody". Proceedings of the National Academy of Sciences. 2015
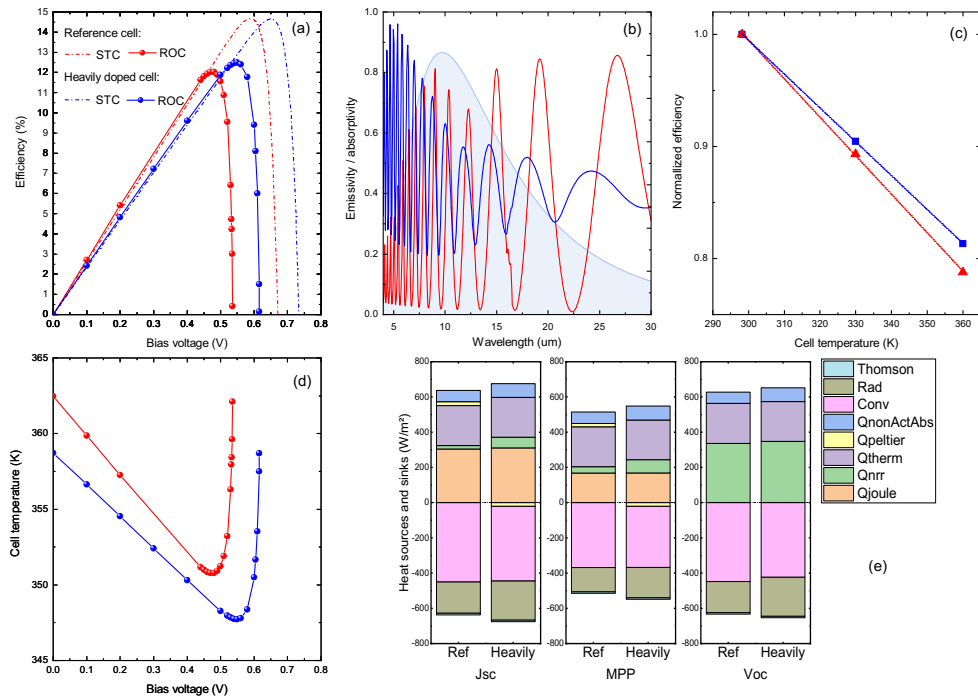
Figure 1 : (a) (a) Power conversion efficiency of the two cells (reference in red and highly doped in green) under standard test conditions (dotted lines) and under real operating conditions (solid lines). (b) Spectral absorptivity under normal incidence of the two solar cells (reference cell in red and heavily doped cells in green), which is the ratio of the absorbed to the incident solar power. According to Kirchhoff's law of radiation, the absorptivity is equal to the spectral emissivity, that is the ratio of the radiation emitted to the radiation emitted by a blackbody at a given wavelength. The emission spectrum of the blackbody at 25°C is shown in the light blue. (c) Normalized efficiency as a function of solar cell temperature, from which the temperature coefficient can be extracted by linear fitting. (d) Temperature-voltage characteristic. (e) Heat sources and sinks of the two cells at three specific operating points: the short-circuit, the maximum power, and the open circuit voltage.

Ferromagnetic Alloys for Integrated Electrical Protection Circuits

ELyT Global
**Theme: Energy
Scientific topic: Materials & Structure design**

Mickaël LALLART[1]   Gaël SEBALD[2]   Hiroyuki MIKI[3]

[1]Univ. Lyon, INSA-Lyon, LGEF EA682, F-69621, France

[2]ELyTMaX UMI 3757, CNRS, Univ. Lyon, INSA Lyon, Centrale Lyon, Université Claude Bernard Lyon 1, Tohoku University, Sendai, Japan

[3]Faculty of Science and Engineering, Ishinomaki Senshu University, Ishinomaki 980-8580, Japan

Abstract

Ferromagnetic materials have the attractive feature of temperature-dependent magnetic properties. Such remarkable characteristics translate into a loose of magnetic properties above a critical temperature (Curie point). Hence, such materials have found extensive applications in the field of cooking tools or energy harvesting devices for instance.

In this study, ferromagnetic materials are included into an electrical conducting circuit in order to provide a safety feature allowing opening the electrical circuit in the case of failure (overcurrent). Compared to conventional electromagnetic breakers, the proposed concept (Fig. 1) features the following advantages:

1. The thermal (moderate overcurrent) and magnetic (high-level surge) are based on the same material
2. No mechanical magnification system is required as circuit opening yields a significant air gap (in conventional breaker, the bimetallic strip displacement caused by temperature rise is too small to ensure circuit opening).

Based on the schematic depicted in Fig. 1, the circuit operations for the can be twofold. First, for a moderate overcurrent, the ferromagnetic device gets heated and eventually looses magnetic properties significantly so that the magnet is attracted by the magnetic core of the coil, hence opening the circuit. The second possibility arises on high overcurrent. In this case, in a similar way than conventional breaker, the magnetic field induced by the coil is sufficiently

high to attract the magnet attached to the switch in a very fast way (within a few milliseconds). When the circuit is opened, the device also includes a security feature preventing self-rearming as the switch is magnetically stuck to the fixed magnetic core of the coil.

Results are depicted in Fig. 2. Three zones can be observed. The first one, corresponding to normal operating conditions, shows that the circuit keeps closed for current lower than 2.3A (which thus corresponds to the rated current). Then, when a moderate overcurrent arises, the thermal protection mechanism is operating, yielding an almost exponentially decreasing opening time with the current. Finally, a high current surge appears, the magnetic protection is enabled, leading to very fast opening within 10 ms. Such characteristics are matching very well with expected characteristics of conventional electrical breaker, and can be tailored from the material aspects, or through device design, for instance through distances between the two terminals of the breaker.

Acknowledgements
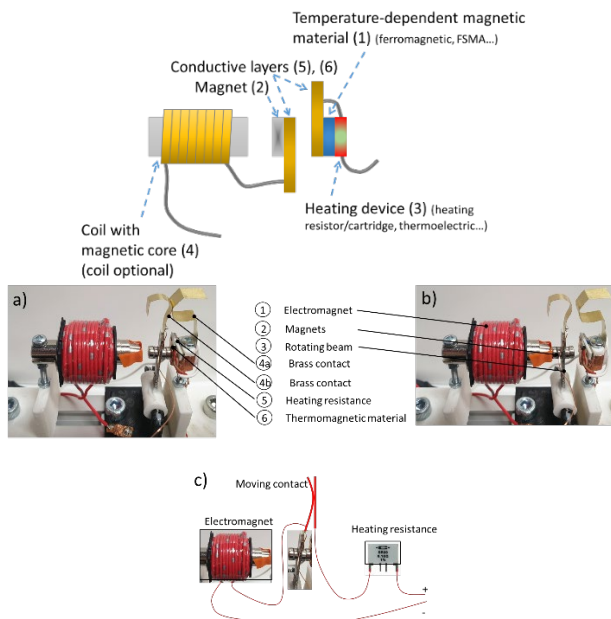
Fig. 1 Device schematic and experimental proof-of-concept picture.
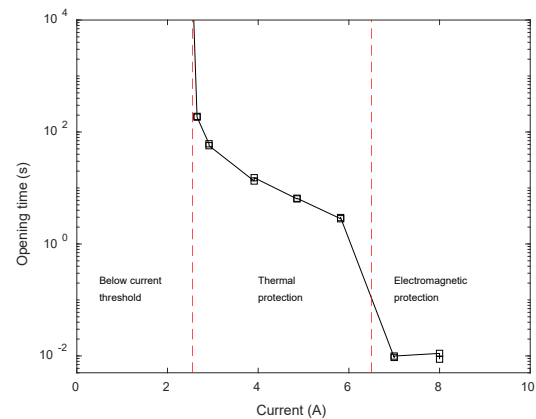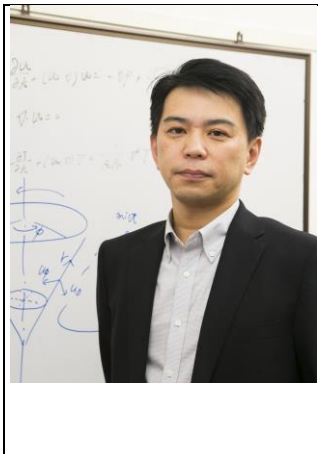
Fig. 2 Protection device experimental characteristics.

Thermodynamic Analysis of a New Electric Environmental Control System

ELyT Global
Electrification of commercial aircraft.
Energy recovery from the exhaust air.

Prof. Takahiro ADACHI

Abstract

A new electric environmental control system for aircraft is investigated, focusing on energy recovery from the exhaust air. The air has a higher energy level in the cabin than outside during the cruise because the outside air is at low pressure and low temperature. In this system, by setting a recovery turbine behind the cabin, the discharged energy can be collected from the exhaust air from the cabin to the exterior. We perform a thermodynamic cycle analysis, where the temperature, pressure and entropy are calculated at each position of the cycle by considering the pressure ratios of the compressors as variable parameters. From the results of cycle analysis, we obtain a T-s diagram, an energy recovery rate of the collected energy from the recovery turbine to the required power to operate the electric compressor, a coefficient of performance(COP), and heat transfer in heat exchangers. It is found that the energy recovery rate and COP in our system have maximum values at the tip point condition and show better performance compared to the literature. In particular, it is shown that the energy recovery rate may exceed 85% under the tip conditions.

CarboEDiffSim :Molecular Theory Analysis of Carbon Diffusion in Iron which is Happened Phase Transformation under Electric Field

ELyT Global
Theme: Energy
Scientific topic: Modelisation/Simulation

	Mr.Ryuta Onozuka[1,2]		**Assistant Prof. Takuya Mabuchi [2,3]**
	Prof. Patrice Chantrenne[4]		**Prof. Takashi Tokumasu[2]**

Affiliation

1) Finemechanics, Graduate School of Engineering, Tohoku University

2) Institute of Fluid Science, Tohoku University

3) Frontier Research Institute for Interdisciplinary Sciences, Tohoku University

4) MATEIS, INSA de Lyon, Université de Lyon

Abstract

Steel is a widely used as structural material used for centuries which still experiences developments to get enhanced mechanical properties. Within all the metallurgical processes, induction heating is more and more used. Its main advantages lie in the direct Joule heating of the matter, significantly increasing the energy efficiency, and the reduced volume. However, it has been demonstrated that the electric current has a significant influence on the carbon diffusion in iron. It is really important to manage these phenomena to get the expected microstructure and mechanical properties of steel. Unfortunately, there is a lack of knowledge to explain physically the mechanisms leading to electromigration of carbon in iron. Thus, in

this research project, the goal is to get fundamental knowledge in order to analyze the mechanisms of carbon diffusion in iron with the presence of an electric field. To investigate these mechanisms, atomic scale simulation approach is used. Molecular Dynamics simulation is an appropriate tool as we will need to tackle with numerous atoms.

Iron is a material that experience allotropic phase change (from BCC to FCC) depending on the temperature level and carbon concentration. In a previous work, an EAM based interatomic potential was used. However, it has been difficult to correctly analyze the temperature dependence of carbon diffusion because the phase transformation temperature is much lower than the experimental value (550 K instead of 1183 K). We have attempted to overcome these problems by using the ABO potential developed by Nguyen et al. as an intermolecular potential. Firstly, we performed test calculations to investigate the validity of the potential. Specifically, we checked the energy conservation law of the calculation system and dissolution energy.

Firstly, how to confirm the energy conservation law of the calculation system is described. Figure 1 shows the structure. Orange indicates iron atoms. There were 2000 iron atoms. The initial temperature was 400[K] and timestep were 0.1[fs] and 1.0[fs]. After we minimized total energy of the calculation system, we simulated for 0.1[ns] using NVE ensemble. From the calculation results, we found that energy conservation law was satisfied when timestep was 0.1[fs].

To verify that we used the interatomic potentials correctly, we compared our results with previous studies. Specifically, we calculated dissolution energy. The calculation method is described. Figure 2 shows the structure. Orange indicates iron atoms and gray indicates carbon atom. Firstly, after minimizing the total energy of the Fe-C system, the carbon atoms were removed. After that, the system of iron was minimized again. Prior to this simulation, the energy per carbon atom was calculated for a system of carbon atoms with a diamond structure. We calculated the dissolution energy by subtracting the total energy of the iron system and the energy of the extracted carbon atom from the calculated total energy of the Fe-C system. In the case that we placed carbon atom to the octahedral void, the calculation results relatively agreed with previous study.

The goal of future works is to determine the phase transformation and carbon atoms diffusion coefficients in austenite and ferrite. From the results of these calculations, we will analyze the temperature dependence and electric field dependence of carbon diffusion in the system that takes phase transformation into account.
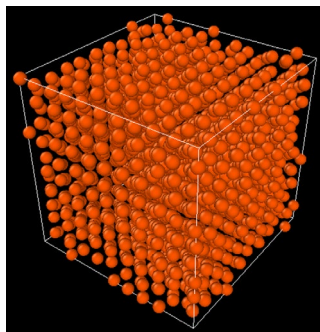

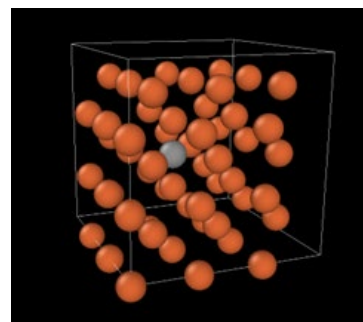Fig1. atomic configuration used for energy conservation test

Fig2. Atomic configuration used for C dissolution energy determination

POSTERS

Magnetostrictive and Inverse Magnetostrictive Properties of Fe-Co-V Particle dispersed Polyurethane matrix composites

ELyT Global
Energy
Materials & Structure design

	Takumi KEINO		**Assist. Prof. Hiroki KURITA**		**Prof. Fumio NARITA**

Abstract

Wearable and flexible magnetostrictive materials are required to realize devices related to the Internet of Things. Soft magnetostrictive materials are also expected to be applied as tactile devices in telemedicine. This study aims to fabricate a material made up of $Fe_{49}Co_{49}V_2$ alloy particles dispersed in a polyurethane (PU) matrix (PU–FeCoV). This material makes soft magnetic composites with a positive magnetostrictive effect. It was shown that several PU–FeCoV soft composites also have a negative magnetostrictive effect on one side of the composites. This study revealed that the large pores produce the bending behaviour in the PU–FeCoV soft composite. The magnetic flux density of the PU–FeCoV soft composites was shown to vary with cyclic loading. Therefore, we believe that PU–FeCoV soft composites may have potential applications as flexible sensing, vibration energy harvesting, and haptic devices.

Introduction

Magnetostrictive materials have been applied in various fields, such as sensors, actuators, and energy harvesting devices [1]. In recent years, wearable and flexible magnetostrictive materials have been used as flexible vibration energy harvesters to realize the Internet of Things (IoT). Moreover, soft magnetostrictive materials are expected to be applied as haptic devices for telemedicine. Sandlund et al. [2] have reported the magnetostrictive behavior of polymer-bonded Terfenol-D composite.

It is well known that the giant magnetostrictive materials, including Terfenol-D and Fe–Ga alloy, are expensive and brittle. Fe–Co alloys attract attention as magnetostrictive alloys due to their excellent mechanical properties and low cost, despite their magnetostriction (approximately 80–140 ppm) being lower than that of Terfenol-D and Fe–Ga alloy [3]. Consequently, the Fe–Co and Fe–Co–V alloys have great potential for practical use as magnetostrictive materials in many industrial applications.

This work fabricated a $Fe_{49}Co_{49}V_2$ alloy particle-dispersed PU matrix (PU–FeCoV) in the form of soft composites and measured their direct and inverse magnetostrictive properties. In addition, the microstructure of PU–FeCoV soft composites was observed using a three-dimensional X-ray computed tomography machine.

Results and Discussion

The addition of $Fe_{49}Co_{49}V_2$ alloy particle produced positive magnetostriction in the PU (i.e., the PU–FeCoV soft composites extended in the direction parallel to the magnetic field). The PU–FeCoV soft composites exhibited a magnetostrictive effect equal to or higher than the $Fe_{49}Co_{49}V_2$ alloy plate. Furthermore, it was shown that the magnetostriction of the PU–FeCoV soft composites does not saturate, while that of the $Fe_{49}Co_{49}V_2$ alloy plate is saturated at 70 ppm. This apparent positive magnetostriction is due to the attraction between the $Fe_{49}Co_{49}V_2$ alloy particles and the electromagnets. It is notable that several PU–FeCoV soft composites exhibited negative magnetostrictive effects on the opposite surface of the PU–FeCoV soft composites, regardless of the $Fe_{49}Co_{49}V_2$ alloy particle volume fraction. This result indicates that these PU–FeCoV soft composites were bent due to the applied magnetic field.

Fig. 1(a) shows the three-dimensional X-ray computed tomography images of the PU–FeCoV soft composites with 40 vol.% of $Fe_{49}Co_{49}V_2$. We present a possible bending mechanism behind the deformation of the PU–FeCoV soft composites in

Figure. 1 (a) CT scan image and (b) The assumed bending mechanism of the PU–FeCoV.

the magnetic field. The mechanism is shown in Fig. 1(b). The pores remain in the upper region of the PU–FeCoV soft composites during the cooling process. Therefore, the bottom side of the PU–FeCoV soft composites extend due to both magnetostriction and the attraction of the $Fe_{49}Co_{49}V_2$ alloy toward the electromagnets. On the other hand, the upper side, with a low compressive elastic modulus due to fewer $Fe_{49}Co_{49}V_2$ alloy particles and more pores, is shorter than the lower region due to the expansion of the bottom side.

The magnetic flux density depended on the cyclic loading applied to the PU–FeCoV soft composites, regardless of the $Fe_{49}Co_{49}V_2$ alloy particle volume fraction. This result indicates that the PU–FeCoV soft composites with a small amount of $Fe_{49}Co_{49}V_2$ alloy particles have potential applications as a sensor or energy harvesting devices.

References

[1] F. Narita, M. Fox, *Advanced Engineering Materials*, 20 (2018), 1700743.

[2] L. Sandlund, M. Fahlander *et al.*, *Journal of Applied Physics*, 75 (1994), 5656.

[3] F. Narita, K. Katabira *et al.*, *Materials Transactions*, 58 (2017), 302-304.

Heat Transfer Mechanisms for Spatially Uniform Cooling of Continuous Heating Elements

ELyT Global
**Theme: Heat transfer
Scientific topic: Uniform cooling**

Mamoru YAMAMOTO[1,2]   Yuki KANDA[2]   Atsuki KOMIYA[2]

[1]Graduate School of Engineering, Tohoku University, Sendai, 980-8577, Japan
[2]Institute of Fluid Science, Tohoku University, Sendai, 980-8577, Japan

Abstract

As the performance of electronic devices improves, the heat generation density increases. In general, convective heat transfer cooling with water is generally applied to devices with a large heat generation density ($\sim$100 kW/m^2). In large LEDs and other devices with a continuous and long structure of heat-generating elements, the cooling water takes heat away in the upstream region of the flow path, causing the water temperature to rise, resulting in insufficient cooling in the downstream resion of the flow path. This causes a heat load on the heat-generating elements, resulting in variations in LED light intensity and a reduction in their lifetime. In the case of forced convection cooling using water as the working fluid, Wang et al. confirmed that the sinusoidal shape of the flow path enhances heat transfer by making the flow path sinusoidal[1]. In addition, the nanofluids in which nanoparticles are added to the fluid has been studied to enhance heat transfer[2]. However, although these heat transfer enhancement methods enhance the heat transfer in the entire channel, there is still a difference in heat transfer between the upstream and downstram of the channel and forms non-uniform temperature distribution.

In this study, we focused on the fact that the heat transfer coefficient of a fluid is positively correlated with the flow velocity in forced convection heat transfer. Specifically, by gradually changing the cross-section area in the flow direction, the flow velocity is increased near the outlet of the channel to enhanse heat transfer. This is intended to achieve uniform heat transfer throughout the entire flow path. The objective of this study is to clarify the heat transfer mechanism for uniform cooling of heating elements using forced convection heat transfer. In this study, the numerical simulation using OpenFOAM was performed to evaluate the uniform cooling. In addition thermal boundary layer (TBL) was visualized experimentally using Mach-Zehnder interferometer to confirm the validity of the numerical calculations.

Figure 1 shows a schematic of experimental setup to visualize the TBL of entire channel. By using an interferometer, the TBL was clearly yet precisely visualized. Both upper and lower walls of the channel was made of copper blocks and these temperatures were precisely controlled by PID control system. The wall temperature was fixed to 28 °C and water temperature was 25°C.
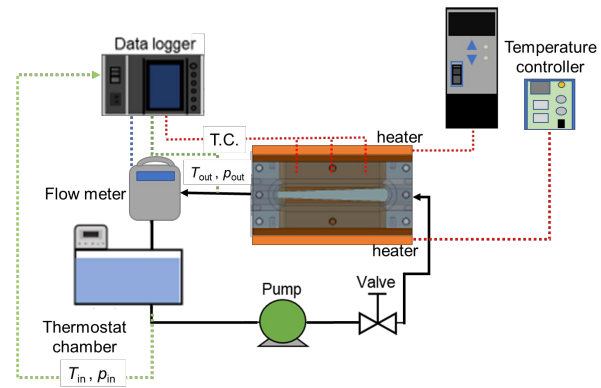

Fig. 1 Schematic diagram of experimental setup.

Figure 2 shows the typical image of visualized TBL. Clearly the layer was visualized and the Nusselt number could be determined from the thickness of the TBL. Comparing the distribution of TBL's thickness between straight channel and tapered one, the latter could form more uniform TBL and it might deliver to uniform cooling along the flow direction.

To quantitatively evaluate the effect of channel tapering, we have performed numerical simulations and obtained the distributions of TBL's thickness and Nusselt numbers. Figure 3 shows their distributions of Nu and temperature of solid. As is obvious from Fig. 3, as the channel is narrowed, TBL's thickness becomes uniformly oriented, resulting in a uniform Nusselt number distribution, and as a result, temperature rise of solids in the latter half of the channel is suppressed and , enabling uniform cooling in long pipes. Future plans include changing the refrigerant to dry air and evaluating the uniform cooling capacity with respect to flow velocity.
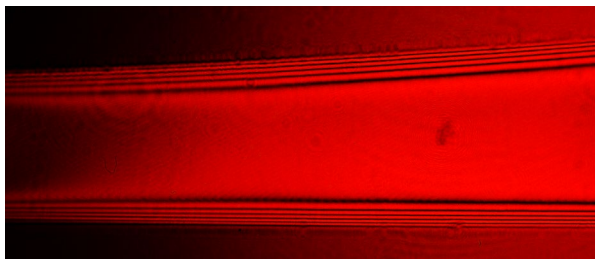
Fig. 2 Visualized image of thermal boundary layer.
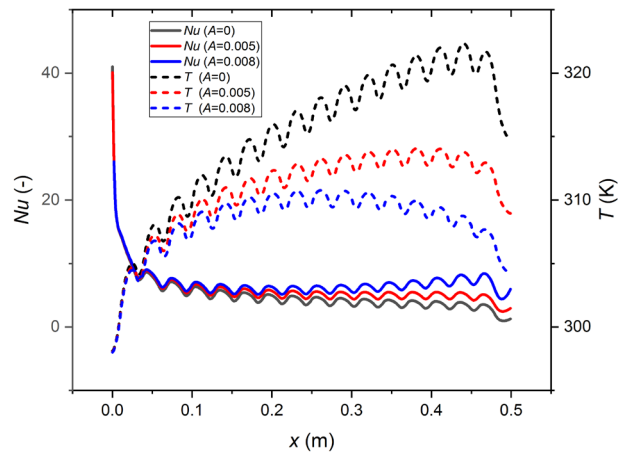
Fig. 3 Visualized image of thermal boundary layer.

References

[1] C.-C. Wang, C.-K. Chen, *International Journal of Heat and Mass Transfer*, 45, (2002), 2587–2595.
[2] Beybin_Ilhan, Hakan Ertürk, *International Journal of Heat and Mass Transfer*, 111, (2017), 500–507.

Design and optimization of elastocaloric refrigeration systems: development of a proof of concept for near-room temperature cooling

ELyT Global
Theme: Energy
Scientific topic: Materials and Structures Design

Marianne SION[a,b,c]	Gaël SEBALD[b]	Atsuki KOMIYA[b,c]	Gildas COATIVY[d]	Jacques JAY[a]

[a] Univ. Lyon, CNRS, INSA-Lyon, CETHIL, UMR5008, F-69621, Villeurbanne, France
[b] ELyTMaX UMI 3757, CNRS – Université de Lyon – Tohoku University International joint Unit, Tohoku University, 980-8577, Sendai, Japan
[c] Institute of Fluid Science, Tohoku University, 980-8577, Sendai, Japan
[d] Univ. Lyon, INSA-Lyon, LGEF, EA682, F-69621, Villeurbanne, France

Abstract

Nowadays, most of the refrigeration systems are using compressed gases, which raises questions about their toxicity, performances and even about their environmental impact. It is needed to find alternatives systems like Peltier or Stirling systems or even using thermoacoustic effect. Another alternative is the use of caloric materials: magnetocaloric, electrocaloric, barocaloric and elastocaloric.

The elastocaloric effect corresponds to the reversible temperature variation of elastocaloric material like natural rubber during its uniaxial loading/unloading, caused by the change in the crystallinity and entropic elasticity of polymer chains. Elastocaloric refrigeration is achieved by mechanical cycles of rubber materials leading to time variations of its temperature. Heat exchangers and cyclic thermal contacts with the rubber material is needed to achieve the creation of the temperature gradient and a volume cooler than ambient temperature.

In the field of elastocaloric systems, the main materials explored were shape memory alloys, such as NiTi alloys. From the state of the art, different elastocaloric systems have been made, such as Shape Memory Alloys heat pumps[1], heat driven heat pumps[2], as well as regenerative systems[3]. It appeared two important routes of innovation that drew our attention. On the one hand, polymers, such as natural rubber, were not yet proposed as plausible candidates for refrigeration although their properties are as high as other caloric materials. On the other hand, currently developed single-stage system do not lead to performances such as large temperature differences combined with large and scalable heat flux and high coefficients of performance because their effective heat exchange and heat loss have not been optimized

A single-stage experimental bench with two linear actuators was implemented (Figure 1) in order to stretch the natural rubber cyclically and to move the exchangers accordingly in order to take heat from a cold reservoir and transport it to a hot reservoir. One actuator was stretching

and releasing the rubber film, the other one was alternatively putting in contact the exchangers with the rubber. Different sensors were placed in the exchangers and fixation in order to obtain parameters such as the force, the position, the heat fluxes and temperatures produced during the cycles.
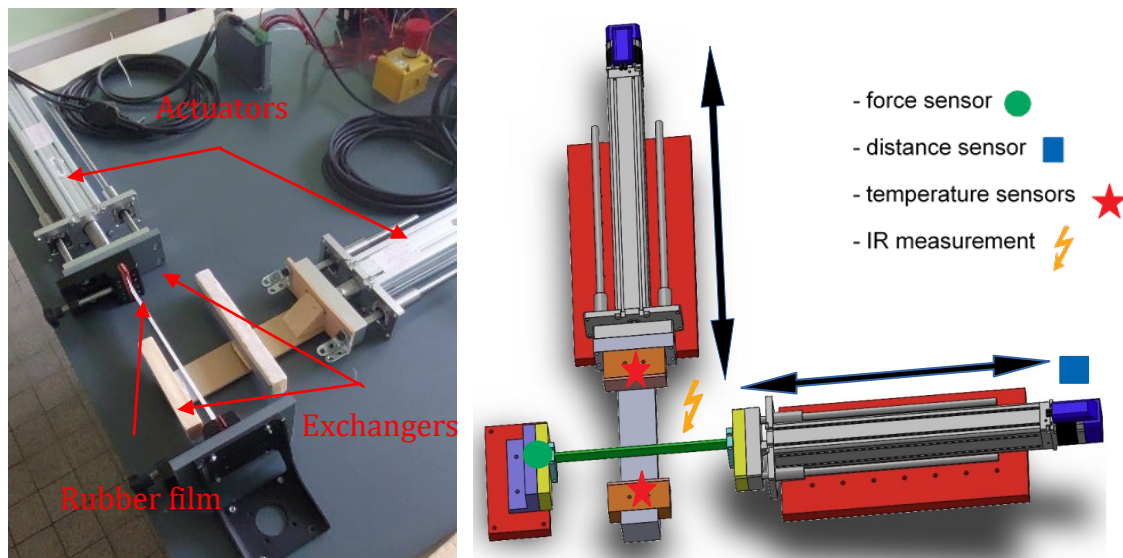
Figure 1: Experimental setup with natural rubber film and exchangers. (right) 3D design of the experimental setup with sensors

The objectives of this work (under progress) is to design a new type of elastocaloric system with natural rubber and to have a better understanding of the energy conversion in order to optimize the heat transfer from the natural rubber to the heat pump and to maximize the cooling power. Also, it is important to obtain better COP and performances by maximizing the heat exchanges while minimizing the heat losses.

Experimental campaigns are planned in order to investigate the impact of the frequency and waveform on the system, the impact of the material (fabrication methods, thickness, height), the impact of the design of the exchangers (surface state, surface value, material) and then the impact of the room temperature by thermalizing the exchangers.

The challenges of this systems are to determine how to obtain an important power, how to measure the temperature gradient correctly in the natural rubber film and to implement a multistage system with great performances. The aims are to allow the design and optimization of an elastocaloric refrigeration system, in order to develop a proof of concept for cooling at near room temperature.

Currently, the development of the experimental setup is in progress with the design of the exchangers and the implementation of the different sensors. During the next three months, the experimental campaign will begin with the investigation of the impact of frequency and waveforms of the mechanical cycles on the elastocaloric performances of our system.

[1]   Ossmer, Hinnerk, Frank Wendler, et al. "Energy-Efficient Miniature-Scale Heat Pumping Based on Shape Memory Alloys." Smart Materials and Structures, vol. 25, Aug. 2016, p. 085037, https://doi.org/10.1088/0964-1726/25/8/085037.
[2]   Ossmer, Hinnerk, Shuichi Miyazaki, et al. Elastocaloric Heat Pumping Using a Shape Memory Alloy Foil Device. 2015, pp. 726–29, https://doi.org/10.1109/TRANSDUCERS.2015.7181026.
[3]   Qian, Suxin, et al. "A Heat Driven Elastocaloric Cooling System." Energy, vol. 182, 2019, pp. 881–99, https://doi.org/https://doi.org/10.1016/j.energy.2019.06.094.
[4]   Tan, Jianming, et al. "Thermodynamic Cycle Analysis of Heat Driven Elastocaloric Cooling System." Energy, vol. 197, 2020, p. 117261, https://doi.org/https://doi.org/10.1016/j.energy.2020.117261.
[5]   Tušek, Jaka, et al. "A Regenerative Elastocaloric Heat Pump." Nature Energy, vol. 1, no. 10, Sept. 2016, p. 16134, https://doi.org/10.1038/nenergy.2016.134.
[6]   Greibich, F., et al. "Elastocaloric Heat Pump with Specific Cooling Power of 20.9 W g–1 Exploiting Snap-through Instability and Strain-Induced Crystallization." Nature Energy, vol. 6, no. 3, Mar. 2021, pp. 260–67, https://doi.org/10.1038/s41560-020-00770-w.
[7]   Engelbrecht, Kurt, et al. "A Regenerative Elastocaloric Device: Experimental Results." Journal of Physics D: Applied Physics, vol. 50, no. 42, Sept. 2017, p. 424006, https://doi.org/10.1088/1361-6463/aa8656.
[8]   Guyomar, Daniel, et al. "Elastocaloric Modeling of Natural Rubber." Applied Thermal Engineering, vol. 57, no. 1, 2013, pp. 33 38,https://doi.org/https://doi.org/10.1016/j.applthermaleng.2013.03.032.

Enhancement of robocasting green body by cellulose nanofiber addition

ELyT Global
Transportation
Materials & Structure design

Teruyoshi KANNO

Assist. Prof. Hiroki KURITA

Prof. Fumio NARITA

Abstract

Silicon carbide (SiC) green body was strengthened by cellulose nanofiber (CNF) addition in the form of an aqueous slurry. The flexural strength of a SiC green body containing 20 wt.% CNF slurry in water dispersant was 813 kPa, 1.5 times larger than the strength of a green body without CNF. CNF increased contact sites between CNF–CNF and CNF–raw particles in the green body, enabling CNF to be subject to load. The enhancement was not observed in a green body containing CNF after annealing at a temperature when bound water on CNF desorbed, which indicated the bond between CNF–raw particles was derived from hydrogen bonding through the bound water.

Introduction

Robocasting is one of the additive manufacturing techniques for ceramic materials, which has an advantage of operation cost due to no need for a special environment such as vacuum, ultraviolet (UV), or laser irradiation. The colloidal slurry is extruded through a syringe and deposited three-dimensionally in this method. Subsequently, the deposited slurry is dried and sintered. The green body, a dried form of ceramic slurry, is fabricated during robocasting, whereas it can easily collapse by shocks that may occur during the process (e.g., transportation from a modeling table to a furnace) due to its low strength. Several studies have been reported concerning enhancing the green body to solve the problem. Pre-heat-treatment under sintering temperature before sintering improved the flexural strength of the alumina green body [1]. Cellulose nanocrystal addition also strengthened that strength by heat treatment at a mild temperature [2]. However, these studies have enhanced only after heat treatment using a furnace. Therefore, other methods that can strengthen it at ambient temperature must be investigated.

Cellulose nanofiber (CNF) is nano-size fibrous cellulose defibrillated from plants. Its aqueous slurry forms a rigid agglomerate after drying at room temperature and shows a rheological behavior suitable for robocasting slurry. Silicon carbide (SiC), one of the high-temperature materials, is particularly difficult to process among ceramics due to its high

hardness. Therefore, novel fabrication procedures of complex shaped SiC products have been desired, and robocasting is expected to be one of them.

In this study, we focused on CNF addition as reinforcement of the ceramic slurry composed of SiC. This work fabricated SiC slurries and robocasting green bodies containing CNF aqueous slurry and evaluated its effect on their rheological property and flexural strength. In addition, the strengthening mechanism is investigated by performing a three-point flexural test of the green bodies after annealing at CNF morphology change.

Results and Discussion

SiC slurries fabricated were classified by the amount of the CNF slurry. In a rheological measurement, the slurry without CNF (100:0 slurry) showed good rheology, Bingham pseudoplastic behavior: yield stress and shear thinning. Another slurry containing 20 wt.% the CNF slurry in water dispersant (80:20 slurry) showed the same rheological behavior as the slurry without CNF, although its yield stress and viscosity of that with CNF were higher than those of that without CNF.
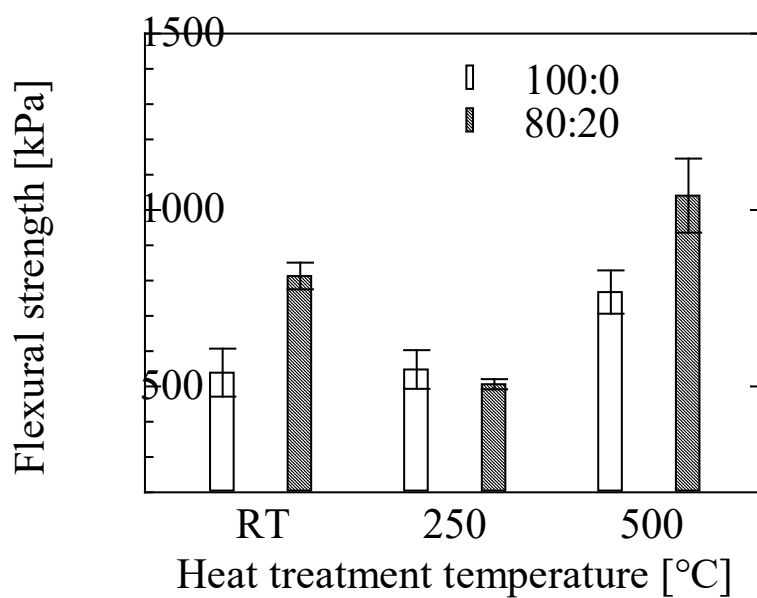
Figure. 1 Flexural strength of SiC green bodies after annealing at some temperatures: the no colors are the green body without CNF and the shaded are that with CNF.

Figure 1 shows the flexural strength of the green bodies after annealing. After room temperature drying (RT in figure 1), the strength of the 80:20 green body was 1.5 higher than that of the 100:0 green body. On the other hand, the strength of the 80:20 green body became as low as that of the 100:0 green body after annealing at 250 °C when bound water on the CNF surface was desorbed. Therefore, green body enhancement by the CNF addition might be caused by hydrogen bonding between CNFs or CNF–particles through the bound water. The bond was broken by desorption of the bound water at 250 °C, and the CNF no longer functioned as a reinforcement.

In contrast, both green bodies were strengthened after annealing at 500 °C when CNF pyrolyzed. The increase might be caused by removing polar groups on the raw particle surface. Subsequently, van der Waals's attractive force between the particles worked stronger.

References

[1]   J.Z. Li, T. Wu *et al.*, *J. Mater. Process. Technol.* 212 (2012) 571–579.

[2]   T. Deng, Y. Wang *et al.*, *Carbohydr. Polym.* 181 (2018) 111–118.

Pseudo-virus Particle Detection using Magnetostrictive Fe–Co/Ni Clad Plate

ELyT Global
Engineering for Health
Materials & Structure design

	Takeru NAKAKI		Assist. Prof. Hiroki KURITA		Prof. Fumio NARITA

Abstract

Self-powered biosensors based on magnetostrictive materials are attracting attention in preparation for new outbreaks of infectious diseases caused by viruses. This study evaluated the energy harvesting performance of Fe-Co/Ni clad plate cantilevers and demonstrated their ability to detect viruses using pseudo-virus particles; the output of the Fe-Co/Ni clad plate cantilever was 0.414 mW (~12.2 mW/cm3). This result suggests that the Fe-Co/Ni clad plate cantilever can detect a mass of 0.1 to 1 μg, assuming that all pseudo-virus (silica) particles are attached to the Fe-Co/Ni clad plate cantilever. Thus, the Fe-Co/Ni clad plate cantilever could lead to the development of a self-powered virus sensor.

Introduction

Piezoelectric and magnetostrictive materials are promising vibrational energy harvesting materials and have been extensively studied for over a decade. Piezoelectric ceramic materials are brittle and easily destroyed by static and cyclic mechanical loading, leading to piezoelectric composite materials. Therefore, many studies and reviews have focused on various piezoelectric energy harvesting materials and devices. However, vibrational energy harvesting using magnetostrictive alloys has potential applications in wireless sensor networks. In addition, flexible magnetostrictive composite materials have been developed to employ wearable vibration energy harvesting. Much research has recently been conducted on magnetostrictive vibrational energy harvesting materials and devices.

Biosensors based on magnetostrictive materials have also been developed, which could detect bacteria and viruses. Even if the current pandemic is overcome, new infectious diseases caused by viruses may occur in the future. Therefore, it is important to maximize the use of piezoelectric and magnetostrictive materials that can be easily integrated with IoT devices, resulting in the development of self-powered energy harvesting systems and

mass sensors for virus detection. Recently, Mori et al. [1] investigated numerically and experimentally the effects of proof mass weight and position on the frequency shift and output voltage of magnetostrictive cladding plates induced by bending vibration. Although magnetostrictive biosensors based on resonant frequency shift have multiple advantages [1, 2], it is necessary to account for the effect of virial mass on the dynamic properties of magnetostrictive biosensors for simultaneous vibration energy harvesting and wireless communication. This study evaluated the energy harvesting performance of Fe-Co/Ni clad plate cantilevers and then demonstrated their virus detection capability using pseudo-virus particles.

Results and Discussion

The mass detection time of the Fe-Co/Ni clad plate was tested for pseudo viral particles due to the low particle concentration. NH$_2$ fluorescent silica microparticles were used to test for the successful formation of -COOH self-assembled monolayers on the cantilevers.

Figure. 1 (a) Steady-state deflections of a frequency shift as a function of time for silica microparticle concentrations of 5 and 10 μg/mL, and (b) Peak-to-peak output voltage change as a function of time for silica microparticle concentrations of 5 and 10 μg/mL

Because the particles are fluorescent, their successful attachment to the surface could be easily confirmed by fluorescence microscopy. Fig. 1(a) shows the dynamic response to silica particles on the surface of a Fe-Co/Ni clad plate with particle concentrations from 0 to 10 mg/mL as a function of immersion time. The cladding plates in high silica particle concentration dispersions showed a large shift Δf in their resonance frequency; the shift in the resonance frequency of the Fe-Co/Ni cladding plates eventually reached a saturation value. The total shift of the resonant frequencies of the cladding plates with silica particle dispersion concentrations of 5 μg/mL and 10 μg/mL were -0.1 and 0.3 Hz, respectively. Fig. 1(b) shows similar results for the change in peak-to-peak output voltage ΔV_{pp} corresponding to Fig. 1(a). No significant change was observed at a concentration of 5 μg/mL even after a reaction time of 2 hours. At a concentration of 10 μg/mL, it can be seen that the peak output voltage changed by about 1.5 V at a reaction time of 30 minutes. As the concentration increases, the peak-to-peak output voltage change is expected to increase; the optimal design and improved performance of the Fe-Co/Ni clad plate will allow particles to be detected from the output voltage change.

Thus, it is demonstrated that the magnetostrictive clad plate energy harvesting device can be used to detect small pseudo viral particles. Since the same signal is used for computation and storage operations, events of interest in the detected signal are continuously monitored without resorting to additional power sources. To demonstrate self-powered virus detection capability, recording the signals produced by the magnetostrictive cladding plate while disconnected from an external power source is necessary.

References

[1] K. Mori et al., Materials 2021, 14, 4486.

[2] F. Narita et al., Advanced Materials 2021, 33, 2005448.

Development of a cerebral artery biomodel for surgery training

	Riko Hasegawa Graduate School of Engineering, Tohoku University		**Hiroyuki Kosukegawa Institute of Fluid Science, Tohoku University Blue Practice Co.Ltd**
	Kaihong Yu Institute of Fluid Science, Tohoku University Blue Practice Co.Ltd		**Makoto Ohta Institute of Fluid Science, Tohoku University**

Abstract

In endovascular treatment, especially for cerebral vascular treatment, catheter insertion is difficult and requires the physicians' experience and skill. A biomodel can provide their training in the technique. However, current biomodels are not enough to reproduce mechanical properties or to acquire sensory knowledge. Furthermore, biomodels are necessary to reproduce vessels with atherosclerotic symptoms requiring catheterization. We have developed the world's first vascular model that reproduces the mechanical properties of blood vessels using polyvinyl alcohol hydrogel (PVA-H) as a material. However, the correlation between the mechanical properties of the PVA-H model and physicians' feeling has not been clarified at this stage. Therefore, this study aims to show the correlation between mechanical properties and physician's feeling. This will make it possible to create a biomodel that more closely resembles actual blood vessels and is expected to improve physicians' catheter manipulation skills.

Acknowledgements

Molecular Dynamics Simulations of Cerium Ion Transport Phenomena in Polymer Electrolyte Membranes of Polymer Electrolyte Fuel Cells

**Mr.
Hiroto Suzuki[1),2)]**

**Assistant Prof.
Takuya Mabuchi[2),3)]**

**Prof.
Takashi Tokumasu[2)]**

Affiliation

1) Graduate School of Engineering, Tohoku University
2) Institute of Fluid Science, Tohoku University
3) Frontier Research Institute for Interdisciplinary Sciences, Tohoku University

Abstract

We analyzed the transport properties of cerium ions, which are added to improve the chemical durability of a polymer electrolyte membrane (PEM), using molecular dynamics simulations. For the analysis, the diffusion coefficient of cerium ions and the radial distribution function around sulfonic acid groups were obtained. The results show that at low water content, the diffusion coefficient is small because of the direct coordination of cerium ions to the sulfonic acid groups due to the small number of water molecules around the sulfonic acid groups. At high water content, water molecules gather around the sulfonic acid groups, and cerium ions are coordinated far from the sulfonic acid groups, resulting in a weaker binding than at low water content and an increase in the diffusion coefficient of cerium ions.

Acknowledgements

Combined Effect of Cr content and Dissolved Oxygen Concentration on Wall Thinning Rate by Low Temperature FAC

Takumi Kishi **Tohoku University**	**Hiroshi Abe** **Tohoku University**	**Yutaka Watanabe** **Tohoku University**	**Kazutoshi Fujiwara** **Central Research Institute of Electric Power Industry**

Abstract

Flow Accelerated Corrosion (FAC) is one of the causes of pipe wall thinning in power plants. It is widely known that FAC is usually experienced between 90 ℃ and 230 ℃, and that the maximum FAC rate is shown at about 150 ℃. Low-temperature FAC (< 90 ℃) has been also reported, however, knowledge of the effects of material and environmental factors on FAC rate at low-temperature is very limited.

In this study, combined effects dissolved oxygen (DO, up to 20 ppb) on FAC rate of carbon steels with different Cr content (up to 1 wt.%) at low temperature (30 ℃, 50 ℃) were investigated.

The results indicate that the amount of DO require to suppress FAC depends on temperature and Cr content of the steel . Visual observations and Raman spectroscopy showed differences in oxide film constituent species depending on DO and Cr content. The combination of Cr content and DO showed differences in the degree of oxide film formation and wall thinning suppression, clearly indicating a combination effect.

Acknowledgements

Numerical Investigation of Liquid Film Thickness

of Adiabatic Two-phase Flow in Microchannel

**Daisuke Tsuneoka**

Abstract

Two-phase flow in a microchannel is recognized as an efficient micro cooling system. Since the slug two-phase flow is frequently observed in practical applications, the heat transfer properties of this regime need to be evaluated. Here, the liquid layer generated between the channel wall and the bubble plays an important role in heat transfer in microchannel. Thus, to achieve an efficient micro cooling system, the behavior of liquid film and its thickness have to be investigated. As an elementary step, a single bubble in an adiabatic microchannel is being numericaly investigated in this study.

The result of this study is as below.

・The flow turbulence in both ends of the bubble seems to affect the liquid film thickness.

・The laminar flow model is applicable when the surface tension is large relatively to the inertial force. When the Capillary number gets higher than 0.05, turbulence model is needed to simulate in high Reynolds number.

・The k-ω SST turbulence model seems to affect the flow in both ends of the bubble and shorten the bubble length.
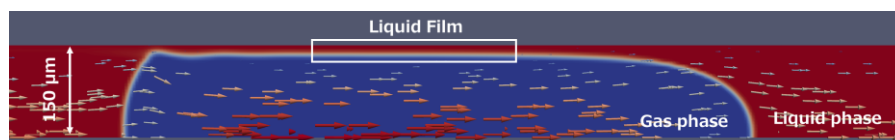
Simulation of the Two-phase slug flow in a microchannel

Acknowledgments

CarboEDiffSim :Molecular Analysis of Carbon Diffusion in Iron with Phase Transformation under Electric Field

Mr.Ryuta Onozuka[1), 2)]

Assistant Prof. Takuya Mabuchi [2), 3)]

Prof. Patrice Chantrenne[4)]

Prof. Takashi Tokumasu[2)]

Affiliation

1) Finemechanics, Graduate School of Engineering, Tohoku University

2) Institute of Fluid Science, Tohoku University

3) Frontier Research Institute for Interdisciplinary Sciences, Tohoku University

4) MATEIS, INSA de Lyon, Université de Lyon

Abstract

In this research project, the goal is to get fundamental knowledge in order to analyze the mechanisms of carbon diffusion in iron under an electric field. To investigate the mechanisms, Molecular Dynamics simulation was used. In a previous work, an EAM based interatomic potential was used. However, it has been difficult to correctly analyze the temperature dependence of carbon diffusion because the phase transformation temperature obtained by this potential is much lower than the experimental value. We have attempted to overcome these problems by using the ABO potential developed by Nguyen et al. We performed test calculations to investigate the validity of the potential. From the results, we found that energy conservation law was satisfied when timestep was 0.1[fs]. In addition, to verify that we used the potentials correctly, we compared our results with previous studies.

Acknowledgements

Microfluidic Experiment about Hypoxic Responses of Vascular Endothelial Cells under Hyperglycemia

Kazuki Sone, Tohoku University

Abstract

Blood glucose and oxygen concentrations are continuously changing in vivo, but the responses of vascular endothelial cells to them have not been completely elucidated. In this study, a vascular endothelial cell monolayer was formed in a microfluidic devise, and the cellular responses were observed under different pericellular glucose and oxygen conditions. As the results, a high glucose condition increased cell migration under normoxia. But, there was no change in cell migration by glucose under hypoxia though it promoted nuclear translocation of hypoxia inducible factors (HIF) -1α. From these it was suggested that the increase in migration induced by high glucose was suppressed by hypoxic response.

Acknowledgements